NOVEL DESIGN FOR PRODUCTION OF LIQUID FUELS WITH NEGATIVE EMISSIONS

NOVEL DESIGN FOR PRODUCTION OF LIQUID FUELS WITH NEGATIVE EMISSIONS

Modeling, design, simulation and techno-economic analysis

By

LEILA HOSEINZADE, B.Sc., M.Sc.

A Thesis Submitted to the School of Graduate Studies in Partial Fulfilment of the Requirements for the Degree Doctor of Philosophy

McMaster University

Ph.D. Candidate (2018) McMaster University

Chemical Engineering Hamilton, Ontario, Canada

TITLE: Novel Design for Production of Liquid Fuels with Negative Greenhouse Gas Emissions

AUTHOR: Leila Hoseinzade

B.Sc. (University of Tabriz)

M.Sc. (Sharif University of Technology)

SUPERVISOR: Dr. Thomas A. Adams II

Number of pages: x, 107

Abstract

Global pressure to reduce greenhouse gas (GHG) emissions, energy security concerns and increasing demand for liquid fuels incentivize the search for more sustainable and secure alternative methods for producing liquid fuels with improved efficiency and reduced environmental impacts. One of the economically attractive examples of these alternate methods is the gas-to-liquid process, however, its environmental impacts are worse than traditional petroleum refining. Carbon capture and sequestration is an option to reduce greenhouse gas emissions of processes, but it decreases the efficiency of the process and often results in economic infeasibility. Instead, integrating different processes and feedstocks was demonstrated to improve the efficiency, economic and environmental performance of the processes.

The focus of this thesis is to design and simulate a novel integrated biomass, gas, nuclear to liquids (BGNTL) process with negative greenhouse gas emissions. In this process, nuclear heat from a high temperature gas-cooled reactor (HTGR) is used as the heat source for a steam methane reforming (SMR) process. The integrated HTGR and SMR process requires detailed analysis and modeling to address key challenges on safety, operability, economic and environmental impacts of the integrated process. To this end, a rigorous first principle based mathematical model was developed in gPROMS modeling environment for the integrated HTGR/SMR process. The results for a large scale design of this system indicate that hydrogen rich syngas with H_2/CO ratio in the range of 6.3 can be achieved.

To meet the desired H_2/CO ratio (around 2) required for the downstream fuel synthesis processes, the HTGR/SMR derived syngas can be blended with a hydrogen lean syngas from biomass gasification. In this thesis, the large scale design of the BGNTL process to synthesize gasoline, diesel and dimethyl ether (DME) is investigated. The results from the gPROMS model of the integrated HTGR/SMR system are used for simulating the BGNTL process in Aspen Plus. The performance of the BGNTL process was compared with a biomass, gas to liquids (BGTL) process. The efficiency, economics, and environmental impact analyses show that the BGNTL process to produce DME is the most efficient, economic and environmentally friendly process among all the considered designs. The results demonstrate that process integration exploits certain synergies that leads to significantly higher carbon and energy efficiencies and lower greenhouse gas emissions. In addition, it was found that all the studied designs yield a net negative greenhouse gas emissions when carbon capture and storage technology is implemented.

As another sustainable alternative to meet the required H_2/CO ratio of the syngas when biomass resources are not available, it is proposed to apply the nuclear heat to the mixed reforming of methane. This represents using steam and waste CO_2 to reform methane into valuable syngas. The developed model for the integrated HTGR/SMR system is extended to the mixed reforming of methane (MRM) process and it was demonstrated that integrated HTGR/MRM process can be a promising option to achieve certain desired H_2/CO ratios for the downstream energy conversion processes.

Research Contributions

- A dynamic and multi-scale model is presented for the integrated high temperature gas-cooled reactor (HTGR) and steam methane reforming (SMR) system.
- The model parameters of the HTGR/SMR system are fitted based on the reported design data in the literature.
- A dynamic and first principle based model is developed for the novel integrated HTGR and mixed reforming of methane (MRM) process.
- The model of the HTGR/MRM process is validated using up to 25 lab scale data sets reported in the literature.
- Several novel biomass, gas, nuclear to liquids (BGNTL) processes are proposed which considers applying nuclear heat to drive the energy intensive steam methane reforming process.
- The proposed designs were simulated based on rigorous model developed for the HTGR/SMR process.

Acknowledgments

First and foremost, my deepest gratitude is extended to my supervisor Dr. Thomas A. Adams II. I am grateful for his support, constant encouragement, positive attitude and invaluable guidance. He will always remain one of the most inspiring people with whom I have had the fortune to work with and who would have contributed to whatever success I achieve in my life ahead.

I would like to thank my committee members, Drs. Mhaskar and Cotton for their insightful questions and suggestions that have improved the quality of this work. I'm also grateful to Dr. Mahalec for his encouragement and support. Special thanks to the McMaster Advanced Control Consortium and the Department of Chemical Engineering at McMaster University for their financial support.

A particularly special thanks to Ikenna Okeke and Pranav Madabhushi for their intellectual and moral support during this project. I would also like to thank Jaffer Ghouse, Yaser Khojasteh, Pedro Castillo, Farid Afzali, Chinedu Okoli, Jake Nease, Vida Meidanshahi, Lingyan Deng, Hundey Lai, Daniela Dering, Anthony Quarshie, Hao Li and other MACC members.

Last but not least, I would like to thank my family and express my love and gratitude to my husband Mahdi Eskandari, my parents Mrs. Masoumeh Hassan nejad and Mr. Karim Hoseinzade for their constant love, support and patience.

Table of contents

Nomenclature

SMR	Steam methane reforming
HTGR	High temperature gas-cooled reactor
HTTR	High temperature test reactor
GHG	Greenhouse gases
JAERI	Japan Atomic Energy Research Institute
PDAE	Partial differential algebraic equation
DRM	Dry reforming of methane
MRM	Mixed reforming of methane
FT	Fischer-Tropsch
POM	Partial oxidation of methane
WGS	Water gas shift
GHSV	Gas hourly space velocity
STP	Standard temperature and pressure
BGNTL	Biomass-gas-nuclear heat-to-liquid
DME	Dimethyl ether
BGTL	Biomass-gas-to-liquid
CCS	carbon capture and storage
GTL	Gas-to-liquids process
MHR	Modular helium reactor
CGNTL	Coal-gas-and-nuclear-to-liquids
CTL	Coal-to-liquids
CGTL	Coal-and-gas-to-liquids

MeOH	Methanol
RSC	Radiant syngas cooler
HHV	High heating value
LHV	Low heating value
LHS	Latin hypercube sampling
GT	Gas turbine
ASU	Air separation unit
LPS	Low pressure steam
MPS	Medium pressure steam
HPS	High pressure steam
NG	Natural gas
MDEA	Methyl di-ethanolamine
CEPCI	Chemical Engineering Plant Cost Index
NPV	Net present value
FCI	Fixed capital investment
TPC	Total production cost

Chapter 1

Introduction

1.1. Background and Motivation

To synthesize liquid fuels, a source of carbon, electricity and heat is required. Traditionally, petroleum oil is used as the main source of carbon, electricity and heat to produce liquid fuels. However, oil is a non-renewable energy resource and its prices are generally high. Moreover, as Figure 1 shows, the demand for the liquid fuels are always increasing [1]. All of these challenges incentivize industry and government to use alternative methods of producing liquid fuels such as the gas-to-liquids process (GTL). The high natural gas prices limited GTL process applications for a decade [2, 3]; however, with low natural gas prices, GTL processes are more economical than petroleum-based fuels [4]. Although, GTL processes are economically appealing, they have often worse environmental impacts than traditional petroleum [3].

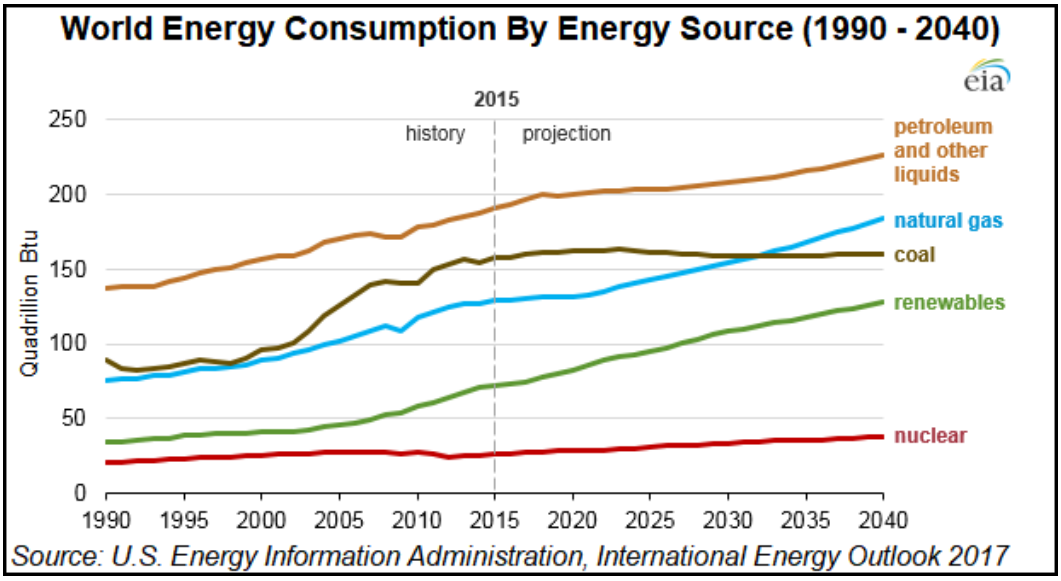

Figure 1. International energy outlook. Taken from U.S. Energy Information Administration (EIA) website [1].

Previous studies by Adams et al. [5,6] and Khojasteh Salkuyeh et al. [7,8] have shown that instead of using gas only, processes which integrate natural gas with other fuels can exploit certain synergies that yield both greater energy and carbon efficiency and significantly lower GHG emissions. In the studies by Khojasteh et al. [7, 8], natural gas and coal are utilized as the source of carbon, while heat and electricity are provided by an advanced type of nuclear energy source called a Modular Helium Reactor (MHR) [7]. This integrated process called coal-gas-and-nuclear-to-liquids (CGNTL), which can be superior both environmentally and economically than coal-to-liquids (CTL), coal-and-gas-to-liquids (CGTL), and other processes. However, even though the CO_2 can be eliminated during processing, one cannot prevent the CO_2 emissions from using the gasoline. Furthermore, coal is not of much interest to Canadian province of Ontario due to lack of coal and the lack of political support. Therefore, a new design is proposed which is meant to specifically take advantage of Ontario's interests and resources. A recent study by Scott et al. [9] presented a biomass-gas-and-nuclear-to-liquids (BGNTL) process to co-produce fuels and power. This study considered using Ontario's interests and resources. In this process, nuclear energy was utilized to power a copper-chloride cycle that produced hydrogen for syngas upgrading. However, it was demonstrated that using nuclear energy in this way is not profitable [9]. Instead, other approaches which take better advantage of the high-temperature (>800°C) heat produced by some nuclear

reactors may be preferable. This study presents the BGNTL process which uses high temperature nuclear heat as the heat source of methane reforming process.

The base case studied BGNTL process is shown in Figure 2. As shown in the figure, biomass is gasified into hydrogen lean syngas (a mixture of hydrogen and carbon monoxide) and some waste carbon dioxide, using high pressure steam (HPS) from heat recovery steam generator (HRSG) section and oxygen from air separation unit (ASU). This syngas has low hydrogen content (H_2/CO ratio of about 0.75); Hence, H_2/CO ratio of 2 is needed for the downstream Fischer-Tropsch (FT) and methanol/DME synthesis.

To meet this ratio, natural gas is reformed into hydrogen rich syngas through the steam methane reforming (SMR) reactions, as given below:

$$CH_4 + H_2O \rightleftharpoons CO + 3H_2 \ \left(\Delta H_{r,T_{ref}} = 206.2 \frac{kJ}{mol}\right) \quad (1)$$

$$CO + H_2O \rightleftharpoons CO_2 + H_2 \ \left(\Delta H_{r,T_{ref}} = -41.2 \frac{kJ}{mol}\right) \quad (2)$$

$$CH_4 + 2H_2O \rightleftharpoons CO_2 + 4H_2 \ \left(\Delta H_{r,T_{ref}} = 165 \frac{kJ}{mol}\right) \quad (3)$$

The SMR process as shown by equations (1) to (3) is highly endothermic and requires a heat source with high temperatures to derive the reaction. Conventionally, the heat required for the SMR process is provided from natural gas combustion which causes huge GHG emissions. Thus, using the carbonless heat from the high temperature gas-cooled reactor is expected to lower the GHG emissions of the SMR process.

The produced syngas from the SMR process has a high H_2 content, and after CO_2 and sulphur removal, it can be mixed with the biomass-derived syngas to adjust syngas with a balanced H_2 amount (H_2/CO~2) needed for downstream FT and MeOH/DME synthesis. Some of the produced

syngas in addition to the waste off-gases from different process sections are sent to power generation section. CO_2 from the process can be sequestered or repurposed to prevent CO_2 emissions, providing a process which produces zero direct CO_2 emissions and consumes enough biomass to compensate the most of GHG emissions from combustion of fuels in the vehicle engine.

Studies by Research Center Julich [10, 11, 12] and Japan Atomic Energy Research Center (JAERC) [10, 13] have examined using helium as a high-temperature transfer medium from nuclear reactor to the SMR process at pilot scale. Those studies were determined the feasibility of the integrated HTGR/SMR process [10] (more details on this system can be found in chapter 2 of the thesis). Although, the feasibility of this system was tested, many key challenges surrounding the steady state and dynamic behaviors of the integrated system needed to be addressed before commercial scale implementation of the system. However, there is no model in the literature to study the dynamic and steady state behaviors of the system, its safety and controllability or analyze its efficiency, economic and environmental impacts.

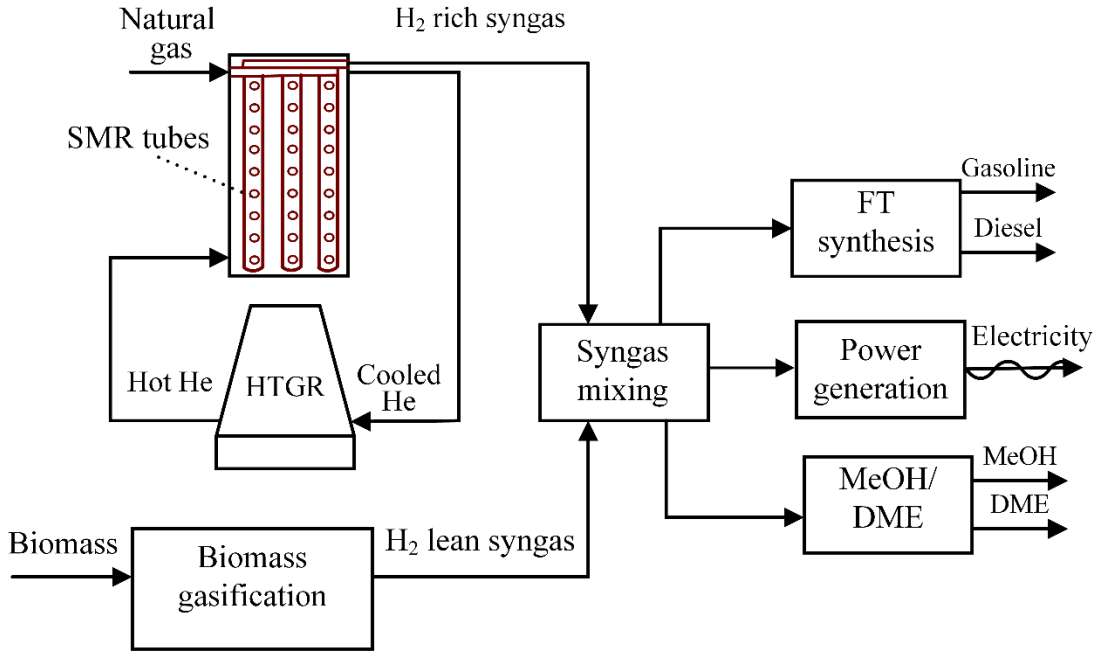

Figure 2. Superstructure of the proposed BGNTL process.

1.2. Research outline

The primary goal of this thesis is to develop sustainable processes with negative GHG emissions to produce liquid fuels and power in Ontario province of Canada using its own resources and technologies. The thesis contains incorporation of novel processes and technologies to co-produce fuels and power and offers novel and sustainable alternatives to the traditional petroleum. The use of Ontario grown woody biomass, natural gas, carbon dioxide and advanced nuclear technology are investigated as the primary alternative feedstock and energy sources.

This thesis contains six chapters including introduction and conclusion chapters. A brief summary for each of the chapters and publications therein is given below:

Chapter 2. This chapter focuses on developing a rigorous dynamic model for the integrated HTGR/SMR system since the dynamics of the high temperature integrated nuclear reactors are poorly understood. This model was developed based on first principles to predict the temporal and spatial variation of the system from the macro to micro level. The developed model is a set of nonlinear partial differential and algebraic equations which was implemented in gPROMS software package (an equation-based modelling and simulation environment). The key design parameters of the integrated system was determined based on the existing data on the integrated HTGR/SMR facilities or model fitting. The model then was used to build a base case large scale design with the cooling duty in the range of 72 MW. The contents of this chapter have been published in the *International Journal of Hydrogen Energy* [14] after peer review.

Chapter 3. The dynamic and multi-scale model developed in the previous chapter was extended to the novel integrated HTGR and combined steam and dry reforming process. The resulting model was validated using reported experimental data at non-equilibrium and equilibrium conditions.

The dynamic and steady state performance of the integrated mixed reforming of methane (MRM) and HTGR system was studied and it was found that in addition to desired H_2/CO ratios, higher methane conversion and lower CO_2 emissions can be achieved using the proposed design compared to HTGR/SMR system. The contents of this chapter have been published in *Industrial & Engineering Chemistry Research* [15] after peer review.

Chapter 4. In this chapter, the base case BGNTL process is presented which uses high-temperature nuclear heat as the heat source for steam methane reforming. This process polygenerates liquid fuels (Fischer-Tropsch liquids, methanol and DME) and power. The scope of this chapter is to present a superstructure rather than an optimal design. Thus, the decision variables of the plant were set to approximately the middle of their feasible range. The BGNTL process was simulated using a combination of different software packages including gPROMS, MATLAB, ProMax, and Aspen Plus. This included the use of a rigorous multi-scale model for the nuclear-heat-powered SMR reactors which was developed in the chapter 2. Energy efficiency and cradle-to-grave life cycle inventory and life-cycle impact analyses of greenhouse gas emissions are accomplished to analyze the efficiency and environmental impacts of the BGNTL system. Plant performance is compared with a non-nuclear base case biomass-gas-to-liquid process at the same size. In all the configurations, carbon capture and storage (CCS) option is considered. The content of this chapter have been published in the *Computer Aided Chemical Engineering* [16] after peer review.

Chapter 5. This chapter focuses on techno-economic and environmental analysis of the BGNTL process. In this chapter, efficient designs of the BGNTL and BGTL processes are presented. Although, a formal optimization of the process as a whole was not carried out in this chapter, the individual sections within the BGNTL and BGTL processes were optimized individually. In

chapter 4, a base case BGNTL process was considered for polygenerating several products and fraction factors to decide on the amount of each product were not optimized. In contrast, in this chapter the BGNTL processes are considered for producing one fuel at a time and the results are compared based on economic and environmental factors. The performance of the BGNTL process was compared against a BGTL process which produces liquid fuels using an optimized integrated biomass gasification and SMR process. The efficiency, economics, and environmental impact analyses show that the BGNTL process to produce DME is the most efficient, economic and environmentally friendly process among the considered designs. As a result of process integration, an efficiency of up to 54 HHV% and a net present value of $600 million can be achieved without using the optional carbon capture system. Furthermore, the cradle-to-grave greenhouse gas emission analysis indicate that BGNTL to DME process without carbon capture and storage has 57% and 25% lower emissions than a coal-to-DME and natural gas-to-DME processes, respectively. In additions, it was found that all the studied designs leads a net negative greenhouse gas emissions when carbon capture and storage option is enabled. The results of this chapter have been submitted for peer review in the *Applied Energy* journal.

Chapter 6. This chapter presents the final conclusions and future directions for this work.

1.3. Author's Contribution to Papers

As the author of this thesis, I can confirm that I was the primary performer of all research and primary author of all the proceeding chapters (including the published works on which they are based).

1.4. Other Contributions

In addition to this thesis findings, I contributed to the field in other two projects during my Ph.D. The first project is the economic modeling and optimization of the "flare gas-to-butanol" process [17] which was carried out in the first year of my Ph.D. In this project, an optimization problem has been developed to predict the best strategy of commercializing Pioneer Energy[1]'s novel and sustainable waste-to-butanol process based on economic and environmental criteria. This study was very insightful on the economic analysis and GHG emission analysis which used in the BGNTL process studies. The results of this research was published in the *Canadian Journal of Chemical Engineering* [17] and I was the first author of this paper.

Furthermore, we published a review paper on the carbon capture technologies [18] in collaboration with other Adams group members. This paper is not going into my thesis, however it was very insightful on the CCS technologies which is a step of BGNTL process design. The paper was published in the *Processes Journal* [18] and I contributed to that as the second author. Since, these two papers are not directly related to this thesis, they are not included in the thesis.

1.5. References

[1] U.S. Energy Information Administration, International Energy Outlook 2017.

[2] Eilers J, Posthuma SA, Sie ST. The shell middle distillate synthesis process (SMDS). Cat Letters 1990;7:256-70.

[1] Pioneer Energy Inc. is a U.S.-based energy technology company.

[3]. Jaramillo P, Griffin WM, Matthews HC. Comparative analysis of the production costs and life-cycle GHG emissions of FT liquid fuels from coal and natural gas. Environ Sci Tech 2008;42:7559-65.

[4]. Baliban RC, Elia JA, Floudas CA. Novel natural gas to liquids processes: Process synthesis and global optimization strategies. AIChE J 2013;59:505-31.

[5] Adams TA II, Barton PI. Combining coal gasification and natural gas reforming for efficient polygeneration. Fuel Process Technol 2011;92:639-55.

[6] Adams TA II, Barton PI. Combining coal gasification, natural gas reforming, and solid oxide fuel cells for efficient polygeneration with CO_2 capture and sequestration. Fuel Process Technol 2011;92:2105-15.

[7] Khojasteh SY, Adams TA II. Combining coal, natural gas, and nuclear heat for liquid fuels production with reduced CO_2 emissions. Comput Aid Chem Eng 2012; 30:247-51.

[8] Khojasteh Salkuyeh Y, Adams TA II. Combining coal gasification, natural gas reforming, and external carbonless heat for efficient production of gasoline and diesel with CO_2 capture and sequestration. Energ Convers Manage 2013;74:492-504.

[9] Scott JA, Adams TA II. Biomass-gas-and-nuclear-to-liquids (BGNTL) processes Part I: model development and simulation. Canadian J Chem Eng 2018; in press, CJCE-18-0053.R2.

[10] Yan XL, Hino R. Nuclear hydrogen production handbook. CRC Press; 2011.

[11] Fedders H, Harth R, Höhlein B. Experiments for combining nuclear heat with the methane steam-reforming process. Nucl Eng Des 1975;34(1):119-27.

[12] Höhlein B, Niessen H, Range J, Schiebahn HJ, Vorwerk M. Methane from synthesis gas and operation of high-temperature methanation. Nucl Eng Des 1984;78(2):241-50.

[13] Inagaki Y, Nishihara T, Takeda T, Hada K, Ogawa M, Shiozawa S, Miyamoto Y. Development programme on hydrogen production in HTTR. No. IAEA-TECDOC--1210 2001.

[14] Hoseinzade L, Adams TA II. Modeling and simulation of an integrated steam reforming and nuclear heat system. Int J Hydrogen Energy 2017;42(39): 25048-62.

[15] Hoseinzade L, Adams TA II. Dynamic modeling of integrated mixed reforming and carbonless heat systems. Ind Eng Chem Res 2018;57:6013-23.

[16] Hoseinzade L, Adams TA II. Combining biomass, natural gas, and carbonless heat to produce liquid fuels and electricity. Comput Aided Chem Eng 2018;43:1401-06.

[17] Hoseinzade L, Adams TA II. Supply chain optimization of flare-gas-to-butanol processes in Alberta. Can J Chem Eng 2016;94: 2336-54.

[18] Adams TA II, Hoseinzade L, Madabhushi PB, Okeke IJ. Comparison of CO_2 Capture Approaches for Fossil-Based Power Generation: Review and Meta-Study. Processes 2017;5:44.

Chapter 2

Modeling and simulation of an integrated steam reforming and nuclear heat system

The contents of this chapter have been published in the following peer reviewed journal:

Hoseinzade, L. and Adams II, T.A., 2017. Modeling and simulation of an integrated steam reforming and nuclear heat system. *International Journal of Hydrogen Energy, 42*(39), pp.25048-25062.

INTERNATIONAL JOURNAL OF HYDROGEN ENERGY 42 (2017) 25048–25062

Available online at www.sciencedirect.com

ScienceDirect

journal homepage: www.elsevier.com/locate/he

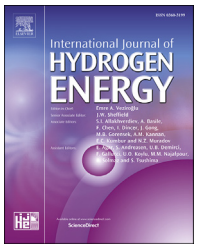

Modeling and simulation of an integrated steam reforming and nuclear heat system

*Leila Hoseinzade, Thomas A. Adams II**

Department of Chemical Engineering, McMaster University, 1280 Main St W, Hamilton, Ontario, L8S 4L7, Canada

ARTICLE INFO

Article history:
Received 25 May 2017
Received in revised form
25 July 2017
Accepted 4 August 2017
Available online 1 September 2017

Keywords:
Dynamic modeling
Steam methane reforming
Syngas
Integrated systems
Nuclear heat

ABSTRACT

In this study, a dynamic and two-dimensional model for a steam methane reforming process integrated with nuclear heat production is developed. The model is based on first principles and considers the conservation of mass, momentum and energy within the system. The model is multi-scale, considering both bulk gas effects as well as spatial differences within the catalyst particles. Very few model parameters need to be fit based on the design specifications reported in the literature. The resulting model fits the reported design conditions of two separate pilot-scale studies (ranging from 0.4 to 10 MW heat transfer duty). A sensitivity analysis indicated that disturbances in the helium feed conditions significantly affect the system, but the overall system performance only changes slightly even for the large changes in the value of the most uncertain parameters.

Introduction

Syngas is an important feedstock for the production of electricity and various chemicals such as methanol, ammonia, dimethyl ether, and Fischer-Tropsch liquids. The steam methane reforming (SMR) process is a common method of producing syngas [1]. The SMR reaction is endothermic and requires high temperatures in order to achieve high conversions of methane [2]. Conventionally, the required heat for the reforming process is provided by combustion (typically using natural gas) in a furnace, through the auto-thermal reforming process, or through partial oxidation. However, there has been research into using alternative sources of providing the required high-temperature heat that could reduce the total greenhouse gas emissions (GHG) of the process [3], such as nuclear energy. For example, a study by Khojasteh-Salkuyeh and Adams [4] examined the concept from a systems perspective for the production of Fischer-Tropsch liquids, in which helium gas was heated in a nuclear reactor to about 1200 °C and then used to provide heat for natural gas reforming to produce syngas. It was determined that using nuclear heat reduces direct fossil fuel consumption for the process as a whole by about 22%, leading to carbon efficiencies of up to 72%. A follow up study examining similar ideas for methanol and dimethyl ether production found similar advantages [5]. Other studies have investigated a similar approach for using nuclear-heat-driven SMR reactions with hydrogen as the final product. Several studies were carried out in Germany and Japan on the integrated HTGR/SMR systems [2,3,6,7]. In these studies, it has been demonstrated that nuclear energy is a safe, abundant and economically viable alternative to produce liquid fuels which can significantly decrease GHG emissions. In each of these cases, the key

* *Corresponding author.*
E-mail address: tadams@mcmaster.ca (T.A. Adams).
http://dx.doi.org/10.1016/j.ijhydene.2017.08.031

component of the system is the high temperature gas-cooled reactor (HTGR), in which a hot gas (usually helium above 800 °C) provides the heat necessary to drive the endothermic SMR reaction.

The first pilot plant of an integrated SMR/HTGR was tested in 1972 in Germany [6]. This facility was called EVA-I (meaning "single splitting tube") and used a 1 MW electric heater to heat helium at 4 MPa up to 950 °C in order to mimic the conditions of high-temperature helium in an actual nuclear facility. This pilot used a single tube-and-shell type configuration. The helium entered the shell, delivering heat through the wall of a single tube. The tube was filled with SMR catalyst in which natural gas and steam would be fed for the reforming reaction countercurrent to the helium. A second, helical inner tube was embedded inside of the main tube, such that the products of the SMR reaction would enter the inner tube, and reverse course to proceed in the co-current to the helium. The inner tube did not contain catalyst, and instead served strictly to provide additional heat to the catalyst zone and increase the total amount of heat transfer and thereby the methane conversion.

The original design concept used a "direct cycle" in which the helium coolant leaving the nuclear reactor directly entered the integrated SMR/HTGR. This is desirable from an efficiency point of view because the helium could be obtained at temperatures as high as 1200 °C, leading to high methane conversions in the SMR. However, later studies by the Japan Atomic Energy Research Institute (JAERI) showed that it is necessary to consider an intermediate heat exchanger (IHX) and use indirect cycle. In an indirect cycle, high temperature helium leaving the nuclear reactor does not enter the SMR/HTGR directly but instead heats a second helium stream in the IHX before returning to the nuclear reactor. The second helium stream enters the SMR/HTGR instead, which significantly enhances that safety and reliability of the process, but with the downside that the second helium stream enters at a lower temperature, making it more difficult to achieve high methane conversion.

Both EVA I and its advanced version EVA II were built, tested, and achieved their design objectives. The results from these studies were used to inform the design of a commercial scale version called the HTR-Module, with the intent of using an HTR-Module pebble bed nuclear reactor integrated with SMR, but this has not yet been constructed to the best of our knowledge [2,7]. Later, another test facility with different design was constructed and tested by JAERI to establish a design for a larger scale integrated SMR/HTGR with 10 MW thermal output [2]. Therefore, the feasibility and satisfactory operability of the integrated SMR/HTGR system has been proven at the pilot scale.

However, many key questions must be answered before the concept can be implemented at the commercial scale. The first set of questions concerns unknowns surrounding the dynamic behaviour of the SMR/HTRG during transient conditions such as when experiencing disturbances, when starting up or shutting down the system, or when transitioning between operating modes. Understanding the dynamics of the system is critical for creating an effective control system, which is of the highest priority for nuclear-based energy systems. The second set of question concerns the unknown optimal design of the SMR/HTRG itself at commercial scale and the larger energy conversion system in which it is used. This information is critical for creating a design that is safe, reliable, and commercially viable.

Therefore, in order to answer either set of questions, a rigorous model is needed because many factors need to be considered for safety purposes, such as the avoidance of hot spots in the steel or catalysts, the non-linear effects of diffusions in complex mixtures which may have unexpected contributions during transients, and the avoidance of excessive thermal gradients during transients to avoid thermal stress on the steel tubes and shell. Due to the high temperatures involved, it is not possible to measure many of these effects directly by experiment, and therefore a sufficiently detailed model is needed. Although one prior work has examined the control system of an SMR/HTRG system [8], the study was limited to examining the controllability of the pressure difference between the shell and the tube sides and the controllability of the other balance of plant equipment not relevant to the present study. In addition, the model used for the study was not provided in the open literature, which was based on a simplified model using transfer functions identified by experiment. As such, the model does not have predictive or generalized capability to be used in other designs. Ghouse and Adams [9] presented a rigorous model of a large-scale SMR process. They developed a two-dimensional heterogeneous model that accounts for the inter- and intra-particle mass and heat transfer with detailed diffusional correlations.

Therefore, this work focuses on the development of a dynamic model for the integrated steam reforming and nuclear heat system shown in Fig. 1. In this system, hot helium from an intermediate heat exchanger flows into the shell side and transfers heat through the wall to the tube. In the tube side, process gas flows through the catalyst particles, receives heat from the hot gas in the shell, and converts to syngas. Then, hot syngas passes through an inner tube to transfer heat to the catalytic region. The model of the system is based on first principles and well-known correlations for heat and mass transfer coefficients, diffusion, and reaction kinetics. The model is an extension of the previous study by Ghouse and Adams [9] to the integrated HTGR/SMR system. The resulting model is a set of non-linear partial differential and algebraic equations which is solved using the finite difference method. The validity of the model is tested using available pilot plant data and only a few of the model parameters need to be fitted within small regions of uncertainty. The dynamic trajectories and steady state conditions of the key variables of the system are analyzed and the effects of disturbances on the system behaviour are investigated. Finally, a sensitivity analysis on the model parameters is conducted to demonstrate the impact of parameter changes on system performance.

Model development

The proposed dynamic, heterogeneous model of integrated nuclear heat and SMR is described in this section. As shown in Fig. 2, the model includes seven sub-models: (1) refractory lining of the shell, (2) gas phase in the shell side, (3) outer tube

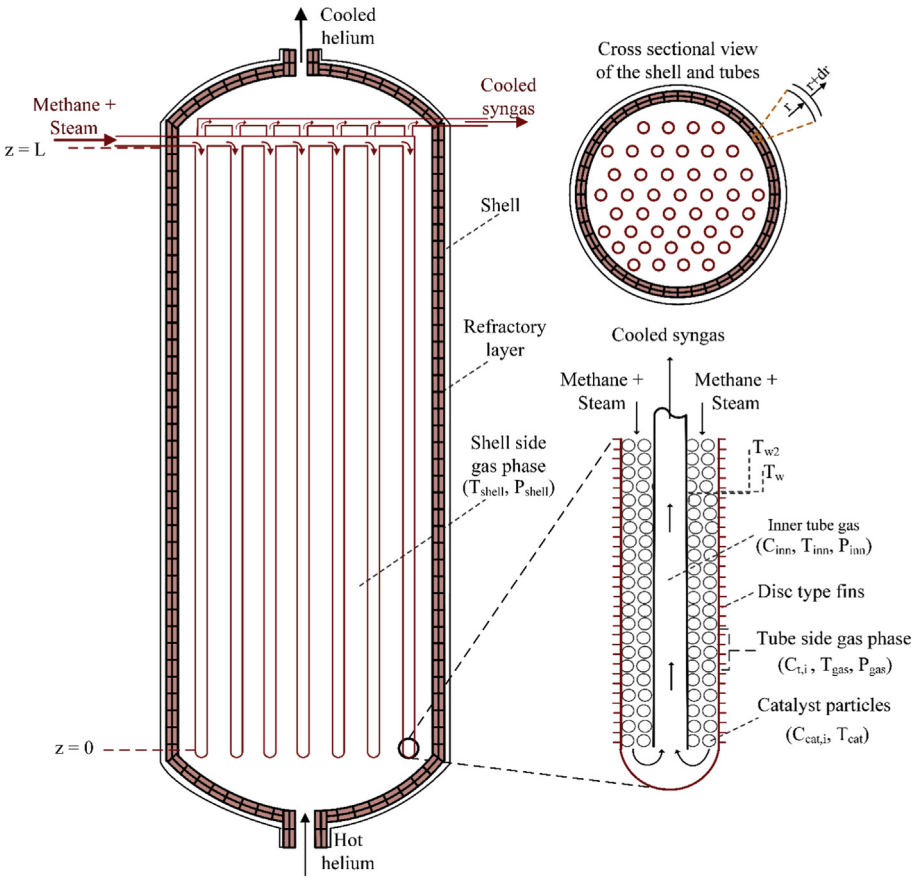

Fig. 1 – Schematic of integrated SMR/HTGR system with key variables of the model.

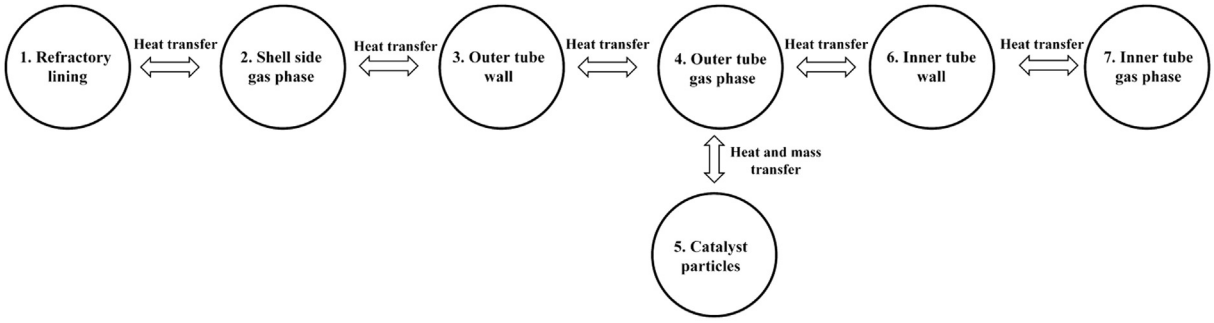

Fig. 2 – Integrated SMR/HTGR sub-models.

wall of the steam reforming tubes, (4) gas phase in the tubes, (5) catalyst particles which are packed inside the tubes, (6) inner tube wall and (7) gas phase in the inner tubes. It should be noted that the nuclear reactor has not been modelled in this work.

Refractory lining

In this model, it is assumed that the refractory layer, which is used as lining to protect the shell from high temperatures, is composed of a single material. In practice, the refractory layer may be a complex layout of several different types of refractory brick such as fireclay brick, insulating brick and a castable layer [10], but the overall system performance varies very little with the type and amount of brick. Therefore, for simplicity, this model considers a single layer consisting of the average properties of the actual refractory lining layers in the energy balance equation as follows:

$$\frac{\partial T_{rfct}}{\partial t} = \frac{K_{rfct}}{\rho_{rfct} C_{p_{rfct}}} \left(\frac{\partial^2 T_{rfct}}{\partial z^2} + \frac{\partial^2 T_{rfct}}{\partial r^2} \right) \quad (1)$$

where T_{rfct} is the refractory temperature, K_{rfct} is the refractory thermal conductivity (1.8 w/m K), ρ_{rfct} is the refractory density (2645 kg/m^3), $C_{p_{rfct}}$ is the specific heat capacity of the refractory

(960 J/kg-K) [11], and r and z stand for the radial and axial positions, respectively.

To solve Eq. (1), four boundary conditions are required. Two of the boundary conditions are zero heat flux at the top and bottom of the refractory lining, due to the relatively small cross-sectional area [9]. These boundary conditions are given as follows:

$$\frac{\partial T_{rfct}}{\partial z}|_{z=0} = \frac{\partial T_{rfct}}{\partial z}|_{z=L} = 0 \tag{2}$$

The other boundary condition is the equivalency of the conductive heat with the convective and radiative heat of the gas phase at the inner wall (R_{in}) of the refractory lining and can be represented as follows:

$$-K_{rfct}\frac{\partial T_{rfct}}{\partial r}|_{r=R_{in}} = h_{shell,rfct}\left(T_{shell} - T_{rfct}|_{r=R_{in}}\right) + \sigma\varepsilon_{shell}\varepsilon_{rfct}\left(T_{shell}^4 - T_{rfct}^4|_{r=R_{in}}\right) \tag{3}$$

where $h_{shell,rfct}$ is the convective heat transfer coefficient from the shell gas to the refractory lining inner wall given in the next section and T_{shell} is the shell gas phase temperature. σ is the Stefan-Boltzmann constant $\left(5.67\times10^{-8}\frac{W}{m^2\ K^4}\right)$, ε_{shell} and ε_{rfct} are the emissivity of the gas phase and refractory, respectively. ε_{rfct} is commonly assumed to be constant in the literature, however it changes significantly as the temperature changes. Ghouse et al. [12] proposed a correlation for ε_{rfct} which is given as follows:

$$\varepsilon_{rfct} = -10^{-7}T_{rfct}^2 + 8\times10^{-5}T_{rfct} + 0.8935 \tag{4}$$

The last boundary condition denotes that the conductive heat transfer at the outer surface of the refractory is equal to the convective heat transfer at this surface. This boundary condition is given as follows:

$$-K_{rfct}\frac{\partial T_{rfct}}{\partial r}|_{r=R_o} = h_{rfct,amb}\left(T_{rfct|r=R_o} - T_{amb}\right) \tag{5}$$

where $h_{rfct,amb}$ is the convective heat transfer between the refractory outer surface and the ambient and T_{amb} is the ambient temperature.

Shell gas phase

This sub-model contains mass and energy balances of the helium gas flows in the shell side. The pressure drop in the shell is small (as 1 bar) and assumed to be constant [12]. The mass balance equation is given as follows:

$$\frac{\partial \rho_{shell}}{\partial t} = -\frac{\partial(\rho_{shell}v_{shell})}{\partial z} \tag{6}$$

where ρ_{shell} is the molar density and v_{shell} is the velocity of helium gas in the shell. The boundary condition of this equation is $\rho_{shell}(t, z=0) = \rho_{shell-inlet}$.

The energy balance equation of the shell gas phase is presented as follows:

$$\frac{\partial(\rho_{shell}H_{shell})}{\partial t} = -\frac{\partial(\rho_{shell}v_{shell}H_{shell})}{\partial z} - N_{tube}\left(q_{tube_{rad}} + q_{tube_{conv}}\right) - \left(q_{rfct_{rad}} + q_{rfct_{conv}}\right) \tag{7}$$

where H_{shell} is the helium gas molar enthalpy, N_{tube} is the number of tubes inside the shell, $q_{tube_{rad}}$ and $q_{rfct_{rad}}$ are the radiative heat duties per volume of the gas transferred from the helium gas to each tube wall and refractory lining, respectively and $q_{tube_{conv}}$ and $q_{rfct_{conv}}$ are the convective heat transferred from gas to the each tube wall and refractory lining, respectively. The enthalpy of helium gas in the shell is defined as follows:

$$H_{shell} = \Delta H_f + \int_{T_{ref}}^{T_{shell}} C_{p_{shell}}dT \tag{8}$$

where ΔH_f is the heat of formation (which is equal to zero for helium at the reference temperature $T_{ref} = 298.15$ K) and $C_{p_{shell}}$. is the specific heat capacity, which is essentially constant for helium gas in the temperature range of interest [13].

The other terms of Eq. (7) are given as follows:

$$q_{tube_{rad}} = \frac{\sigma\varepsilon_{shell}\varepsilon_{tube}(\pi D_{t,o})\left(T_{shell}^4 - T_w^4|_{r=R_{t,o}}\right)}{A_{shell}} \tag{9}$$

$$q_{tube_{conv}} = \frac{h_{shell,w}(\pi D_{t,o})\left(T_{shell} - T_w|_{r=R_{t,o}}\right)}{A_{shell}} \tag{10}$$

$$q_{rfct_{rad}} = \frac{\sigma\varepsilon_{shell}\varepsilon_{rfct}(\pi D_{in})\left(T_{shell}^4 - T_{rfct}^4|_{r=R_o}\right)}{A_{shell}} \tag{11}$$

$$q_{rfct_{conv}} = \frac{h_{shell,rfct}(\pi D_{in})\left(T_{shell} - T_{rfct}|_{r=R_o}\right)}{A_{shell}} \tag{12}$$

where ε_{tube} is the tube emissivity, $h_{shell,w}$ is the convective heat transfer coefficient from gas to the tubes, $D_{t,o}$ is the tube outer diameter, T_w is the tube wall temperature and A_{shell} is the cross-sectional area of the shell. The convective heat transfer coefficient between the shell gas phase and tube walls ($h_{shell,w}$) is given by the correlation provided by Geankopolis [1] as follows:

$$h_{shell,w} = \frac{K_{shell}}{D_{t,o}}\left(0.163\ Re_{tube}Pr_{shell}^{1/3}\right) \tag{13}$$

where $Re_{tube} = \frac{D_{t,o}v_{shell}\rho_{mass}}{\mu_{shell}}$ is the Reynolds number over the tubes, ρ_{mass} is the mass density, μ_{shell} is the dynamic viscosity of the gas, $Pr_{shell} = \frac{C_{p_{shell}}\mu_{shell}}{K_{shell}}$ is the Prandtl number of the gas and K_{shell} is the conductive heat transfer coefficient of the shell gas.

In addition, the convective heat transfer coefficient between the shell gas phase and the refractory lining ($h_{shell,rfct}$) is given by Gneilinski as follows [10]:

$$h_{shell,rfct} = \frac{\frac{ff}{8}(Re_{rfct} - 1000)Pr_{shell}}{1 + 12.7\left(\frac{ff}{8}\right)^{\frac{1}{2}}\left(Pr_{shell}^{\frac{2}{3}} - 1\right)} \tag{14}$$

where $ff = 0.316Re_{rfct}^{-1/4}$ is the friction factor [10] and $Re_{rfct} = \frac{D_o v_{shell}\rho_{mass}}{\mu_{shell}}$ is the Reynolds number of the shell gas. The boundary condition of Eq. (7) is. $T_{shell}(t, z=0) = T_{shell-inlet}$.

Tube wall

Tube wall temperature variations are considered in radial and axial axis as follows:

$$\frac{\partial T_w}{\partial t} = \frac{K_w}{\rho_w C_{p_w}}\left(\frac{\partial^2 T_w}{\partial z^2} + \frac{\partial^2 T_w}{\partial r^2}\right) \tag{15}$$

where K_w is the wall thermal conductivity (25.5 w/m K), ρ_w is the wall density (7940 kg/m^3) and C_{p_w} is the specific heat capacity of the wall (500 J/kg K) [14]. The tube material is Incoloy 800H and the average properties are used in Eq. (15).

To solve Eq. (15), again four boundary conditions are required. One of the boundary conditions states that convective and radiative heat in the outer layer (R_{to}) of the tube is equal to the conductive heat transferred at that layer. This boundary condition is given as follows:

$$K_w \frac{\partial T_w}{\partial r}|_{r=R_{to}} = h_{shell,w}\left(T_{shell} - T_w|_{r=R_{to}}\right) + \sigma\varepsilon_{shell}\varepsilon_w\left(T_{shell}^4 - T_w^4|_{r=R_{to}}\right) \tag{16}$$

where $h_{shell,w}$ is the convective heat transfer coefficient between the shell gas and tube outer layer, and ε_w is the emissivity of the tube wall.

In the inner layer of the tube wall, temperature is lower and radiative heat can be neglected, thus the boundary condition at this layer (R_{ti}) can be written as:

$$K_w \frac{\partial T_w}{\partial r}|_{r=R_{ti}} = h_w\left(T_w|_{r=R_{ti}} - T_{gas}\right) \tag{17}$$

where h_w is the convective heat transfer between the tube inner wall and the gas in the tube and given by Eq. (31) in Section Tube gas phase.

At the top and bottom of the tube wall, heat flux can be assumed to be zero since the cross sectional area is small. Thus, the boundary conditions can be stated as follows:

$$\frac{\partial T_w}{\partial z}|_{z=0} = \frac{\partial T_w}{\partial z}|_{z=L} = 0 \tag{18}$$

Tube gas phase

In the tube side, steam and natural gas are mixed and converted to the syngas on the catalyst surface based on the following reactions [15]:

$$CH_4 + H_2O \rightleftharpoons CO + 3H_2 \left(\Delta H_{r,T_{ref}} = 206.2\frac{kJ}{mol}\right) \tag{19}$$

$$CO + H_2O \rightleftharpoons CO_2 + H_2 \left(\Delta H_{r,T_{ref}} = -41.2\frac{kJ}{mol}\right) \tag{20}$$

$$CH_4 + 2H_2O \rightleftharpoons CO_2 + 4H_2 \left(\Delta H_{r,T_{ref}} = 165\frac{kJ}{mol}\right) \tag{21}$$

These reactions are highly endothermic and the required heat is provided by hot helium in the shell side. Conversion of these reactions are limited by equilibrium [9].

Key assumptions of the tube gas phase model are: ideal gas law is used for approximations [16], radial variations in the reformer tubes are negligible [17,18], the conditions of one tube represent the other tubes as well, a pre-reformer converts C_2^+ hydrocarbons into methane, hydrogen or carbon monoxide, so heavier-than-methane hydrocarbons are neglected in this model, and the steam/carbon ratio is high enough such that carbon deposition will not happen in the reformer [19].

The mass balance equation of gas phase in the tube is given as follows:

$$\frac{\partial C_{gas,i}}{\partial t} = \frac{\partial\left(C_{gas,i} v_{gas}\right)}{\partial z} - \kappa_{gas,i}\left(C_{gas,i} - C_{cat,i}|_{r=R_p}\right)\left(\frac{a_v}{\varepsilon}\right), \quad i = CH_4, H_2O, CO, H_2, CO_2, N_2 \tag{22}$$

where $C_{gas,i}$ is the concentration (mol/m^3) of each component in the gas phase, v_{gas} is the interstitial velocity of the gas, $\kappa_{gas,i}$ is the mass transfer coefficient of the component i (given in Eq. (24)), $C_{cat,i}|_{r=R_p}$ is the molar concentration of the component i on the catalyst surface, $a_v = 6(1-\varepsilon)/D_p$ is the catalyst particle surface area, ε is the bed porosity and D_p is the particle diameter. The interstitial velocity of the gas is approximated by Ref. [16]:

$$v_{gas} = \frac{F_{gas}}{A_{tube}\varepsilon}\frac{RT_{gas}}{P_{gas}} \tag{23}$$

where F_{gas} is the total inlet molar flow rate, T_{gas} is the gas phase temperature, P_{gas} is the pressure of gas, $A_{tube} = \frac{\pi}{4}(D_{ti}^2 - D_{t2,o}^2)$ is the cross sectional area of the tube and $D_{t2,o}$ is the inner tube outer diameter. Furthermore, mass transfer coefficient $\kappa_{gas,i}$ is given by Ref. [20]:

$$\kappa_{gas,i} = \frac{v_{gas_s}}{\varepsilon} Sc_{gas,i}^{-2/3}\left(\frac{0.765}{Re_{gas}^{0.82}} + \frac{0.365}{Re_{gas}^{0.386}}\right) \tag{24}$$

where $Sc_{gas,i} = \mu_{gas}/\rho_{gas}D_{i,mix}$ is Schmidt number, $Re_{gas} = D_p\rho_{gas}v_s/\mu_{gas}$ is Reynolds number, $v_{gas_s} = v_{gas}\varepsilon$ is the superficial velocity, ρ_{gas} is the mass density of process gas, and μ_{gas} is the dynamic viscosity of the gas mixture and $D_{i,mix}$ is the diffusivity of the component i in the mixture.

Considering the counter-current configuration, the boundary condition for Eq. (22) is given by:

$$C_{gas,i}(t, z = L) = C_{gas,i,inlet} \tag{25}$$

The pressure drop is computed using the Ergun equation [23] as Eq. (26). Due to numerical stiffness, the dynamic term in the momentum balance equation is not considered [9]. It should be noted that, in packed bed reactors pressure drop is mostly due to friction, therefore the dynamic term can be neglected [16].

$$\frac{\partial P_{gas}}{\partial z} = \frac{G}{\rho_{gas}D_p}\frac{1-\varepsilon}{\varepsilon^3}\left(\frac{150(1-\varepsilon)\mu_{gas}}{D_p} + 1.75G\right) \tag{26}$$

where $G = \rho_{gas}v_{gas_s}$ is the mass velocity. Furthermore, the boundary condition of Eq. (26) is given as $P_{gas}(L) = P_{inlet}$.

In this study, the temperature in the tube side is low enough such radiative heat can be neglected. Therefore, the energy balance is written as:

$$\frac{\partial\left(\rho_{m,gas}H_{gas}\right)}{\partial t} = \frac{\partial\left(\rho_{m,gas}v_{gas}H_{gas}\right)}{\partial z} + q_w + q_{w_2} - q_{cat} + \sum_{i=1}^{6} q_i \tag{27}$$

where $\rho_{m,gas}$ is the molar density, H_{gas} is the enthalpy of the gas mixture. q_w is the convective heat transferred from the tube wall to the gas phase (per unit volume of the gas phase), q_{w_2} is the convective heat transferred from the inner tube wall to the gas phase, q_{cat} is the convective heat transferred from the gas phase to the catalyst particles and q_i is the energy of component i carried from the catalyst phase to the tube gas phase or

vice-versa in the form of enthalpy of the mass being transferred. The enthalpy and convective heat transfer terms are given as:

$$H_{gas} = \sum_{i=1}^{6} y_i H_{i,gas} \tag{28}$$

$$H_{i,gas} = \Delta H_{i,f} + \int_{T_{ref}}^{T_{gas}} C_{p,i} dT, i = CH_4, H_2O, CO, H_2, CO_2, N_2 \tag{29}$$

where y_i is the mole fraction, $\Delta H_{i,f}$ is the formation enthalpy in the vapour state and $C_{p,i}$ is the specific heat capacity of component i in the gas phase.

$$q_w = \frac{h_w(\pi D_{ti})\left(T_w|_{r=R_{ti}} - T_{gas}\right)}{A_{tube}\varepsilon} \tag{30}$$

where h_w is the convective heat transfer coefficient between the process gas and inner layer of the tube and D_{ti} is the inner diameter of the tube. h_w is calculated as follows [24]:

$$h_w = 0.4\frac{K_g}{D_p}\left(2.58Re_{gas}^{\frac{1}{3}}Pr_{gas}^{\frac{1}{3}} + 0.094\,Re_{gas}^{0.8}Pr_{gas}^{0.4}\right) \tag{31}$$

where K_g is the thermal conductivity of the gas mixture, $Pr_{gas} = C_{p,mix}\mu_{gas}/K_{gas}$ is the Prandtl number and $C_{p,mix}$ is the specific heat capacity of the gas mixture.

$$q_{w_2} = \frac{h_{w_2}(\pi D_{t2,o})\left(T_{w_2}|_{r=R_{t2,o}} - T_{gas}\right)}{A_{tube}\varepsilon} \tag{32}$$

where h_{w_2} is the convective heat transfer coefficient between the process gas and outer layer of the inner tube, $D_{t2,o}$ is the outer diameter of the inner tube and T_{w2} is the inner tube wall temperature.

Convective heat transfer from the gas to the catalyst is defined as follows:

$$q_{cat} = \frac{h_{cat}a_v\left(T_{gas} - T_{cat}|_{r=R_p}\right)}{\varepsilon} \tag{33}$$

where h_{cat} is the convective heat transfer coefficient between the gas phase and catalyst particles and T_{cat} is the catalyst temperature [25]. h_{cat} is defined as follows:

$$h_{cat} = \frac{1.37C_{p,mix}G}{\varepsilon}\left(\frac{0.765}{Re_{gas}^{0.82}} + \frac{0.365}{Re_{gas}^{0.386}}\right)Pr_{gas}^{-2/3} \tag{34}$$

q_i is computed based on the species concentration difference between the bulk gas and catalyst surface as follows [9]:

$$\text{if } C_{gas,i} \geq C_{cat,i}|_{r=R_p} \rightarrow q_i = -\frac{H_{i,gas}\kappa_{gas,i}\left(C_{gas,i} - C_{cat,i}|_{r=R_p}\right)a_v}{\varepsilon} \tag{35}$$

$$\text{if } C_{gas,i} < C_{cat,i}|_{r=R_p} \rightarrow q_i = -\frac{H_{i,cat}\kappa_{gas,i}\left(C_{gas,i} - C_{cat,i}|_{r=R_p}\right)a_v}{\varepsilon} \tag{36}$$

where $H_{i,gas}$ is the component i enthalpy at T_{gas} as given in Eq. (29) and $H_{i,cat}$ is the enthalpy of component i at T_{cat}.

The boundary condition of Eq. (27) is given by:

$$T_{gas}(t, z = L) = T_{gas,inlet} \tag{37}$$

Catalyst particles

The mass balance equation in the catalyst phase is given as follows:

$$\theta_{cat}\frac{\partial C_{cat,i}}{\partial t} = \frac{2}{r}D_{ei,mix}\frac{\partial C_{cat,i}}{\partial r} + \frac{\partial}{\partial r}\left(D_{ei,mix}\frac{\partial C_{cat,i}}{\partial r}\right) + r_i\rho_{cat}, \quad i = CH_4, H_2O, CO, H_2, CO_2, N_2 \tag{38}$$

It is assumed that particles are a homogenous mixture of solid catalyst and gas in the catalyst pores, where θ_{cat} (void fraction of catalyst particles) represents the pores' volumetric fraction in the catalyst. In Eq. (38) r_i is the rate of reaction of component i, ρ_{cat} is the catalyst density and $D_{ei,mix}$ is the effective diffusivity of species i. The definition of $D_{ei,mix}$ can be found in the prior study [9]. The boundary conditions of this equation are as follows:

$$\frac{\partial C_{cat,i}}{\partial r}|_{r=0} = 0 \tag{39}$$

$$D_{ei,mix}\frac{\partial C_{cat,i}}{\partial r}|_{r=R_p} = \kappa_{gas,i}\left(C_{gas,i} - C_{cat,i}|_{r=R_p}\right) \tag{40}$$

The energy balance equation for the catalyst particles can be written as follows:

$$\left[(1-\theta_{cat})\rho_{cat}C_{p_{cat}} + \theta_{cat}\sum_{i=1}^{6}C_{cat,i}C_{p_{cat,i}}\right]\frac{\partial T_{cat}}{\partial t} = K_{cat}\frac{1}{r^2}\frac{\partial}{\partial r}\left(r^2\frac{\partial T_{cat}}{\partial r}\right) + \sum_{i=1}^{6}C_{p_{cat,i}}D_{ei,mix}\frac{\partial C_{cat,i}}{\partial r}\frac{\partial T_{cat}}{\partial r} + \rho_{cat}\sum_{i=1}^{6}r_iH_{i,cat} \tag{41}$$

where $C_{p_{cat}}$ is the specific heat capacity of the catalyst particle, K_{cat} is the thermal conductivity of the catalyst particle and $C_{p_{cat,i}}$ is the specific heat capacity of component i in the catalyst phase. The boundary conditions of catalyst particles are given as follows:

$$\frac{\partial T_{cat}}{\partial r}|_{r=0} = 0 \tag{42}$$

$$\left[K_{cat}\frac{\partial T_{cat}}{\partial r} + \sum_{i=1}^{6}D_{ei,mix}H_{i,cat}\frac{\partial C_{cat,i}}{\partial r}\right]_{r=R_p} = h_{cat}\left(T_{gas} - T_{cat}|_{r=R_p}\right) - \frac{\varepsilon}{a_v}\sum_{i=6}^{6}Q_i \tag{43}$$

Steam reforming kinetics

The steam reforming reaction kinetics equation are presented by Xu and Froment [26] for the Ni-alumina catalyst. These kinetics have been widely accepted and cited for the steam reforming reaction. The reaction rates for Eqs. (19)–(21) are given by Eqs. (44)–(46), respectively.

$$r_1 = \frac{k_1}{p_{H_2}^{2.5}\,DEN^2}\left[p_{CH_4}\,p_{H_2O} - \frac{p_{H_2}^3 p_{CO}}{K_1}\right] \tag{44}$$

$$r_2 = \frac{k_2}{p_{H_2}\,DEN^2}\left[p_{CO}\,p_{H_2O} - \frac{p_{H_2}p_{CO_2}}{K_2}\right] \tag{45}$$

$$r_3 = \frac{k_3}{p_{H_2}^{3.5}\,DEN^2}\left[p_{CH_4}\,p_{H_2O}^2 - \frac{p_{H_2}^4 p_{CO_2}}{K_3}\right] \tag{46}$$

$$DEN = 1 + K_{CO}p_{CO} + K_{H_2}p_{H_2} + K_{CH_4}p_{CH_4} + \frac{K_{H_2O}p_{H_2O}}{p_{H_2}} \tag{47}$$

where $p_i = C_{cat,i}RT_{cat}$ is the partial pressure of the corresponding species according to the ideal gas assumption. k_1, k_2 and k_3 are the reaction coefficients and defined by:

$$k_1 = 9.49 \times 10^{16}\exp\left(-\frac{28879}{T_{cat}}\right), kmol\frac{kPa^{0.5}}{kg\,h} \tag{48}$$

$$k_2 = 4.39 \times 10^{4}\exp\left(-\frac{8074.3}{T_{cat}}\right), \frac{kmol}{kPa\,kg\,h} \tag{49}$$

$$k_3 = 2.29 \times 10^{16}\exp\left(-\frac{29336}{T_{cat}}\right), kmol\frac{kPa^{0.5}}{kg\,h} \tag{50}$$

The equilibrium constants are defined as:

$$K_1 = 10266.76\exp\left(-\frac{26830}{T_{cat}} + 30.11\right), kPa^2 \tag{51}$$

$$K_2 = \exp\left(\frac{4400}{T_{cat}} - 4.063\right) \tag{52}$$

$$K_3 = K_1K_2 \tag{53}$$

The adsorption constants in the *DEN* expression are defined by:

$$K_{CH_4} = 6.65 \times 10^{-6}\exp\left(\frac{4604.28}{T_{cat}}\right), kPa^{-1} \tag{54}$$

$$K_{H_2O} = 1.77 \times 10^{3}\exp\left(-\frac{10666.35}{T_{cat}}\right) \tag{55}$$

$$K_{H_2} = 6.12 \times 10^{-11}\exp\left(\frac{9971.13}{T_{cat}}\right), kPa^{-1} \tag{56}$$

$$K_{CO} = 8.23 \times 10^{-7}\exp\left(\frac{8497.71}{T_{cat}}\right), kPa^{-1} \tag{57}$$

Based on Eqs. (19)–(21), reaction rates of the components can be written as:

$$r_{CH_4} = -(r_1 + r_3) \tag{58}$$

$$r_{H_2O} = -(r_1 + r_2 + 2r_3) \tag{59}$$

$$r_{CO} = r_1 - r_2 \tag{60}$$

$$r_{H_2} = 3r_1 + r_2 + 4r_3 \tag{61}$$

$$r_{CO_2} = r_2 + r_3 \tag{62}$$

$$r_{N_2} = 0 \tag{63}$$

More details on the tube model can be found in the prior work [9].

Inner tube wall

Similar to the tube model, the inner tube wall temperature variations are considered in radial and axial dimensions as follows:

$$\frac{\partial T_{w2}}{\partial t} = \frac{K_{w2}}{\rho_{w2}C_{p_{w2}}}\left(\frac{\partial^2 T_{w2}}{\partial z^2} + \frac{\partial^2 T_{w2}}{\partial r^2}\right) \tag{64}$$

where K_{w2} is the wall thermal conductivity (28.5 w/m K), ρ_{w2} is the wall density (7880 kg/m^3) and $C_{p_{w2}}$ is the specific heat capacity of the wall (741 J/kg K) [27]. It should be noted that, the inner tube material is austenitic cast steel made up of alloy IN 519.

The boundary conditions of the inner tube wall are given as follows:

$$K_{w2}\frac{\partial T_{w2}}{\partial r}|_{r=R_{t2,o}} = h_{w2}\left(T_{w2}|_{r=R_{t2,o}} - T_{gas}\right) \tag{65}$$

The boundary condition at the inner layer of the inner tube ($R_{t2,i}$) are:

$$K_{w2}\frac{\partial T_{w2}}{\partial r}|_{r=R_{t2,i}} = h_{inn}\left(T_{w2}|_{r=R_{t2,i}} - T_{inn}\right) \tag{66}$$

where h_{inn} is the convective heat transfer between the inner tube inner wall and the syngas.

At the top and bottom of the inner tube wall, heat flux can be assumed to be zero since the cross sectional area is small. Thus, the boundary conditions can be stated as follows:

$$\frac{\partial T_{w2}}{\partial z}|_{z=0} = \frac{\partial T_{w2}}{\partial z}|_{z=L} = 0 \tag{67}$$

Inner tube gas phase

As shown in Fig. 1, an inner tube is embedded inside the SMR tubes to recover heat from the hot syngas produced in the tube side. It has been shown that this helps increasing the heat transfer efficacy and methane conversion as well [2].

It should be noted that there is no reaction in the inner tube. Therefore, the mass balance equation can be written as:

$$\frac{\partial C_{inn,i}}{\partial t} = -\frac{\partial\left(C_{inn,i}v_{inn}\right)}{\partial z} \tag{68}$$

where $C_{inn,i}$ is the concentration of the component i the syngas and v_{inn} is the velocity of the gas in the inner tube and computed as follows:

$$v_{inn} = \frac{F_{gas}(0,t)}{A_{inn}}\frac{RT_{inn}}{P_{inn}} \tag{69}$$

where $F_{gas}(0,t)$ is the exit molar flow rate of the tube, T_{inn} is the syngas temperature, P_{inn} is the pressure of the syngas in the inner tube and A_{inn} is the cross-sectional area of the inner tube.

The initial and boundary conditions of this equation are $C_{inn,i}(t, z = 0) = C_{gas,i}(0,t)$. This means that the concentration of the components at the inlet of the inner tube is the same as the tube outlet concentration.

The energy balance equation of the inner tube gas phase is given by:

$$\frac{\partial(\rho_{inn}H_{inn})}{\partial t} = -\frac{\partial(\rho_{inn}v_{inn}H_{inn})}{\partial z} - \frac{1}{A_{inn}}Q_{inn} \quad (70)$$

where $\rho_{inn} = \sum_{i=1}^{6} C_{inn,i}$ is the molar density of the syngas in the inner tube, H_{inn} is the enthalpy of the syngas and Q_{inn} is the convective heat transferred from the syngas to the inner tube wall.

The enthalpy of the syngas in the inner tube, H_{inn} is defined as:

$$H_{inn} = \sum_{i=1}^{6} y_{inn,i}H_{inn,i} \quad (71)$$

where $y_{inn,i}$ is the mole fraction of the component i in the gas phase and $H_{inn,i}$ is the enthalpy of the component i in the gas phase and defined in the same way as Eq. (29) at T_{inn} temperature.

Convective heat transferred from the gas to the inner tube wall, Q_{inn} is given by:

$$Q_{inn} = h_{inn}(\pi D_{t2,i})\left(T_{inn} - T_{w2}|_{r=R_{t2,i}}\right) \quad (72)$$

where h_{inn} is the convective heat transfer between the inner tube gas phase and the inner tube inner wall and given by Dittus-Boelter equation [10] as follows:

$$h_{inn} = \frac{K_{inn}}{D_{t2,i}}(0.0265\ Re_{inn}^{0.8}Pr_{inn}^{0.3}) \quad (73)$$

where K_{inn} is the thermal conductivity of the syngas (which is a function of temperature), Re_{inn} is the Reynolds number of the gas and Pr_{inn} is the Prandtl number of the syngas in inner tube.

The boundary condition for the energy balance equation is $T_{inn}(z = 0, t) = T_{gas}(0, t)$.

Similar to the shell gas phase, the pressure drop in the inner tube is small and fixed at 1 bar.

The model developed in Section Model development is a set of partial differential and algebraic equations (PDAE) implemented in the gPROMS software package [28] which is an equation-oriented modeling and simulation environment. This software uses finite difference methods (FDM) to discretize the PDEs in space. The selection and spacing of the grid points was chosen on a case-by-case basis based on error measurements and are described in later sections.

Model validation and parameter estimation

A survey of the literature shows that several integrated SMR/nuclear heat plants have been designed and tested for hydrogen production. As mentioned earlier, most of these studies were performed by Research Center Julich, SIEMENS-INTERATOM research groups in Germany [6,7] or by JAERI [2,3,29]. The designs developed in Germany usually use a helical or other complex geometry for the inner tubes, and thus cannot be used for validation without making significant modifications to the proposed model. However, the JAERI design uses a straight inner tube design which can be used to validate the presented model with very few modifications.

The JAERI design uses a high temperature test reactor (HTTR) to produce hydrogen from natural gas via the SMR reaction using the heat from a nuclear reactor. The safety and feasibility of the HTTR plant has been investigated by JAERI using a smaller scale test facility called the "mock-up". The mock-up reactor is 1/30th of the size of the HTTR. Table 1 shows the key design specification of the HTTR and the mock-up reactors. As shown in the table, the mock-up reactor includes only one SMR tube inside the shell. It should be noted that, in both designs, an intermediate heat exchanger has been used between the nuclear reactor and the SMR system for safety and operability reasons [2], with helium gas chosen as the heat transfer medium in both cases. However, the temperature of the helium in the secondary cycle is lower than the primary helium cycle.

In the HTTR design, the temperature in the shell side is significantly lower than in conventional fossil-based SMR plants, such that radiative heat transfer is small, and the heat flux is lower as a result. To compensate for this, the HTTR uses disc-type fins around the outer surface of the tubes to increase the convective heat transfer coefficient and area. As a result, the heat transfer coefficient increases by 2.7 times and the heat transfer area increases by 2.3 times [3]. Therefore, in order to account for the effect of the fins in our model, values of the corresponding heat transfer coefficient and heat transfer area were scaled up by a factor of 2.7 and 2.3, respectively.

The key design parameters of the mock-up and HTTR pilots such as number of the tubes, tube diameter, thickness, length and material, shell diameter, inner tube diameter, thickness and material, catalyst particle size, etc., are necessary for model validation. Table 2 shows the values of these parameters wherever they are given, however as shown in the table some of these parameters have not been reported in the literature. Therefore, these missing parameters had to be estimated in order to validate the model.

The missing model parameters were estimated and their values are given in Table 3. The parameters were estimated such that the outlet temperature of the helium gas, the outlet temperature of the syngas, and the rate of hydrogen production meet the design specifications given in Table 1. Note, however, that for all of these missing parameters, the range of

Table 1 – Design specification for the High Temperature Test Reactor (HTTR) integrated with SMR.

Specification	Mock-up facility	HTTR facility
Process gas conditions		
Inlet pressure	4.3 MPa	4.5 MPa
Inlet temperature	450 °C	450 °C
Natural gas feed	43.2 kg/h (2.7 kmol/h)	1296 kg/h (81 kmol/h)
Outlet temperature	600 °C	580 °C
Steam to carbon ratio (S/C)	3.5	3.5
Helium gas conditions		
Inlet pressure	4.0 MPa	4.1 MPa
Inlet temperature	880 °C	880 °C
Feed rate	327.6 kg/h	8748 kg/h
Outlet temperature	650 °C	585 °C
Hydrogen product	120 Nm^3/h	4200 Nm^3/h

Taken from Ref. [29].

Table 2 – Key design parameters of the HTTR and out of pile facilities [3].

Parameter	Mock-up	HTTR
Number of tubes	1	30
Catalyst type	Ni-Alumina	Ni-Alumina
Tube material	Incoloy 800 H	Incoloy 800 H
Tube length	6.54 (m)	6.54 (m)
Tube thickness	1 cm	1 cm
Tube inner diameter	12.8 cm	12.8 cm
Inner tube thickness	–	–
Inner tube inner diameter	–	–
Catalyst particle diameter	–	–
Refractory inner diameter	16.2 cm	–
Inner tube material	–	–

Table 3 – Estimated parameters.

Parameter	Mock-up	HTTR
Inner tube thickness	0.165 cm	0.165 cm
Inner tube inner diameter	5.72 cm	5.72 cm
Catalyst particle diameter	1.2 cm	1.2 cm
Refractory inner diameter	–	0.86 m
Inner tube material	Alloy IN 519	Alloy IN 519

practical values the parameters can take is actually rather small, and do not actually have a strong influence on the reactor exit conditions. For example, the possible choices for the inner tube diameter and thickness are selected from a small subset of Japanese industrial standard sizes for alloy IN 519 pipes at relevant temperatures and pressures [30]. The diameter of the inner and outer tubes are likewise constrained to a small range of acceptable values based on geometrical limitations and reasonable spacing requirements. The average catalyst particle diameter is perhaps the most influential parameter, but again, it is limited to a very small range of possibilities given the tight spaces available. Because the parameter estimates are limited to small ranges, the estimation was carried out "by hand" via a guess-and-check approach. There were no other model parameters that needed to be estimated.

The results of the model fitting via parameters estimation are shown in Figs. 3 and 4. Fig. 3 indicates the model prediction of the mock-up design. The model predicts that cooled helium exits the shell at 908 K, which compares well to the actual design criteria of 923 K. On the tube side, syngas leaves the inner tube at 883 K, where the design data is 873 K. Also, the model predicts the amount of hydrogen produced to be 127 Nm^3/h, where the given design data is 120 Nm^3/h. Fig. 4 shows the model prediction performance of the HTTR design; in this case, model predicts the shell outlet temperature as 869 K compared to the pilot of 853 K, and the syngas outlet temperature as 873 K, compared to the design data of 858 K. The model prediction of the hydrogen production rate is 4221 Nm^3/h and the HTTR design data for this variable is 4200 Nm^3/h. These results depict that model can predict the mock-up and HTTR plants' behaviour with high accuracy. The maximum error of the temperature prediction is 1.7% and the maximum error of the hydrogen rate production is 5.8%.

Considering the limitations in the validation of the proposed model, the results indicate that the model parameters were estimated properly and can be used to analyze and design the integrated SMR/nuclear heat systems.

Furthermore, choosing the number of nodes to solve the PDAE is a trade-off between the computational load and accuracy of the results. The finite differences method by its nature introduces error into the estimation of derivatives such that it does not conserve energy or mass. Therefore, the accuracy of the results is tested based on mass and energy conservations errors within the system boundaries. These errors are defined as follows:

$$\Delta e_{m1} = \Delta m_{shell} \tag{75}$$

$$\Delta e_{m2} = m_{tube} - m_{inn} \tag{76}$$

$$\Delta e_{E} = \Delta E_{shell} - (\Delta E_{t} + \Delta E_{r} - \Delta E_{inn}) \tag{77}$$

where Δe_{m1} is the overall mass balance error in the shell side and Δm_{shell} is the mass flow rate difference between the shell inlet and exit. Δe_{m2} is the mass balance error in the tube and

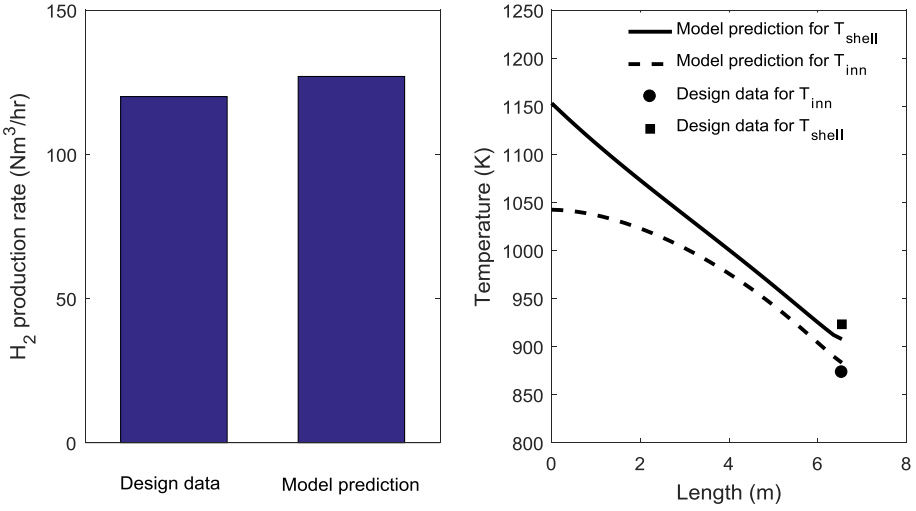

Fig. 3 – Model fitting using mock-up facility data.

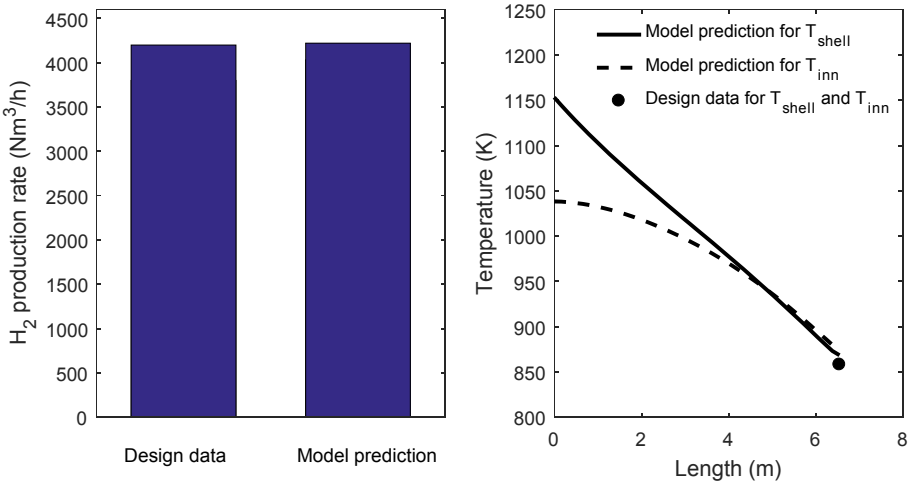

Fig. 4 – Model fitting using HTTR facility data.

inner tube side, m_{tube} and m_{inn} are the masses in the inlet of the outer tube and outlet of the inner tube, respectively. Δe_E is the global energy balance error, ΔE_{shell}, ΔE_t, ΔE_r and ΔE_{inn} are the energy differences between the inlet and outlet of the shell, tube, refractory and inner tube, respectively. Results show that mass balances errors are as small as 10^{-8} kg/s; however, the energy balance error changes significantly with the grid size. Table 4 shows the results of the energy balance error and CPU time at different grid sizes for the HTTR system. It can be concluded from the table that specifying axial nodes as 40, radial nodes as 60 and lateral nodes as 10 is the most efficient choice for the HTTR system considering both energy conservation error and CPU time. The error in this situation is limited to about 0.25% of the total energy transferred.

Results and discussion

Although the 10 MW scale studies were useful for validation of the model, the purpose of this work is to present and study an industrial scale design for the integrated system. On such industrial-scale design is provided by SIEMENS-INTERATOM [2] to produce hydrogen via the SMR process using nuclear heat from a HTR-Module pebble bed reactor with 60 MW thermal power. The key differences between this design and HTTR facility is higher inlet temperatures and pressure of helium in the HTR-Module design. This is due to using the direct helium cycle in the HTR-Module design. In addition, the helical inner tube design in the HTR-Module rather than the straight one in the HTTR is the other key difference of these two facilities. The design specification for this system is given in Table 5.

The design parameters are also given in Table 6. Some of the parameters such as inner tube diameter, thickness, catalyst particle size, and the refractory diameter are not reported, those parameters except refractory inner diameter are fixed at the values estimated in the previous section. It is assumed that a triangular arrangement of tubes with the C/D ratio (which is center-to-center distance of tubes/tube outer diameter) of 2 [12] is applied in this design. Therefore, the refractory inner diameter is selected based on this assumption and the correlations and guidance presented by Kern [31] on heat exchanger design.

It should be noted that in the large scale design used in this work, the inner tubes are straight with disc-type fins on the outer surface of inner tubes to increase the convective heat transfer coefficient and area.

Table 4 – Energy balance error vs grid size.

Number of nodes	Δe_E (MW)	CPU time (s)
Axial nodes = 60, Radial nodes = 50, Lateral nodes = 10	0.0105	809
Axial nodes = 50, Radial nodes = 50, Lateral nodes = 10	0.0112	635
Axial nodes = 40, Radial nodes = 50, Lateral nodes = 10	0.0113	436
Axial nodes = 40, Radial nodes = 60, Lateral nodes = 10	0.0091	463
Axial nodes = 40, Radial nodes = 40, Lateral nodes = 10	0.0121	362
Axial nodes = 40, Radial nodes = 50, Lateral nodes = 5	0.0123	394

Table 5 – Design specification for an industrial scale SMR/HTGR system [2].

Specification	Large scale design
Process gas conditions	
Inlet pressure	5.6 MPa
Inlet temperature	347 °C
Feed rate	34.8 kg/s
Steam to carbon ratio (S/C)	4
Helium gas conditions	
Inlet pressure	4.987 MPa
Inlet temperature	950 °C
Feed rate	50.3 kg/s

Table 6 – Design parameters for the SMR/HTGR used in this work.

Parameter	
Reported parameters [2]	
Number of tubes	199
Catalyst type	Ni-Alumina
Tube material	Incoloy 617
Tube length	14 (m)
Tube wall thickness	1 (cm)
Tube inner diameter	12 (cm)
Estimated parameters	
Inner tube thickness	0.165 (cm)
Inner tube inner diameter	5.72 (cm)
Catalyst particle diameter	1.2 (cm)
Refractory inner diameter	2.7 (m)
Inner tube material	Alloy IN 519

Base-case simulation results

Based on the above operating conditions and design parameters, the proposed model was used to simulate the proposed industrial design and analyze the key process variables as a function of space and time. However, because the model is complex and contains over 200,380 variables and equations, *a priori* initialization is very difficult. Therefore, a workaround was used in which an initial state was given that was fictional but consistent with the model equations, such that initialization was possible *a priori*. From that fictional initial point, the simulation was run with various changes in the inlet boundary conditions that allowed the simulation to arrive at a realistic steady state. In this case, all variables were set at time zero to be either pure nitrogen on the tube side or pure helium on the shell side at 620.15 K, with the inlet boundary conditions set to pure nitrogen in the tube side and helium in the shell side flowing in at 620.15 K. This made it possible for gPROMS to successfully initialize the simulation and permit dynamic simulation to continue. The inlet feed was maintained until steady-state was reached. Then, the inlet boundary conditions were step-changed to the feed conditions given in Table 5, and the dynamic simulation continued until new steady state conditions attained. Although this final steady state condition is meaningful, the transition getting to it is not since it began from a fictional initial state. This final steady state condition was saved and then used as the initial condition to initialize future runs of the simulation. The results are discussed next.

The steady state performance of the integrated system is shown in Fig. 5 as a function of axial variations of the shell, outer tube, and inner tube gas phase temperatures, and methane conversion in the outer tube section. It has been shown that the helium temperature in the shell drops from 1223 K in the inlet to 944 K in the shell exit, which results in 72.9 MW cooling duty. In the tube side, methane and steam mixture enter the SMR tubes at 620 K, receive heat from the shell and inner tube, convert to syngas with 73% methane conversion, then exit the tube at 1126 K. The hot syngas proceeds through the inner tube to recover its heat and exits at 864 K. Methane conversion in this system is in the range of 65%–90% which reported in the literature for SMR processes [12], but not as high as we would like. As mentioned in Section

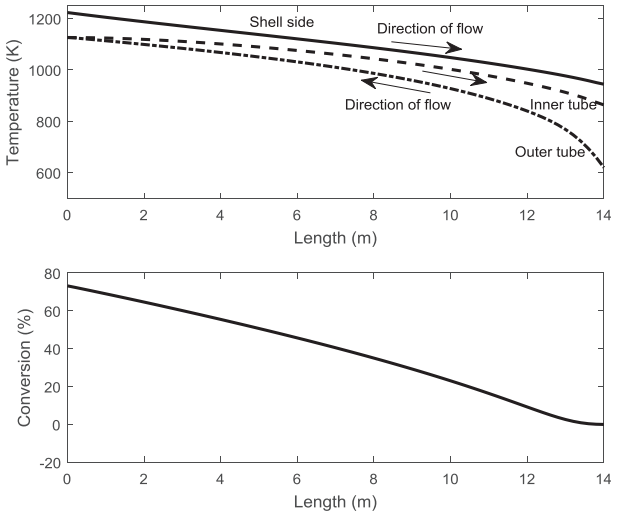

Fig. 5 – Temperature and conversion profiles at steady-state conditions.

Model validation and parameter estimation, due to the low temperature in the shell side comparing conventional SMR processes, radiative heat transfer accounts for 5.2% of the total heat transfer in the shell and this is one of the reasons for low conversion. In addition, high pressure (5.6 MPa) in the tubes causes lower conversion. In integrated SMR/HTGR systems, low pressure SMR cannot be applied since high pressure helium is required for the nuclear reactor.

Fig. 6 shows the mole fraction profiles of the CO and H_2 in the tube side at the steady state condition. The results show that in the reactor outlet, hydrogen mole fraction reaches to the 0.38 while the CO mole fraction is only 0.06. This achieves a H_2/CO ratio of 6.3 which is significantly high. This is due to the high steam to carbon ratio in the feed which is required for higher methane conversions. This process with the given operating condition in Table 5 is designed for the hydrogen production. However, if it is used for the Fischer-Tropsch applications, CO and H_2 required to be separated then mixed to obtain the proper ratio.

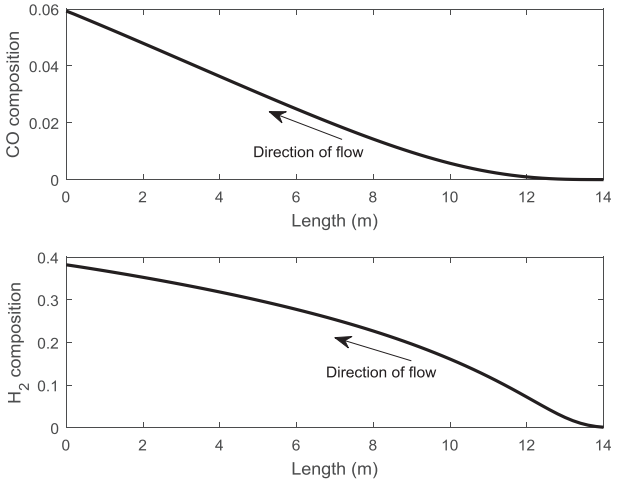

Fig. 6 – Composition profiles of CO and H_2 at steady-state condition.

Effect of disturbances

In order to demonstrate the impacts of disturbances on the system performance, common disturbances in the process gas (methane/steam mixture) and helium feeds such as changes in the feed temperature were studied.

The first disturbance investigated is a step increase of 100 K in the tube-side gas feed temperature from base-case steady state conditions. Fig. 7 shows the trajectories of the shell temperature, inner tube temperature, and methane conversion at the shell and inner tube outlets (z = 14 m). As a result of this change the shell outlet temperature reaches a new steady state of 959 K which increased 18 K from the previous steady state; inner tube gas outlet temperature also increases 29 K from the previous steady state. Furthermore, cooling duty drops from 72.9 MW to 68.3 MW. Methane conversion in the inner tube outlet increases only 1.2% points from the previous steady state. Therefore, this disturbance does not significantly affect the overall system behaviour.

The second disturbance considered in this study, is 100 K increase in the helium gas inlet temperature starting from the base case steady-state. This can happen due to an increase in the nuclear reactor temperature or feed flow rate fluctuations in the primary helium cycle. The system response to this disturbance is given in Fig. 8. As shown in the figure, methane conversion significantly increases by this change. It shows a 15 percentage-point increase in the conversion from the previous steady state condition. The shell and inner tube outlet temperatures increase remarkably, also. Shell outlet temperature increased by 45 K and inner tube outlet temperature grows by 37 K from the previous steady state. Due to the larger temperature difference between the shell and tube, the cooling duty of the system also increases by 13.5 MW (18.5%).

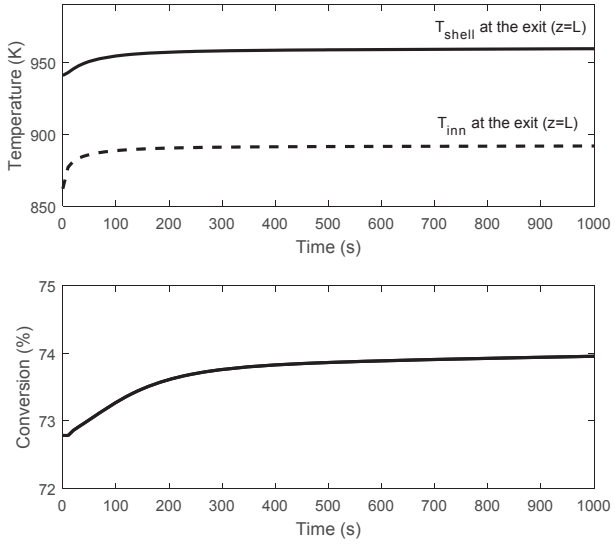

Fig. 7 – Effect of 100 K increase in the process gas feed at t = 0 (s) on the outlet temperatures of the shell and inner tube gases and methane conversion.

Sensitivity analysis

It was noted in Section Results and discussion that some of the system parameters such as catalyst particle size, inner tube diameters, and refractory inner diameter have some uncertainty since they were estimated based on reported design data combined with engineering intuition. Even though the range of feasible values for these parameters is small, it is still important to investigate the sensitivity of the system to changes in those uncertain parameters. The system performance was analyzed for 10% and 20% changes in the nominal values of the catalyst particle size, inner tube diameters and refractory inner diameter. It should be noted that, inner tube inner and outer diameters were simultaneously changed by the same magnitude due to geometric limitations.

The sensitivity of the system is best demonstrated by the shell and inner tube exit temperatures, the methane conversion, and the cooling duty of the system, as they are the most important representatives of the integrated system behaviour. Fig. 9 shows the percentage of change from the base case values by ±10% and ±20% changes in the base case values of the parameters which are given in Table 6.

This figure indicates that a ±20% change in the value of the parameters changes the outlet temperatures of the shell and tube by at most ±0.7%, meaning that they are not very sensitive to changes in the uncertain parameters. Unlike the outlet temperatures, the methane conversion and cooling duty of the system change up to ±4.9% and ±2.7%, which depicts those variables are more sensitive to changes in those parameters, even though the overall impact is still relatively small. This indicates that the model is meaningful and useful even considering these uncertain parameters.

Generally, in most of the cases, the average catalyst particle diameter is the most influential of the uncertain parameters. The methane conversion is impacted the strongest, because smaller particle diameters can be packed together more tightly, have reduced impacts of diffusion within the catalyst, and increase the pressure drop, all of which lead to either faster reaction kinetics and/or higher equilibrium constants. However, this does not imply that smaller particle diameters are necessarily better, because the negative effects of pressure loss at the system level can be significant in terms of both operational safety and balance-of-plant effects. The optimal particle diameter can only be determined at the systems level and is a subject of future study.

The same idea applies to the shell and tube diameters. While a smaller refractory inner diameter or greater tube diameter causes greater heat transfer from the helium gas (and thus increased methane conversion) when varied independently, shrinking the refractory inner diameter or increasing the tube diameter requires squeezing the tubes closer together, which quickly becomes impractical without removing some of the tubes. There is a lower bound on tube pitch ratio (C/D) of 1.25 for the triangular and square tube arrangements [32,33] to allow mechanical cleaning of the tubes, and for a clear line-of-sight between the hot helium gas (for radiative heat transfer) and the tube surface, and for adequate space for gas to flow between the tubes without

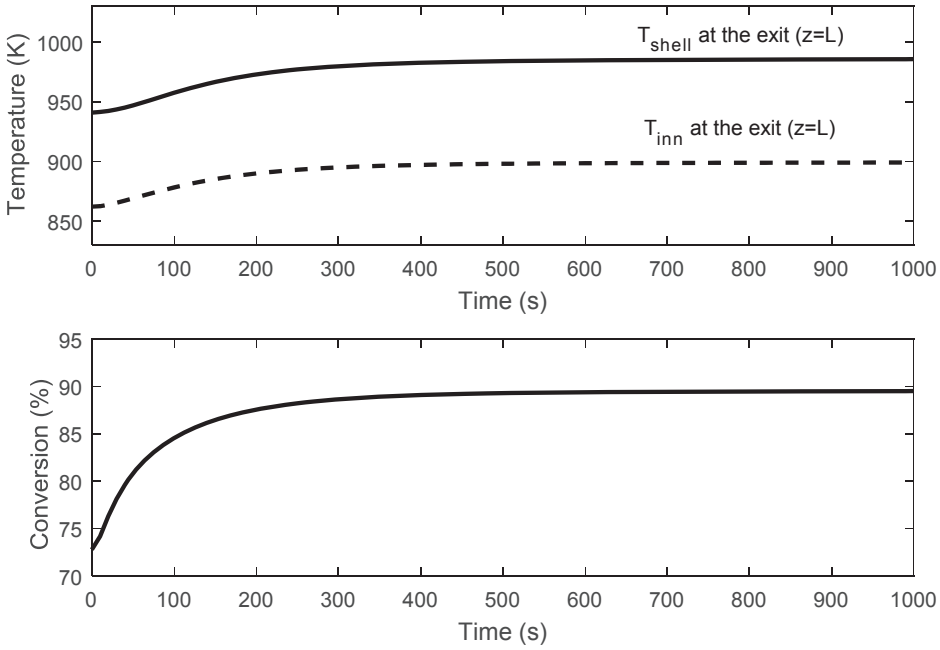

Fig. 8 – Dynamic response of the shell and inner tube outlet temperatures and methane conversion to the 100 K increase in the shell inlet temperature at t = 0 (s).

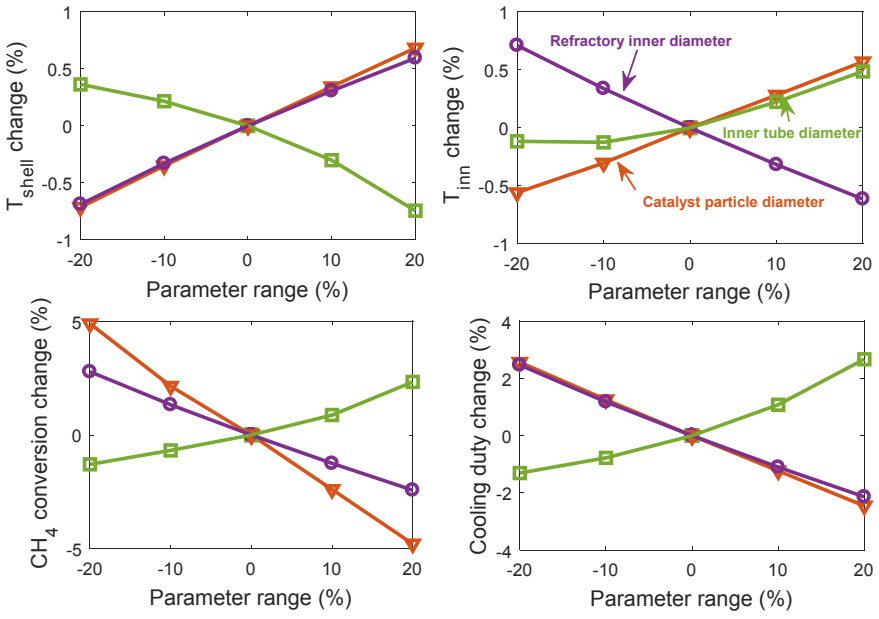

Fig. 9 – Sensitivity of exit temperatures of the shell and inner tube, CH_4 conversion and cooling duty of the system to some of the model parameters.

causing a significant pressure drop. The general conclusion here from an optimal design perspective is somewhat obvious in that the shell size and tube spacing should not be bigger than it needs to be.

Conclusion

This work presents, to the best of our knowledge, the first dynamic two-dimensional model for the integrated steam methane reforming and nuclear heat system. Because the model itself is based on first principles and commonly used empirical correlations of physical properties, it requires no general parameter fitting, which makes it very general and suitable for a wide variety of design applications. The model only requires information which is either known by design, or, can be readily determined experimentally at the laboratory scale, such as kinetic rate equations, common catalyst characteristics such as density and tortuosity, and basic physical property information such as heat capacity, thermal

conductivity, and density. Because the model considers space-time transients within the catalyst particles themselves, it does not make use of effectiveness factors, and instead considers the transient effects of diffusion on overall reaction rates. The model was validated with two steady-state designs and predicted the output conditions of the reactors extremely well. Unfortunately, no experimental information is available on transient behaviour to use for validation of the transient portions of the model.

The model is useful for many applications such as finding the optimal design of the SMR/HTGR device and the system in which it is used, and the control of the SMR/HTGR unit which is extremely important for safety-critical systems. In particular, the model is useful for predicting phenomena which are extremely difficult to measure directly, such as the internal temperature and composition profiles inside the catalyst particles, both in steady-state or during transients. The latter is of particular importance for the design and operability of the SMR/HTGR unit because, disturbances can lead to inverse responses caused by sudden shifts in reaction rates that could cause hot spots, cold spots, or other negative effects which are hard to measure can greatly impact long-term performance or cause safety issues.

In future work, this model will be used to help determine optimal designs for the SMR/HTGR device in the context of the entire nuclear hydrogen production system. In addition, the model will be used to develop control systems to ensure robust, safe, and stable operation. Finally, the model will be expanded to include other forms of methane reforming, such as dry reforming (reacting methane with CO_2 instead of stream) and mixed-reforming (having both steam reforming and dry reforming simultaneously) by using different catalysts and system arrangements. The incorporation of CO_2 as a reagent has certain potential benefits such as CO_2 emission reduction in applications such as synthetic Fischer-Tropsch fuels or mixed alcohols synthesis.

Acknowledgment

Financial support from the Ontario Ministry of Innovation via Early Researcher Award ER13-09-213 with matching support from the McMaster Advanced Control Consortium is gratefully acknowledged. The authors would also like to acknowledge Dr. Jaffer H. Ghouse (U.S. Department of Energy, National Energy Technology Laboratory) for assistance in developing the gPROMS code.

Nomenclature

Subscripts

rfct	refractory
in	Refractory inner surface
o	Refractory outer surface
shell	Shell
conv	convection
rad	radiation
w	Tube wall
t, o	Tube outer surface
tube	Tube
ti	Tube inner surface
gas	Mixture of gases in the tube
cat	Catalyst phase
i	Component counter
p	Particle
w_2	Inner tube wall
f	formation
mix	Mixture
t_2, o	Inner tube outer surface
t_2, i	Inner tube inner surface
inn	Inner tube gas
E	Energy balance
m_1	Shell side mass
m_2	Tube side mass

Acronyms

SMR	Steam methane reforming
HTGR	High temperature gas-cooled reactor
HTTR	High temperature test reactor
GHG	Greenhouse gases
JAERI	Japan Atomic Energy Research Institute
PDAE	Partial differential algebraic equation

Greek letters

ρ	Density
ε	emissivity
σ	Stefan-Boltzmann constant
μ	dynamic viscosity
ε	Bed porosity
π	mathematical constant
κ	Mass transfer coefficient
θ	Catalyst void fraction

REFERENCES

[1] Kvamsdal HM, Svendsen HF, Olsvik O, Hertzberg T. Dynamic simulation and optimization of a catalytic steam reformer. Chem Eng Sci 1999;54(13):2697–706.
[2] Yan XL, Hino R, editors. Nuclear hydrogen production handbook. CRC Press; 2011.
[3] Inagaki Y, Nishihara T, Takeda T, Hada K, Ogawa M, Shiozawa S, et al. Development programme on hydrogen production in HTTR. 2001. No. IAEA-TECDOC–1210.
[4] Khojasteh Salkuyeh Y, Adams II TA. Combining coal gasification, natural gas reforming, and external carbonless heat for efficient production of gasoline and diesel with CO_2 capture and sequestration. Energy Convers Manag 2013;74:492–504.
[5] Khojasteh Salkuyeh Y, Adams II TA. A new power, methanol, and DME polygeneration process using integrated chemical looping systems. Energy Convers Manag 2014;88:411–25.
[6] Fedders H, Harth R, Höhlein B. Experiments for combining nuclear heat with the methane steam-reforming process. Nucl Eng Des 1975;34(1):119–27.
[7] Höhlein B, Niessen H, Range J, Schiebahn HJ, Vorwerk M. Methane from synthesis gas and operation of high-temperature methanation. Nucl Eng Des 1984;78(2):241–50.
[8] Inaba Y, Ohashi H, Nishihara T, Sato H, Inagaki Y, Takeda T, et al. Study on control characteristics for HTTR hydrogen production system with mock-up test facility: system

controllability test for fluctuation of chemical reaction. Nucl Eng Des 2005;235(1):111–21.
[9] Ghouse JH, Adams II TA. A multi-scale dynamic two-dimensional heterogeneous model for catalytic steam methane reforming reactors. Int J Hydrogen Energy 2013;38(24):9984–99.
[10] Monaghan RF, Ghoniem AF. A dynamic reduced order model for simulating entrained flow gasifiers: part I: model development and description. Fuel 2012;91(1):61–80.
[11] Bergman TL, Incropera FP. Introduction to heat transfer. John Wiley & Sons; 2011.
[12] Ghouse JH, Seepersad D, Adams II TA. Modelling, simulation and design of an integrated radiant syngas cooler and steam methane reformer for use with coal gasification. Fuel Process Technol 2015;138:378–89.
[13] Perry RH, Green DW. Perry's chemical engineers' handbook. McGraw-Hill Professional; 1999.
[14] The story of the "INCOLOY alloys series," from 800, through 800H, 800 HT. Special Metals Corporation; Sep 2004. Publication number: SMC-047.
[15] Abbas SZ, Dupont V, Mahmud T. Kinetics study and modelling of steam methane reforming process over a NiO/Al_2O_3 catalyst in an adiabatic packed bed reactor. Int J Hydrogen Energy 2017;42(5):2889–903.
[16] Adams II TA, Barton PI. A dynamic two-dimensional heterogeneous model for water gas shift reactors. Int J Hydrogen Energy 2009;34(21):8877–91.
[17] Pantoleontos G, Kikkinides ES, Georgiadis MC. A heterogeneous dynamic model for the simulation and optimisation of the steam methane reforming reactor. Int J Hydrogen Energy 2012;37(21):16346–58.
[18] Nandasana AD, Ray AK, Gupta SK. Dynamic model of an industrial steam reformer and its use for multiobjective optimization. Ind Eng Chem Res 2003;42(17):4028–42.
[19] Dybkjær I. Tubular reforming and autothermal reforming of natural gas—an overview of available processes. Fuel Process Technol 1995;42(2–3):85–107.
[20] Dwivedi PN, Upadhyay SN. Particle-fluid mass transfer in fixed and fluidized beds. Ind Eng Chem Proc DD 1977;16(2):157–65.
[23] Fogler HS. Elements of chemical reaction engineering. 4th ed. Upper Saddle River, NJ: Prentice Hall; 2006.
[24] Singh CP, Saraf DN. Simulation of side fired steam-hydrocarbon reformers. Ind Eng Chem Proc Des Dev 1979;18(1):1–7.
[25] Satterfield CN. Mass transfer in heterogeneous catalysis. 1st ed. Cambridge: Massachusetts Institute of Technology Press; 1970.
[26] Xu J, Froment GF. Methane steam reforming, methanation and water-gas shift I Intrinsic kinetics. AIChE J 1989;35(1):88–96.
[27] IN-519 cast chromium–nickel–niobium heat-resisting steel. INCO Databook; 1976.
[28] gPROMS, process systems enterprise. 2015.
[29] Inagaki Y, Nishihara T, Takeda T, Hayashi K, Inaba Y, Ohashi H. Research and development program on HTTR hydrogen production system. In: Proceedings of the international conference on global environment and advanced nuclear power plants, Kyoto, Japan; September 2003. p. 15–9.
[30] JIS specification for piping. Retrieved from The engineering toolbox, http://www.engineeringtoolbox.com/jis-pipes-tubes-fittings-d_758.html.
[31] Kern DQ. Process heat transfer. McGraw-Hill; 1950.
[32] Mukherjee R. Effectively design shell-and-tube heat exchangers. Chem Eng Prog 1998;94(2):21–37.
[33] Sanaye S, Hajabdollahi H. Multi-objective optimization of shell and tube heat exchangers. Appl Therm Eng 2010;30(14):1937–45.

Chapter 3

Dynamic modeling of integrated mixed reforming and carbonless heat systems

The contents of this chapter have been published in the following peer reviewed journal:

Hoseinzade, L. and Adams II, T.A., 2017. Dynamic modeling of integrated mixed reforming and carbonless heat systems. *Industrial & Engineering Chemistry Research, 57* (17), 6013-6023.

I&EC research
Industrial & Engineering Chemistry Research

Article

Cite This: Ind. Eng. Chem. Res. 2018, 57, 6013–6023

pubs.acs.org/IECR

Dynamic Modeling of Integrated Mixed Reforming and Carbonless Heat Systems

Leila Hoseinzade and Thomas A. Adams II*

Department of Chemical Engineering, McMaster University, 1280 Main Street West, Hamilton, Ontario, L8S 4L8, Canada

ABSTRACT: In the previous study, a dynamic and two-dimensional model for a steam methane reforming process integrated with nuclear heat production was developed. It was shown that the integrated high temperature gas-cooled reactor (HTGR)/steam methane reforming (SMR) is an efficient process for applications such as hydrogen production. In this study, it is demonstrated that combining nuclear heat with the mix of steam and dry reforming process can be a promising option to achieve certain desired H_2/CO ratios for Fischer–Tropsch or other downstream energy conversion processes. The model developed in the previous study is extended to the combined steam and dry reforming process. The resulting model was validated using reported experimental data at nonequilibrium and equilibrium conditions. The dynamic and steady state performance of the integrated mixed reforming of methane and nuclear heat system was studied, and it was found that in addition to desired H_2/CO ratios, higher methane conversion and lower CO_2 emissions can be achieved using the proposed design compared to the HTGR/SMR system.

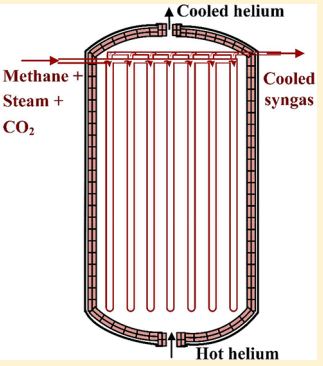

1. INTRODUCTION

Syngas, a mixture of hydrogen and carbon monoxide, is an important feedstock to produce various products such as electricity, methanol, dimethyl ether, ammonia, synthetic fuels by the Fischer–Tropsch (FT) process, and so on.[1] The steam reforming of methane process is a well-established and economical method for syngas production,[2,3] which yields a hydrogen rich syngas. However, when using steam as the feed, the hydrogen to carbon monoxide ratio is often too high to be used directly for the FT process.[4,5] CO_2 reforming of methane (also known as dry reforming of methane or DRM) is a potentially attractive method of producing syngas, since it converts captured carbon dioxide (a waste and greenhouse gas (GHG)) into valuable syngas.[6,7] The resulting syngas from dry reforming has an H_2/CO molar ratio of around 1, which is suitable for the production of dimethyl ether (DME) but too low for FT production. However, due to carbon deposition and rapid catalyst deactivation during the dry reforming reaction, the application is limited in practice.[6]

Different catalysts have different potentials for carbon formation in the CO_2 reforming reaction. Many studies investigated the activity and resistance of various catalysts (including noble metals, Ni, and graphite-based catalysts) to carbon deposition in the dry reforming reaction.[7,8] The results generally demonstrated that in the absence of steam, carbon deposition occurs for all of the studied catalyst types; however, noble-metal- and Ni-based catalysts have less selectivity for carbon deposition than graphite.[8] Furthermore, among the noble metals, Ru and Rh have the highest activity and the highest resistance to carbon formation.[7,8] Although the activities of the Ru- and Rh-based catalysts are about 10 times larger than the activity of Ni, the latter is still a promising catalyst for industrial applications considering its reasonable performance, low cost, and availability.[7,9]

Due to the catalyst deactivation issue, the dry reforming process has not been commercialized at large scales. However, combined dry and steam reforming processes have been commercialized in several countries.[2] Using steam in the dry reforming feedstock converts higher hydrocarbons (which are often present in natural gas) into H_2 and CO and reduces the risk of carbon deposition.[2] There is a certain minimum amount of steam necessary to prevent carbon deposition which depends on the catalyst type and the CO_2/CH_4 ratio in the feed.[2] Moreover, the H_2/CO ratio of the syngas produced by the combined process is in between that of dry reforming and steam reforming, much closer to the 2.0 ratio required for the FT process.

The steam reforming and water gas shift (WGS) reactions are given as follows:[10]

$$CH_4 + H_2O \rightleftharpoons CO + 3H_2 \quad \left(\Delta H_{r,25^\circ C} = 206.3 \frac{kJ}{mol}\right) \tag{1}$$

$$CO + H_2O \rightleftharpoons CO_2 + H_2 \quad \left(\Delta H_{r,25^\circ C} = -41.1 \frac{kJ}{mol}\right) \tag{2}$$

$$CH_4 + 2H_2O \rightleftharpoons CO_2 + 4H_2 \quad \left(\Delta H_{r,25^\circ C} = 164.9 \frac{kJ}{mol}\right) \tag{3}$$

Special Issue: PSE Advances in Natural Gas Value Chain

Received: September 7, 2017
Revised: December 23, 2017
Accepted: December 26, 2017
Published: December 26, 2017

DOI: 10.1021/acs.iecr.7b03726
Ind. Eng. Chem. Res. 2018, 57, 6013–6023

The dry reforming reaction proceeds as follows:[9]

$$CH_4 + CO_2 \rightleftharpoons 2CO + 2H_2 \quad \left(\Delta H_{r,298k} = 247 \frac{kJ}{mol}\right) \tag{4}$$

All of the dry and steam reforming reactions are highly endothermic and require a large amount of heat in order to reach equilibrium.

The SMR reaction mechanism and kinetics are well studied and understood. The well-known kinetic model of this reaction based on the nickel catalyst was presented using a Langmuir–Hinshelwood type model by Xu and Froment.[11] However, the reaction kinetics and mechanisms of the dry reforming process are still less well-known.

Richardson et al.[7] studied the kinetics of the DRM reaction on a Rh/γ-Al_2O_3 catalyst and presented a model based on the Langmuir–Hinshelwood framework and a redox mechanism. Their results showed that for low CO_2/CH_4 ratios there is no carbon deposition at temperatures of 600–800 °C. Bradford et al.[12] investigated the dry reforming reaction on a Ni catalyst with different supports (TiO_2, C, SiO_2, and MgO) and indicated that catalyst activity significantly varies for different supports. They found Ni/MgO to be the most stable and active catalyst between the studied cases. They also developed an expression for the reaction rate for the Ni catalysts based on assuming CH_4 and CH_xO decompositions as the slow kinetic steps.[13]

In addition, Olsbye et al.[14] developed a kinetic model for the CO_2 reforming of methane based on the Langmuir–Hinshelwood type equation on the Ni/La/α-Al_2O_3-based catalyst and showed that experimental data is consistent with this type of model. Wang et al.[15] studied the kinetics of the dry reforming reaction over a Ni/γ-Al_2O_3 catalyst and presented a Langmuir–Hinshelwood mechanism similar to Olsbye's model. The results of this study indicated that Ni/γ-Al_2O_3 is an effective catalyst for this reaction and a Langmuir–Hinshelwood equation is a proper model to represent the kinetics of the reaction. Maestri et al.[16] developed a detailed microkinetic model for the SMR and DRM reaction kinetics on a Rh/Al_2O_3 catalyst. The results of this study showed that methane activation is the rate-determining step of the dry reforming reaction.

Based on Zhao et al.[17] and our survey of the literature, the best kinetic model to describe the combined dry and steam reforming kinetics is the model presented by Park et al.[18] This kinetic model is a combination of the SMR kinetic model proposed by Xu et al.[11] and the dry reforming kinetic model presented by Olsbye et al.[14] These kinetic models, as briefly explained above, are Langmuir–Hinshelwood type expressions developed for Ni-based catalysts. This study provided correlations for the equilibrium and reaction coefficients based on lab scale data from a fixed-bed microreactor. In Park's study, the reaction was under nonequilibrium conditions by using inert solids and high feed flow rate to catalyst ratios. The model also was validated using lab scale experimental data for various ranges of pressure, temperature, and feed flow rates. Their results indicated consistency between the experiments and model prediction.[18]

As mentioned earlier, both the dry and steam reforming processes are highly endothermic and energy intensive. Conventionally, reforming tubes are placed inside a furnace and heat is provided by combusting a fuel. In addition, the endothermic reforming process can be combined with the exothermic partial oxidation of methane (POM) process to provide the required heat in which high purity oxygen is injected as an additional reagent. However, it has some disadvantages such as forming hot spots in the catalyst which results in catalyst deactivation[19,20] and the expense of adding an air separation unit to produce the necessary high purity oxygen.[18] Furthermore, either using a furnace or partial oxidation causes large GHG emissions; thus, it is important to investigate alternate sources to reduce total greenhouse gas emissions of the process.

Several researchers studied nuclear energy as an alternate source of heat for the steam reforming process.[21−26] Researchers in Germany and Japan tested the integrated high temperature gas-cooled reactor (HTGR) and SMR processes for hydrogen production at pilot scale and demonstrated that nuclear heat is a safe, clean, and economically feasible source of energy to produce hydrogen.[21−24] Khojasteh Salkuyeh and Adams also showed that by integrating the HTGR with the SMR process, direct fossil fuel consumption significantly decreases and carbon efficiency increases.[25,26]

The feasibility and operability of the integrated HTGR/SMR process were demonstrated by pilot scale facilities by research groups in Germany and Japan Atomic Energy Research Institute.[21−24] The dynamic modeling of the process was also developed in the previous work[27] to address the key challenges of the process concerning dynamic behavior, such as start-up, shutdown, and response to disturbances. In the previous work, the dynamic model was developed based on first-principles using a multiscale model, considering phenomena such as gas diffusion inside catalysts.[27] The validity of the model was tested using available data, and very few model parameters needed to be fit based on the reported design data. The dynamic and steady state variations of the key variables of the system were analyzed, and it was found that, to obtain higher methane conversions, a high steam to methane ratio in the feed is required. This leads to a large H_2/CO ratio which is more suitable for hydrogen production than for FT processes.

Therefore, as mentioned earlier, to obtain lower H_2/CO ratios which is suitable for the FT process, the mixed reforming process is preferable. The required heat for the MRM process can be provided by high temperature gas-cooled reactors, as was previously considered for the SMR process. However, to the best of the authors' knowledge, integrating nuclear heat and mixed reforming process has not been investigated.

The purpose of this study is to propose a large scale design for the novel integrated nuclear heat and mixed reforming process. To do this, the dynamic model which was developed in the previous study is extended to the mixed reforming process. The model is based on the conservations of mass, momentum, and energy within the system, and common correlations for physical properties, heat and mass transfer coefficients, and diffusion. Also, Park's kinetic model for the MRM reactions is applied. The final model (a set of partial differential and algebraic equations, or PDAEs) is implemented and solved using the finite differences method with the gPROMS software package, an equation-oriented modeling and simulation environment. To the best of our knowledge, there is no large scale experimental data on the integrated HTGR/MRM process, so the validity of the model for the mixed reforming process is checked using lab scale data. After verifying the validity of the model, the dynamic and steady state performance of the system is analyzed, as well as its transient behavior in the presence of disturbances. Finally, a sensitivity analysis on the key parameters of the system is accomplished to investigate the

DOI: 10.1021/acs.iecr.7b03726
Ind. Eng. Chem. Res. 2018, 57, 6013−6023

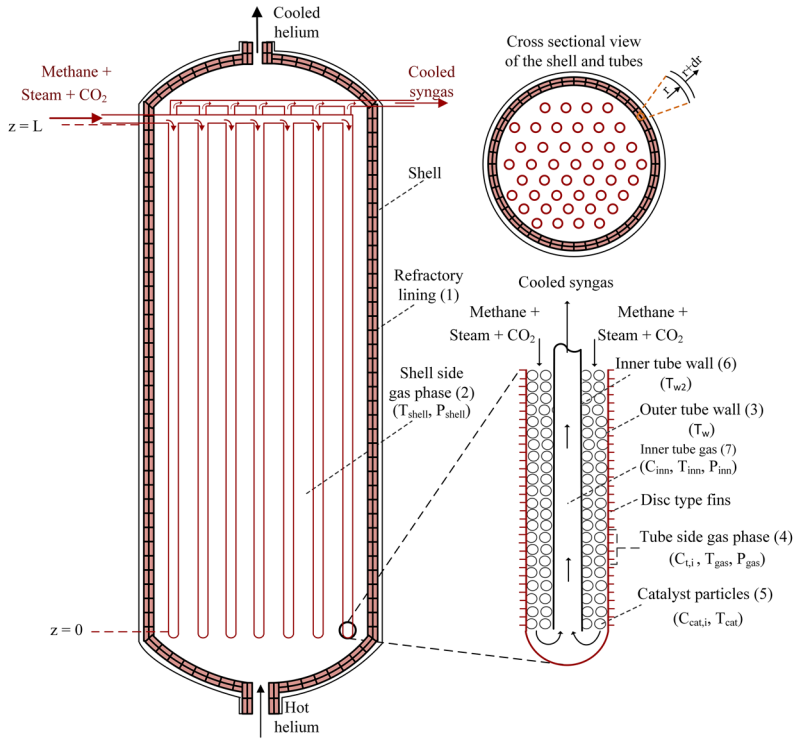

Figure 1. Schematic of the integrated HTGR/MRM system. This figure was adapted from the study by Hoseinzade et al.[27]

Table 1. Description of the Submodels

submodel	description
(1) refractory lining of the shell	Considers the temperature gradient in the axial and radial directions of the refractory lining based on the conductive heat transfer, as given by eqs 1−5 of the study by Hoseinzade et al.[27]
(2) gas phase in the shell side	Considers the concentration, pressure, and temperature variations in the shell side in the axial direction, convective (estimated based on empirical correlations empirical correlations) and radiative heat transfer from the gas to the refractory lining and tubes outer surface according to eqs 6−14 of the study by Hoseinzade et al.[27]
(3) outer tube wall of the mixed reforming tubes	Considers the temperature gradient in the axial and radial directions of the outer tube based on conductive heat transfer, as given by eqs 15−18 of the study by Hoseinzade et al.[27]
(4) gas phase in the reforming tubes	Considers the concentration, pressure (pressure drop was estimated based on the Ergun equation), and temperature variations in the gas phase of the tubes in the axial direction, convective heat transfer from the gas to the outer and inner tube walls and the catalyst surface, as given by eqs 19−37 of the study by Hoseinzade et al.[27]
(5) catalyst particles	Considers temperature and concentration gradients within the catalyst particles, surface-to-gas mass and heat transfer, multispecies diffusion correlations, heat transfer correlations according to eqs 38−43 of the study by Hoseinzade et al.[27] and reaction kinetics as given by eqs 5−27 of section 2.1 of this work
(6) inner tube wall	Considers the temperature gradients in the axial and radial directions of the inner tube based on the conductive heat transfer correlation according to eqs 64−67 of the study by Hoseinzade et al.[27]
(7) gas phase in the inner tubes	Considers the concentration, pressure, and temperature gradients in the inner tube in the axial direction, convective heat transfer from the gas to the inner tube inner surface according to eqs 68−73 of the study by Hoseinzade et al.[27]

system performance in the presence of parameter uncertainty. This information was used to develop a final recommended design for the integrated HTGR/MRM reactor.

2. MODEL DEVELOPMENT

A schematic of the proposed integrated HTGR/MRM system is shown in Figure 1. The model of this system contains seven submodels at different scales including (1) refractory lining of the shell, (2) gas phase in the shell side, (3) outer tube wall of the mixed reforming tubes, (4) gas phase in the reforming tubes, (5) catalyst particles which are packed inside the reforming tubes, (6) inner tube wall, and (7) gas phase in the inner tubes. Table 1 briefly describes each submodel. The model and the assumptions are the same as those in the previous study except the reaction kinetics which are presented in section 2.1 below. Key assumptions of the model are given in Table 2. To avoid repetition, the model equations are not presented here. The only difference between the models is that eqs 44−63 of the previous study have to be replaced by eqs

Table 2. Model Assumptions

assumptions	reference
Ideal gas law	28
Radial gradients in the reformer tubes are negligible.	29
Conditions of one tube represent the other tubes as well.	30
Heavier than methane hydrocarbons are converted in a pre-reformer, and thus neglected from the model.	31
Carbon deposition will not occur due to high steam to carbon ratio.	2
The pressure drop in the shell and inner tube side is small and fixed at 1 bar.	27, 32

DOI: 10.1021/acs.iecr.7b03726
Ind. Eng. Chem. Res. 2018, 57, 6013−6023

5−27 of this study to represent the MRM reaction kinetics and rates properly. The rest of the model equations are the same, and the detailed model equations can be found in the study by Hoseinzade et al.[27]

2.1. Mixed Reforming Kinetics. The kinetic model of the combined reforming reaction is presented by Park et al.[18] for the Ni-based catalyst. As mentioned earlier, Park et al.[18] combined the kinetics provided by Xu and Froment,[11] a well-known kinetic model for the SMR reaction, and the kinetic expression provided by Olsbye et al.[14] for the dry reforming process. The model is a Langmuir−Hinshelwood type equation, and Park et al. developed correlations for coefficients based on their experimental data. The reaction rates for eqs 1−4 are given by eqs 5−8, respectively.

$$r_1 = \frac{k_1\left[p_{CH_4}p_{H_2O} - \frac{p_{H_2}^{3}p_{CO}}{K_1}\right]}{p_{H_2}^{2.5}\left(1 + K_{CO}p_{CO} + K_{H_2}p_{H_2} + K_{CH_4}p_{CH_4} + \frac{K_{H_2O}p_{H_2O}}{p_{H_2}}\right)^2} \quad (5)$$

$$r_2 = \frac{k_2\left[p_{CO}p_{H_2O} - \frac{p_{H_2}p_{CO_2}}{K_2}\right]}{p_{H_2}\left(1 + K_{CO}p_{CO} + K_{H_2}p_{H_2} + K_{CH_4}p_{CH_4} + \frac{K_{H_2O}p_{H_2O}}{p_{H_2}}\right)^2} \quad (6)$$

$$r_3 = \frac{k_3\left[p_{CH_4}p_{H_2O}^{2} - \frac{p_{H_2}^{4}p_{CO_2}}{K_3}\right]}{p_{H_2}^{3.5}\left(1 + K_{CO}p_{CO} + K_{H_2}p_{H_2} + K_{CH_4}p_{CH_4} + \frac{K_{H_2O}p_{H_2O}}{p_{H_2}}\right)^2} \quad (7)$$

$$r_4 = \frac{k_4\left[p_{CH_4}p_{CO_2} - \frac{p_{H_2}^{2}p_{CO}^{2}}{K_4}\right]}{(1 + K_{CO}p_{CO} + K_{CH_4}p_{CH_4})(1 + K_{CO_2}p_{CO_2})} \quad (8)$$

where $p_i = C_{cat,i}RT_{cat}$ is the partial pressure of the corresponding species (calculated by assuming the ideal gas law), $C_{cat,i}$ is the molar concentration of component i on the catalyst surface, and T_{cat} is the catalyst temperature. k_1, k_2, k_3, and k_4 are the reaction coefficients defined by

$$k_1 = 4.72 \times 10^{6} \exp\left(-\frac{232{,}477}{R}\left(\frac{1}{T_{cat}} - \frac{1}{1123.15}\right)\right), \quad \frac{\text{mol Pa}^{0.5}}{\text{g h}} \quad (9)$$

$$k_2 = 1.06 \times 10^{-3} \exp\left(-\frac{71{,}537}{R}\left(\frac{1}{T_{cat}} - \frac{1}{1123.15}\right)\right), \quad \frac{\text{mol}}{\text{Pa g h}} \quad (10)$$

$$k_3 = 1.89 \times 10^{3} \exp\left(-\frac{267{,}760}{R}\left(\frac{1}{T_{cat}} - \frac{1}{1123.15}\right)\right), \quad \frac{\text{mol Pa}^{0.5}}{\text{g h}} \quad (11)$$

$$k_4 = 2.91 \times 10^{-7} \exp\left(-\frac{234{,}851}{R}\left(\frac{1}{T_{cat}} - \frac{1}{1123.15}\right)\right), \quad \frac{\text{mol}}{\text{g h Pa}^2} \quad (12)$$

The equilibrium constants are defined as

$$\ln K_1 = 2.48 - \frac{22920.6}{T_{cat}} + 7.19 \ln T_{cat} - 2.95 \times 10^{-3}T_{cat} \quad (13)$$

$$\ln K_2 = -12.11 + \frac{5318.69}{T_{cat}} + 1.01 \ln T_{cat} + 1.14 \times 10^{-4}T_{cat} \quad (14)$$

$$K_3 = K_1K_2 \quad (15)$$

$$K_4 = K_1/K_2 \quad (16)$$

where the unit of K_1 is Pa^2 and K_2 is dimensionless. The adsorption coefficients are defined by

$$K_{CH_4} = 6.65 \times 10^{-9} \exp\left(\frac{38{,}280}{RT_{cat}}\right), \quad \text{Pa}^{-1} \quad (17)$$

$$K_{H_2O} = 1.77 \times 10^{5} \exp\left(-\frac{88{,}680}{RT_{cat}}\right) \quad (18)$$

$$K_{H_2} = 6.12 \times 10^{-14} \exp\left(\frac{82{,}900}{RT_{cat}}\right), \quad \text{Pa}^{-1} \quad (19)$$

$$K_{CO} = 8.23 \times 10^{-10} \exp\left(\frac{70{,}650}{RT_{cat}}\right), \quad \text{Pa}^{-1} \quad (20)$$

$$K_{CO_2} = 5.97 \times 10^{-7} \exp\left(\frac{52{,}670}{RT_{cat}}\right), \quad \text{Pa}^{-1} \quad (21)$$

Based on eqs 1−4, reaction rates of the components can be written as

$$r_{CH_4} = -(r_1 + r_3 + r_4) \quad (22)$$

$$r_{H_2O} = -(r_1 + r_2 + 2r_3) \quad (23)$$

$$r_{CO} = r_1 - r_2 + 2r_4 \quad (24)$$

$$r_{H_2} = 3r_1 + r_2 + 4r_3 + 2r_4 \quad (25)$$

$$r_{CO_2} = r_2 + r_3 - r_4 \quad (26)$$

$$r_{N_2} = 0 \quad (27)$$

The resulting model is a set of PDAEs which is implemented in the gPROMS software package.[33] The PDAEs are discretized in space using the finite difference method. Also, the grid size for the discretization in different axis is chosen based on reducing

DOI: 10.1021/acs.iecr.7b03726
Ind. Eng. Chem. Res. 2018, 57, 6013−6023

the global energy and mass conservation errors as described in the previous work.

3. MODEL VALIDATION

A survey in the literature shows there is no experimental data on the proposed integrated HTGR/MRM process to validate the model predictions. However, some lab scale experimental data on the mixed reforming process are available. As mentioned earlier, the model applied in this study is an extension of the model developed in our previous work[27] to the mixed reforming process. The only difference of the models is the reaction kinetics applied for the tube side. The model of the integrated HTGR/SMR process was validated and fitted in the previous work, and results demonstrated high accuracy of the model in predicting the reported design specifications. Since the shell side model is exactly the same in both models, it is necessary to validate the tube side model only.

Park et al. presented a kinetic model for the mixed reforming process and carried out experiments on the mixed reforming process for the equilibrium and nonequilibrium reactions.[18,34] The results of these experiments are employed here to validate the tube side model. In the latest study by Park et al.,[18] experiments were conducted for nonequilibrium reaction by adding diluents and decreasing the residence time of the components in the reactor. The experiment conditions are briefly described as follows: the fixed bed reforming reactor was embedded inside a heater such that the tube wall temperature was kept constant and equal to the temperature of the inlet process gas; the temperature in the study is in the range 700−900 °C, the pressure is 0.5−1.2 MPa, and the GHSV is 90,000−280,000 mL-CH_4/g_{cat} h. The amounts of the catalyst and diluent (α-Al_2O_3) used in the experiment were 50 mg and 1 g, respectively. The steam to methane and carbon dioxide to methane ratios were kept constant at CO_2/CH_4 = 0.3 and H_2O/CH_4 = 1.7 in this experiment. Furthermore, in the experiment, feed was flowing in the tube filled with catalyst and diluent particles, receiving heat from the heater and converted to the syngas, and then produced hot syngas leaving the tube. To simulate the experiment conditions, the inner tube submodel is removed from the model. More details about the experiment conditions can be found in the study by Park et al.[18]

One of the significant differences between the experiment conditions and large scale design is the bed porosity. In the developed model for large scale systems, bed porosity was approximated using the given correlations in the literature for the fixed bed catalytic reactors based on the diameters of both the tube and catalyst particles.[35] However, in the experiment in order to prevent the reaction from reaching equilibrium, only a small amount of catalyst was loaded in the reactor. By definition, bed porosity in packed bed reactors is the ratio of the free volume to the total volume of the reactor as follows

$$\varepsilon_{cat} = 1 - \frac{V_p}{V_t} = 1 - \frac{m_p \rho_p}{\pi D_t^2 L/4} \tag{28}$$

where ε_{cat} is the bed porosity with respect to the catalyst particles which is used to compute the catalyst surface area ($a_v = 6(1 - \varepsilon_{cat})/D_p$), V_p is the volume occupied by the catalyst particles, m_p is the net weight of the catalyst loaded, ρ_p is the particle density, V_t is the reactor volume, D_t is the reactor inner diameter (10.9 mm), and L is the reactor length (6 mm). The reactor diameter and length were not reported in the article but were provided by the authors via personal communication.[36]

The only parameter fitted for model validations is the catalyst particle size within a tight range known from the Park study.[18]

In those experiments, a portion of the reactor volume was occupied by diluent particles (α-Al_2O_3 balls) to control the mixed reforming reaction progress. There is no reaction on the diluent particles; however, it affects the velocity and pressure drop of the gas stream flowing in the reactor. Therefore, the bed porosity definition was adjusted in the model to reflect the experimental setup, defining it as the ratio of the free volume to the reactor volume:

$$\varepsilon_t = 1 - \frac{V_p + V_d}{V_t} = 1 - \frac{m_p \rho_p + m_d \rho_d}{\pi D_t^2 L/4} \tag{29}$$

where ε_t is the bed porosity considering any particles, V_d is the volume of the diluent particles, m_d is the net weight, and ρ_d is the density of the diluent particles.

With these assumptions, the results of the model prediction at different temperatures, pressures, and gas hourly space velocity (GHSV) are shown in Figure 2. In the figure, the

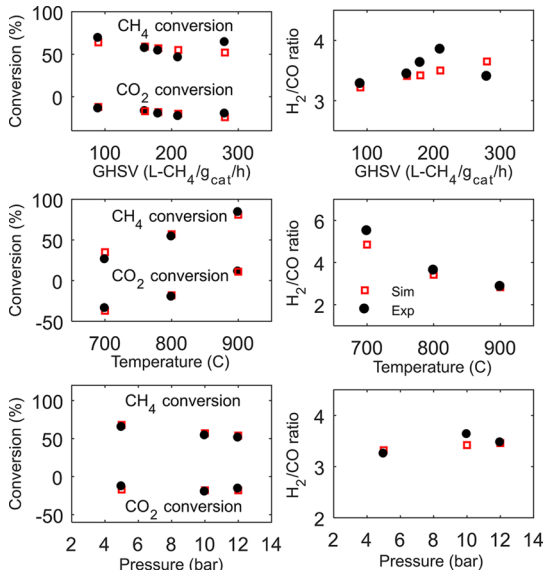

Figure 2. Model validation at nonequilibrium conditions. Experimental data was obtained from the Park study.[18]

model predictions are shown as red squares and the experimental data with black circles. The base condition for the experiments is GHSV = 180,000 mL-CH_4/g_{cat} h, a temperature of 800 °C, and a pressure of 1.0 MPa. At each series of experiments, one of these operating conditions was perturbed from the base condition.

It should be noted that GHSV is measured at the standard temperature and pressure (STP) condition[18] and converted to the methane molar flow rate ($\dot{F}_{CH_4}$) by the following equation

$$\dot{F}_{CH_4} = \frac{GHSV \times m_p \times P_{STP}}{R T_{STP} Z_{STP}} \tag{30}$$

where P_{STP} is the pressure, T_{STP} is the temperature, and Z_{STP} is the methane compressibility factor at STP.

The system performance is shown by variations of the methane and carbon dioxide conversions and the hydrogen to carbon monoxide ratio (H_2/CO) as it is used in Park's study. The results indicate that at each data point, the tube model can predict methane and carbon dioxide conversions and the H_2/

DOI: 10.1021/acs.iecr.7b03726
Ind. Eng. Chem. Res. 2018, 57, 6013−6023

CO ratio with high accuracy. The average absolute error in the CO_2 and methane conversions and H_2/CO ratio predictions is 2%, 4.35% and 0.183, respectively. It should be noted that the presented model indicates better agreement with the experimental data than the simulation results in the Park study.[18] This is because the presented model considers more detailed phenomena, such as multispecies diffusion correlations,[37] temperature and concentration variations in the catalyst phase, as well as heat transfer coefficients and so on. Validating the model in the nonequilibrium condition and with only a single parameter fitting suggests that all of the correlations applied for the diffusion, heat transfer coefficient, reaction kinetics, physical properties, as well as assumptions made to develop the model are reasonable and can be used for the large scale design.

In addition, the tube model is validated using other experimental data sets reported by Jun et al.[34] at equilibrium and nonequilibrium conditions. In this data set, nine cases were studied at equilibrium conditions (cases 1−9 of the study by Jun et al.[34]) and eight cases at nonequilibrium conditions (cases 10−17 of the study by Jun et al.[34]). Similar to the previous case, the fixed bed reactor is embedded inside a heater to keep the tube wall temperature constant, which we replicated in our model for validation purposes by fixing the boundary condition of the inner tube wall temperature accordingly. The temperature in the experiment was in the range of 700−900 °C, the pressure was 0.25−1.0 MPa, the GHSV was 2500−400,000 mL-CH_4/g_{cat} h, and the molar ratios are $CH_4/CO_2/H_2O/N_2$ = 3/1−1.2/2−4/3−4. The reactor inner diameter is 10 mm, and the length is 30 mm. More details about the experiments can be found in the study by Jun et al.[34]

With the given conditions, model predictions and experimental data for the equilibrium and nonequilibrium conditions of methane and carbon dioxide conversions are indicated in Figure 3a. The identity line shown with dashes in Figure 3b clearly demonstrates that the deviation of model predictions from experimental data is low. In the experiments, in order to reach equilibrium, the space velocity of inlet gas was kept low such that sufficient residence time was given for the reactants to reach equilibrium. Figure 3a shows that in many cases methane equilibrium conversion is slightly underestimated by the model, and the average absolute error of prediction is 6.59%. However, as shown by Figure 3b, the equilibrium conversion of CO_2 and model prediction are close and the average absolute error of the prediction is 3.1%.

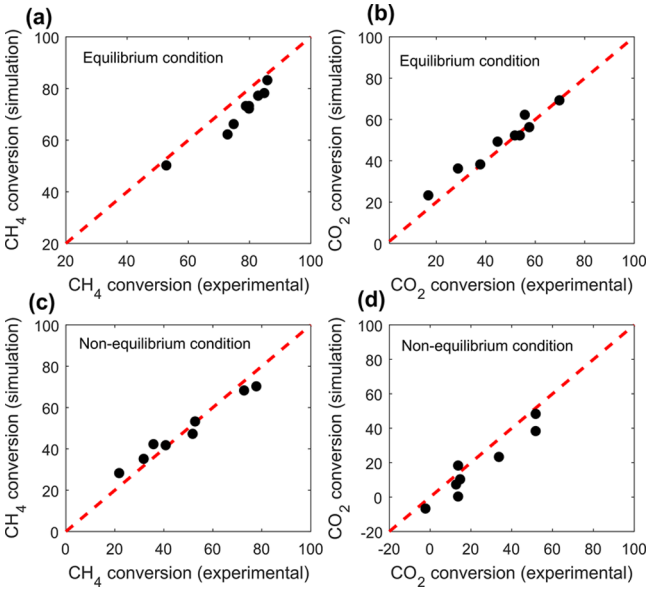

Figure 3. Parity plots of the experimental and simulation results for the methane and CO_2 conversions at equilibrium and nonequilibrium conditions. Experimental data was derived for cases 1−17 from Figure 2 of the study by Jun et al.[34]

Parts c and d of Figure 3 indicate the model prediction and experimental data for the nonequilibrium data set (cases 10−17 of the study by Jun et al.[34]). The nonequilibrium condition in experiments was attained by increasing the feed flow rate up to 80 times from the equilibrium condition, and by adding some diluent solids (alumina balls). The operating conditions for each case are given in the study by Jun et al.[34] The broad range of system behavior explored is evident from the range of methane and carbon dioxide conversions obtained for this data set. The results depict that for all cases, the methane and carbon dioxide conversions compare well with the experimental results. The average absolute errors in the CO_2 and methane conversions are 4.2 and 7.8%, respectively.

4. RESULTS AND DISCUSSION

The objective of this section is to present an analysis of a large scale design for the proposed integrated HTGR/MRM system. SIEMENS-INTERATOM provided a large scale design for the integrated HTGR/SMR system for hydrogen production.[21] The operating conditions of the presented design are extended from this reference to the integrated HTGR/MRM system. Since the DRM reaction is more endothermic than SMR, a lower process gas feed rate (or a higher helium feed rate) is required to obtain the same cooling duty as the SMR process studied in the previous work.[27] Therefore, a lower process gas (mixture of methane, steam, and carbon dioxide) feed rate is required in the MRM process to obtain the same cooling duty as the SMR-only process.

It can be challenging to choose optimal steam to methane and CO_2 to methane ratios in the MRM process. For example, due to the presence of CO_2, carbon deposition is possible, which depends on the steam to methane and CO_2 to methane ratios as well as the type of catalyst.[2] These ratios also affect the heat duties, heat transfer properties, conversion rates, and outlet gas concentrations, all of which have impacts both on the equipment design and on the balance-of-plant. A survey of the literature shows that different ratios are applied depending on the application of syngas in the downstream; however, there is a carbon limit for the H_2O/CH_4 and CO_2/CH_4 ratios for certain types of catalyst.[2] The selected ratios in this study have been derived from the industrial reported data in ref 2. Based on the carbon limit diagram provided in ref 2, the ratios chosen for this work are located in the safe region (no carbon deposition region) for the Ni-based catalyst. Furthermore, the design parameters are taken from either the SIEMENS-INTERATOM design or the fitted parameters in our previous study.[27] The operating conditions and design parameters used for the large scale HTGR/MRM process are given in Tables 3 and 4, respectively. As shown in Table 3, the process gas feed was changed from 35 kmol/h/tube in the HTGR/SMR process[27] to 25.77 kmol/h/tube in this study to obtain the same cooling duty as the HTGR/SMR system. It should be noted that temperatures and pressures as well as helium flow rate in Table 3 are obtained from SIEMENS-INTERATOM design data. These data are based on the results of a pilot scale plant test.[21]

DOI: 10.1021/acs.iecr.7b03726
Ind. Eng. Chem. Res. 2018, 57, 6013−6023

Table 3. Design Specification for the Industrial Scale Integrated HTGR/MRM System

specification	large scale design
Process Gas Conditions	
inlet pressure[21]	5.6 MPa
inlet temperature[21]	347 °C
feed rate	25.77 kmol/h/tube
methane/steam/CO_2 ratio [Mortensen]	1/2.5/1.5
Helium Gas Conditions[21]	
inlet pressure	4.987 MPa
inlet temperature	950 °C
feed rate	50.3 kg/s

Table 4. Design Parameters for the Industrial Scale Integrated HTGR/MRM System[21,27]

parameter	value
number of tubes	199
catalyst type	Ni-alumina
tube material	Incoloy 617
tube length	14 (m)
tube wall thickness	1 (cm)
tube inner outer diameter	12 (cm)
inner tube thickness	0.165 (cm)
inner tube inner diameter	5.72 (cm)
refractory inner diameter	2.7 (m)
inner tube material	Alloy IN 519

Based on the design specifications and parameters in Tables 3 and 4, the system behavior is analyzed in this section. The final model implemented in gPROMS contains 233,538 variables. To initialize the simulations in gPROMS, all tube side gases (including within the catalyst particles) were set at time zero to be pure nitrogen at 347 °C and 56 bar. Similarly, the shell side was set to be pure helium at 347 °C, with the inlet to the shell at 347 °C and 49.87 bar. This created a set of initial conditions that was consistent with the model equations and thus allowed the simulation to initialize. Then, the simulation was run until a steady state was attained. Then, the inlet stream conditions were changed to those given in Table 3 and the dynamic simulation was continued until a new steady state condition was obtained. This new steady state condition was saved for use as a set of consistent initial conditions for use in all future simulations, and all previous time steps were discarded.

The steady state performance of the integrated HTGR/MRM system based on the given operating conditions in Table 3 is shown in Figure 4 as a function of the axial position of the shell, outer tube, and inner tube gas phase temperatures, methane and CO_2 conversions in the outer tube section. Figure 4 shows that helium gas in the shell side transfers heat to the tube wall and its temperature decreases from 950 to 676 °C with a corresponding cooling duty of 72 MW. In the outer tube, process gas receives heat through the outer tube and inner tube walls, converted to the syngas, and its temperature increases from 347 to 886 °C; then, the hot syngas proceeds in the inner tube to transfer its heat to the tube side such that its temperature drops from 886 to 594 °C. Also, the overall methane and CO_2 conversions are 84.8 and 26.9%, respectively. The CO_2 conversion is low due to the high pressure of the feed. One solution to increase CO_2 conversion at the systems level is to separate unreacted CO_2 from the product and recycle that to

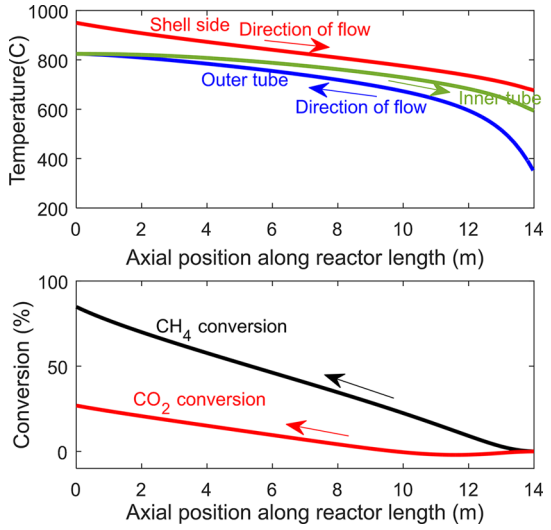

Figure 4. Temperature and conversion profiles of the HTGR/MRM system at the steady state conditions.

the system; however, this is the subject of future study. In addition, the syngas outlet has an H_2/CO ratio of 1.7.

The results show that methane conversion is significantly higher in this system than the integrated SMR/HTGR system (without DRM). In addition to higher methane conversion, 26.9% of the CO_2 converted to syngas. However, in the SMR-only process, some CO_2 is produced during the reaction. This demonstrates the potential for lower GHG emissions of the integrated reforming/HTGR systems by combining steam and dry reforming processes, although a rigorous life cycle analysis in the context of the balance-of-plant is a subject of future work.

Figure 5 shows the steady state temperature in the catalyst surface as a function of axial position based on the given

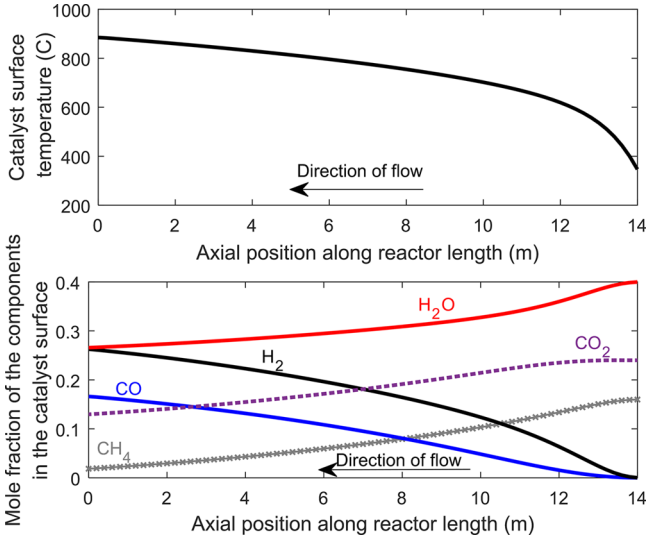

Figure 5. Temperature and mole fraction profiles of the HTGR/MRM system in the catalyst surface at steady state conditions.

operating conditions in Table 3. Based on the results, the catalyst surface temperature reaches 885 °C in the outer tube outlet which is very close to the syngas temperature in the outer tube outlet. Furthermore, Figure 5 shows the mole fraction profile of the components in the catalyst surface at steady state. The profiles indicate that methane is consumed faster than

DOI: 10.1021/acs.iecr.7b03726
Ind. Eng. Chem. Res. 2018, 57, 6013−6023

steam and carbon dioxide within the reactor length. Similarly, the hydrogen production rate is faster than that of carbon monoxide, which leads to a H_2/CO ratio of 1.7. In addition, the results show that more than half of the steam and CO_2 leave the reforming tubes unreacted.

In order to reach higher H_2/CO ratios, extra steam is required. Further analysis found that in order to achieve an H_2/CO ratio of 2 at the given operating conditions in Table 3, $CH_4/H_2O/CO_2$ feed ratios of 1/3.4/1.43 are required. As a result of this change, a methane conversion of 84.3%, a CO_2 conversion of 21.2%, and a cooling duty of 63.1 MW can be achieved. Figure 6 shows the temperature and conversion

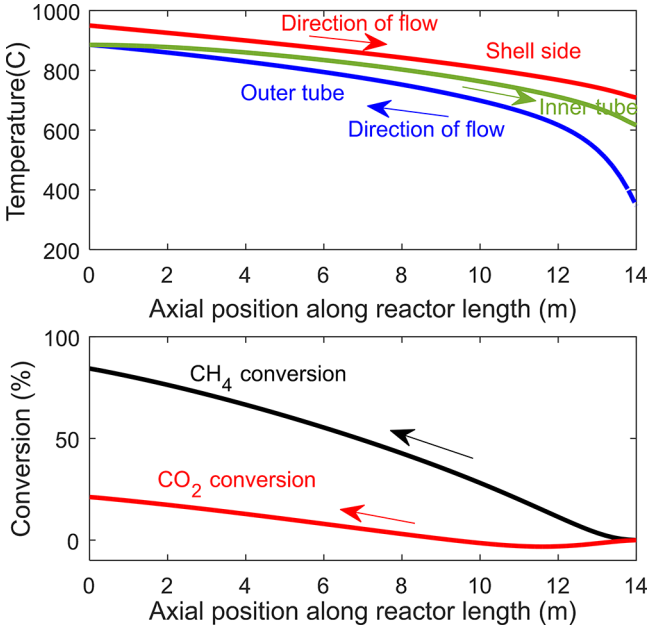

Figure 6. Temperature and conversion profiles of the HTGR/MRM system at steady state conditions for the feed composition of $CH_4/H_2O/CO_2$ equal to 1/3.4/1.43.

profiles for this feed condition at steady state. As shown in the figure, helium gas temperature decreases from 950 to 709 °C. In the outer tube, process gas temperature increases from 347 to 885 °C, and the inner tube temperature drops from 885 to 616 °C.

4.1. Effect of Disturbances. In this section, the impact of the disturbances on the inlet helium or process gas (methane, steam, and CO_2 mixture) feed such as disturbances in the helium and process gas inlet temperatures is presented. The first disturbance studied is a step change of +50 °C in the helium gas feed temperature from steady state. As a result of this change, the shell and inner tube outlet temperatures as well as the methane and CO_2 conversions significantly increased. Figure 7 indicates the response of the key variables of the system at the exit (z = 14 m) to this change. As shown in the figure, the steady state value of the shell exit temperature increased from 676 to 699 °C which resulted in a cooling duty increase of 7.3 MW. The inner tube outlet temperature increased from 594 °C to the new steady state of 611 °C; methane and CO_2 conversions also significantly increased and reached new steady state values of 95.3 and 34.1%, respectively. It can be concluded from the results that helium gas inlet temperature changes remarkably affect the key variables of the system.

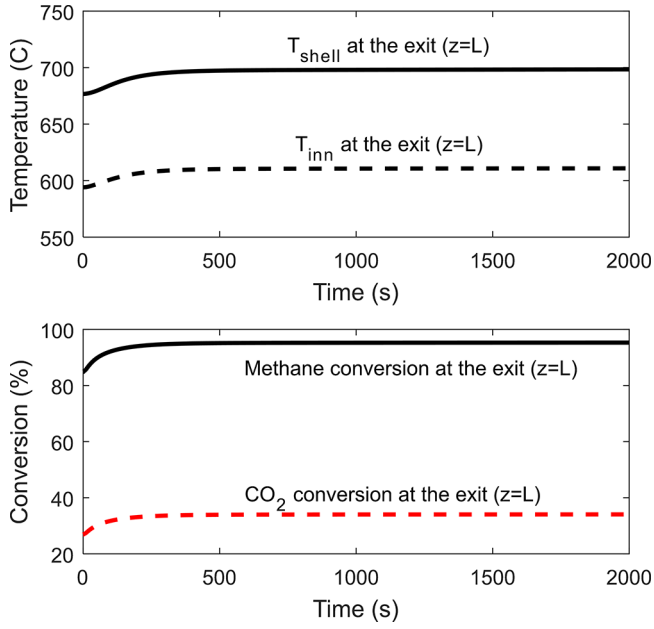

Figure 7. Effect of 50 °C increase in the helium gas feed at t = 0 (s) on the outlet temperatures of the shell and inner tube gases and conversions of methane and CO_2.

The second disturbance investigated here is a 50 °C increase in the process gas inlet feed temperature. Figure 8 shows the

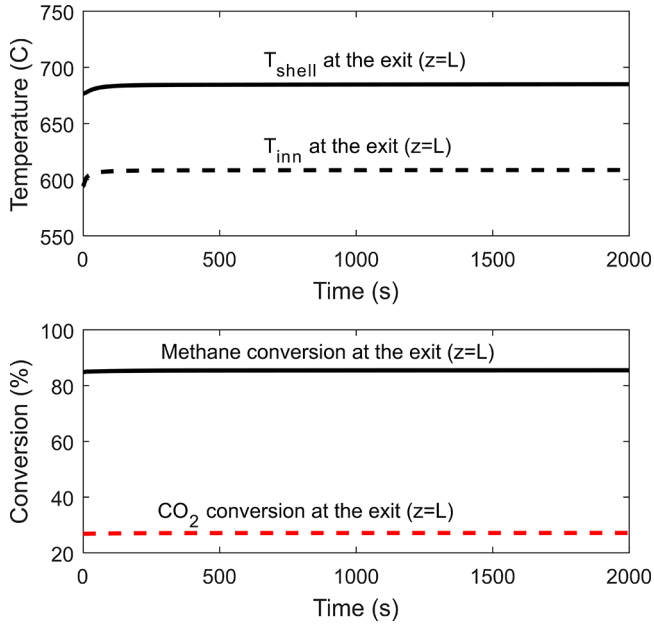

Figure 8. Effect of 50 °C increase in the process gas feed at t = 0 (s) on the outlet temperatures of the shell and inner tube gases and conversions of methane and CO_2.

impact of this change on the shell and inner tube exit temperatures as well as the methane and carbon dioxide conversions in the outlet. As a result of this change, the shell outlet temperature increased from 676 °C to the new steady state of 685 °C, resulting in a decrease in the cooling duty of the system to 69.2 MW. In the inner tube side, the syngas exit temperature increased from 594 °C to 881.8 K. Methane conversion went up only by 0.7 percentage points, and CO_2

DOI: 10.1021/acs.iecr.7b03726
Ind. Eng. Chem. Res. 2018, 57, 6013−6023

conversion only increased by 0.2 percentage points. The results show that disturbances in the process gas inlet temperature have an insignificant impact on the system performance. Since in the tube side, $c_p(\Delta T)$ is small compared to the conv. ΔH_r term, the impact of inlet temperature in the tube side is small.

4.2. Sensitivity Analysis. In this section, the impact of key design parameters on the performance of the system is presented. Although the given parameters reported in Table 4 are the design data from the literature, it is necessary to determine the key parameters of the system and investigate the impact of those on the system performance. The sensitivity of the system to uncertain parameters was analyzed for 5 and 10% changes in the base value of the inner tube diameter, catalyst particle size, and tube length. The key design variables to represent the performance of the system are the shell exit temperature, the cooling duty of the system, the methane and CO_2 conversions, and the exit H_2 to CO ratio in the MRM tubes. Figure 9 shows the percentage of change from the base case values by ±5 and ±10% changes in the base values of the parameters given in Table 4.

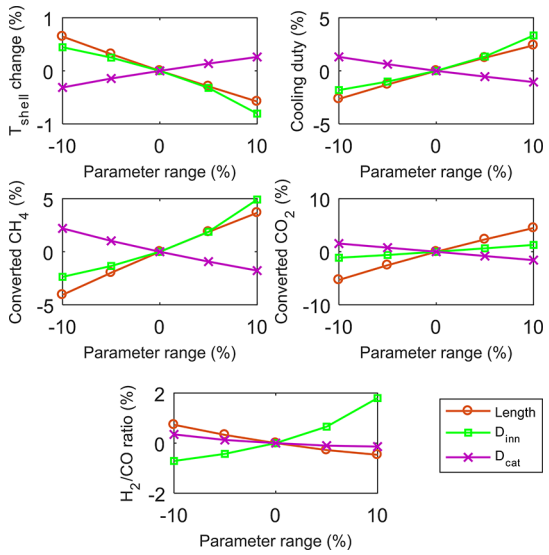

Figure 9. Sensitivity of exit temperatures of the shell, CH_4 and CO_2 exit conversions, cooling duty, and H_2/CO ratio of the system to some of the model parameters (tube length, outer and inner diameters of the inner tube, and catalyst diameter).

This figure indicates that as a result of a ±10% change in the value of the parameters, shell exit temperature shows a maximum change of ±0.8%. This shows that shell outlet temperature is not very sensitive to the parameter uncertainty. The H_2/CO ratio and cooling duty are moderately sensitive to parameter changes. The maximum change of the H_2/CO ratio and cooling duty is 3.3 and 2%, respectively, from a 10% increase in the inner and outer diameters of the inner tube. The methane and carbon dioxide conversions are more sensitive to parameter changes. As a result of ±10% change in the parameters, the moles of converted methane and carbon dioxide change ±4.9 and ±5.3%, respectively. This shows that, for the case of 10% parameter uncertainty, the maximum change in the key variables of the system is 5.3%, which is still small and implies that system performance is not very sensitive to the parameter uncertainty.

In all cases, the catalyst particle diameter is the least influential parameter. However, the impact of the tube length and the inner tube diameter is stronger. It can be concluded from the figure that, despite the inner tube diameter, the tube length affects the system performance roughly linearly. The results show that increasing the inner tube diameter improves the conversions and the cooling duty of the system. This is due to an increase in the heat transfer from the inner tube to the tube. However, increasing the inner tube diameter also leads to the higher pressure drop in the tube side. The same explanation applies for the tube length as well. In addition, increasing the tube length increases the conversions and cooling duty, but it does not mean longer tubes are necessarily optimal due to pressure drops and capital cost limits. Therefore, the optimal values of these parameters must be determined at the systems level depending on how the HTGR/MRM is used.

5. CONCLUSIONS

This study presented a dynamic two-dimensional and multi-scale model for the integrated HTGR/MRM process for syngas production. The model was extended from the previous work by Hoseinzade and Adams[27] to this study. The model is based on first-principles and well-known empirical correlations for physical properties, diffusion, heat and mass transfer coefficients, and reaction kinetics. Due to lack of experimental data on the integrated HTGR/MRM process, the model was validated for the tube side only using the reported experimental data. The shell side model was already validated in the previous study. The developed model for the mixed reforming reactor was validated using over 25 experimental data points for equilibrium and nonequilibrium reactions at steady state conditions. The results demonstrate that the model predicts experimental data well either under equilibrium or non-equilibrium conditions. The model of the integrated HTGR/MRM system was reapplied to commercial scales using design criteria presented in the literature, and that was used to predict key performance criteria such as methane and CO_2 conversions. It has been demonstrated that integrating nuclear heat with the mixed reforming process is a promising option to achieve H_2/CO ratios suitable for FT and MeOH/DME processes. Furthermore, the most important design parameters were identified to be the tube length and the inner tube diameter from a sensitivity analysis, which will help in the design of other HTGR/MRM systems for different applications.

The HTGR/MRM process has potential to be applied in many types of energy conversion systems, such as converting natural gas and nuclear energy into synthetic fuels. Therefore, the presented model is useful to address the key challenges of any applications of integrated HTGR/MRM systems. The inclusion of DRM has the capability to consume CO_2 as a reagent. Thus, depending on the design objectives and how the HTGR/MRM system is integrated with the balance of plant, there is the possibility that it would result in lower lifecycle GHG emissions than using an HTGR/SMR and especially a SMR only approach. The presented model provides the possibility to answer the questions on the life cycle impacts of the HTGR/MRM system. However, analyzing the life cycle of the HTGR/MRM systems in various usage cases is the subject of future study.

AUTHOR INFORMATION

Corresponding Author
*E-mail: tadams@mcmaster.ca.

DOI: 10.1021/acs.iecr.7b03726
Ind. Eng. Chem. Res. 2018, 57, 6013−6023

ORCID

Thomas A. Adams II: 0000-0002-9871-9851

Notes

The authors declare no competing financial interest.

■ ACKNOWLEDGMENTS

Financial support from the Ontario Ministry of Innovation via Early Researcher Award ER13-09-213 with matching support from the McMaster Advanced Control Consortium is gratefully acknowledged.

■ NOMENCLATURE

Subscripts

r = Reaction
p = Particles
d = Diluent
shell = Shell
w = Tube wall
w_2 = Inner tube wall
gas = Mixture of gases in the tube
cat = Catalyst phase
i = Component counter
t = Tube
inn = Inner tube gas

Acronyms

SMR = Steam methane reforming
DRM = Dry reforming of methane
MRM = Mixed reforming of methane
FT = Fischer–Tropsch
POM = Partial oxidation of methane
HTGR = High temperature gas-cooled reactor
WGS = Water gas shift
GHSV = Gas hourly space velocity
GHG = Greenhouse gases
PDAE = Partial differential algebraic equation
STP = Standard temperature and pressure

Greek Letters

ρ = Density
ε = Bed porosity
π = Mathematical constant
κ = Mass transfer coefficient

Variables

r = Reaction rate
C = Molar concentration
p = Partial pressure
T = Temperature
k = Reaction coefficient
K = Equilibrium constant or adsorption coefficient
V = Volume
m = Mass
D = Diameter
L = Length
$\dot{F}$ = Flow rate
Z = Compressibility factor

■ REFERENCES

(1) Rostrup-Nielsen, J. R. Syngas in perspective. *Catal. Today* **2002**, *71* (3), 243.
(2) Mortensen, P. M.; Dybkjær, I. Industrial scale experience on steam reforming of CO_2-rich gas. *Appl. Catal., A* **2015**, *495*, 141.
(3) Abashar, M. E. E. Coupling of steam and dry reforming of methane in catalytic fluidized bed membrane reactors. *Int. J. Hydrogen Energy* **2004**, *29* (8), 799.
(4) O'Connor, A. M.; Schuurman, Y.; Ross, J. R.; Mirodatos, C. Transient studies of carbon dioxide reforming of methane over Pt/ZrO_2 and Pt/Al_2O_3. *Catal. Today* **2006**, *115* (1), 191.
(5) Chen, J.; Wang, R.; Zhang, J.; He, F.; Han, S. Effects of preparation methods on properties of Ni/CeO_2–Al_2O_3 catalysts for methane reforming with carbon dioxide. *J. Mol. Catal. A: Chem.* **2005**, *235* (1), 302.
(6) Sadykov, V. A.; Gubanova, E. L.; Sazonova, N. N.; Pokrovskaya, S. A.; Chumakova, N. A.; Mezentseva, N. V.; Bobin, A. S.; Gulyaev, R. V.; Ishchenko, A. V.; Krieger, T. A.; Mirodatos, C. Dry reforming of methane over Pt/PrCeZrO catalyst: kinetic and mechanistic features by transient studies and their modeling. *Catal. Today* **2011**, *171* (1), 140.
(7) Richardson, J. T.; Paripatyadar, S. A. Carbon dioxide reforming of methane with supported rhodium. *Appl. Catal.* **1990**, *61* (1), 293.
(8) Rostrupnielsen, J. R.; Hansen, J. B. CO_2-reforming of methane over transition metals. *J. Catal.* **1993**, *144* (1), 38.
(9) Wang, S.; Lu, G. Q.; Millar, G. J. Carbon dioxide reforming of methane to produce synthesis gas over metal-supported catalysts: state of the art. *Energy Fuels* **1996**, *10* (4), 896.
(10) Elnashaie, S. S. E. H.; Elshishini, S. S. *Modelling, simulation, and optimization of industrial fixed bed catalytic reactors*; Gordon and Breach Science Publishers: Yverdon, Switzerland, 1994.
(11) Xu, J.; Froment, G. F. Methane steam reforming, methanation and water-gas shift: I. Intrinsic kinetics. *AIChE J.* **1989**, *35* (1), 88.
(12) Bradford, M. C.; Vannice, M. A. Catalytic reforming of methane with carbon dioxide over nickel catalysts I. Catalyst characterization and activity. *Appl. Catal., A* **1996**, *142* (1), 73.
(13) Bradford, M. C.; Vannice, M. A. Catalytic reforming of methane with carbon dioxide over nickel catalysts II. Reaction kinetics. *Appl. Catal., A* **1996**, *142* (1), 97.
(14) Olsbye, U.; Wurzel, T.; Mleczko, L. Kinetic and reaction engineering studies of dry reforming of methane over a Ni/La/Al_2O_3 catalyst. *Ind. Eng. Chem. Res.* **1997**, *36* (12), 5180.
(15) Wang, S.; Lu, G. Q. A comprehensive study on carbon dioxide reforming of methane over Ni/γ-Al_2O_3 catalysts. *Ind. Eng. Chem. Res.* **1999**, *38* (7), 2615.
(16) Maestri, M.; Vlachos, D. G.; Beretta, A.; Groppi, G.; Tronconi, E. Steam and dry reforming of methane on Rh: Microkinetic analysis and hierarchy of kinetic models. *J. Catal.* **2008**, *259* (2), 211.
(17) Zhao, Y. R.; Latham, D. A.; Peppley, B. A.; McAuley, K. B.; Wang, H.; LeHoux, R. Simulation of dry reforming of methane in a conventional downfired reformer. *AIChE J.* **2017**, *63* (6), 2060.
(18) Park, N.; Park, M. J.; Baek, S. C.; Ha, K. S.; Lee, Y. J.; Kwak, G.; Park, H. G.; Jun, K. W. Modeling and optimization of the mixed reforming of methane: maximizing CO_2 utilization for non-equilibrated reaction. *Fuel* **2014**, *115*, 357.
(19) Larentis, A. L.; De Resende, N. S.; Salim, V. M. M.; Pinto, J. C. Modeling and optimization of the combined carbon dioxide reforming and partial oxidation of natural gas. *Appl. Catal., A* **2001**, *215* (1), 211.
(20) Koh, A. C.; Chen, L.; Leong, W. K.; Johnson, B. F.; Khimyak, T.; Lin, J. Hydrogen or synthesis gas production via the partial oxidation of methane over supported nickel–cobalt catalysts. *Int. J. Hydrogen Energy* **2007**, *32* (6), 725.
(21) Yan, X. L.; Hino, R. *Nuclear hydrogen production handbook*; CRC Press: Boca Raton, 2011.
(22) Inagaki, Y.; Nishihara, T.; Takeda, T.; Hada, K.; Ogawa, M.; Shiozawa, S.; Miyamoto, Y. Development programme on hydrogen production in HTTR. *No. IAEA-TECDOC--1210*. 2001, 213.
(23) Fedders, H.; Harth, R.; Höhlein, B. Experiments for combining nuclear heat with the methane steam-reforming process. *Nucl. Eng. Des.* **1975**, *34* (1), 119.
(24) Höhlein, B.; Niessen, H.; Range, J.; Schiebahn, H. J.; Vorwerk, M. Methane from synthesis gas and operation of high-temperature methanation. *Nucl. Eng. Des.* **1984**, *78* (2), 241.

DOI: 10.1021/acs.iecr.7b03726
Ind. Eng. Chem. Res. 2018, 57, 6013–6023

(25) Khojasteh Salkuyeh, Y.; Adams, T. A., II Combining coal gasification, natural gas reforming, and external carbonless heat for efficient production of gasoline and diesel with CO_2 capture and sequestration. *Energy Convers. Manage.* **2013**, *74*, 492.
(26) Khojasteh Salkuyeh, Y.; Adams, T. A., II A new power, methanol, and DME polygeneration process using integrated chemical looping systems. *Energy Convers. Manage.* **2014**, *88*, 411.
(27) Hoseinzade, L.; Adams, T. A., II Modeling and simulation of the integrated steam reforming and nuclear heat systems. *Int. J. Hydrogen Energy* **2017**, *42*, 25048.
(28) Adams, T. A., II; Barton, P. I. A dynamic two-dimensional heterogeneous model for water gas shift reactors. *Int. J. Hydrogen Energy* **2009**, *34* (21), 8877.
(29) Nandasana, A. D.; Ray, A. K.; Gupta, S. K. Dynamic model of an industrial steam reformer and its use for multiobjective optimization. *Ind. Eng. Chem. Res.* **2003**, *42* (17), 4028.
(30) Pantoleontos, G.; Kikkinides, E. S.; Georgiadis, M. C. A heterogeneous dynamic model for the simulation and optimization of the steam methane reforming reactor. *Int. J. Hydrogen Energy* **2012**, *37* (21), 16346.
(31) Dybkjær, I. Tubular reforming and autothermal reforming of natural gas-an overview of available processes. *Fuel Process. Technol.* **1995**, *42* (2−3), 85.
(32) Ghouse, J. H.; Seepersad, D.; Adams, T. A., II Modelling, simulation and design of an integrated radiant syngas cooler and steam methane reformer for use with coal gasification. *Fuel Process. Technol.* **2015**, *138*, 378.
(33) gPROMS. *Process Systems Enterprise*, 2011.
(34) Jun, H. J.; Park, M. J.; Baek, S. C.; Bae, J. W.; Ha, K. S.; Jun, K. W. Kinetics modeling for the mixed reforming of methane over Ni-CeO_2/$MgAl_2O_4$ catalyst. *J. Nat. Gas Chem.* **2011**, *20* (1), 9.
(35) Francesconi, J. A.; Mussati, M. C.; Aguirre, P. A. Analysis of design variables for water-gas-shift reactors by model-based optimization. *J. Power Sources* **2007**, *173* (1), 467.
(36) Park, M. J. Personal communication. Feb 13, 2017.
(37) Ghouse, J. H.; Adams, T. A., II A multi-scale dynamic two-dimensional heterogeneous model for catalytic steam methane reforming reactors. *Int. J. Hydrogen Energy* **2013**, *38* (24), 9984.

DOI: 10.1021/acs.iecr.7b03726
Ind. Eng. Chem. Res. 2018, 57, 6013−6023

Chapter 4

Combining biomass, natural gas, and carbonless heat to produce liquid fuels and electricity

The contents of this chapter have been accepted in the following peer reviewed conference proceeding:

Hoseinzade L, Adams TA II. Combining biomass, natural gas, and carbonless heat to produce liquid fuels and electricity. Computer Aided Chemical Engineering 2018;43:1401-06.

Anton Friedl, Jiří J. Klemeš, Stefan Radl, Petar S. Varbanov, Thomas Wallek (Eds.)
Proceedings of the 28th European Symposium on Computer Aided Process Engineering
June 10th to 13th, 2018, Graz, Austria.
http://dx.doi.org/10.1016/B978-0-444-64235-6.50245-X

Combining Biomass, Natural Gas, and Carbonless Heat to Produce Liquid Fuels and Electricity

Leila Hoseinzade, Thomas A. Adams II*

Department of Chemical Engineering, McMaster University, 1280 Main St W, Hamilton, Ontario, L8S 4L8, Canada
tadams@mcmaster.ca

Abstract

In this study, a new Biomass-Gas-Nuclear heat-To-Liquid fuel (BGNTL) process is presented which uses high-temperature nuclear heat as the heat source for steam methane reforming (SMR). This process co-produces liquid fuels (Fischer-Tropsch liquids, methanol and DME) and power. The BGNTL process was simulated using a combination of different software packages including gPROMS, MATLAB, ProMax, and Aspen Plus. This included the use of a rigorous multi-scale model for the nuclear-heat-powered SMR reactor which was developed in a prior work in gPROMS. Energy efficiency and cradle-to-grave life cycle inventory and life-cycle impact analyses of greenhouse gas (GHG) emissions were accomplished to analyze the environmental impacts of the BGNTL system. Plant performance was compared with a base case Biomass-Gas-To-Liquid (BGTL) process at the same size. In both processes, a carbon capture and storage (CCS) option is considered. It has been found that both processes result in negative total life cycle GHG emissions due to the use of biomass as one of the feedstocks and CCS. Furthermore, the results of this study demonstrate that BGNTL process has 5% lower direct GHG emissions and 13% lower life cycle GHG emissions compared to the BGTL process due to the nuclear heat integration. Also, by using nuclear heat, fossil fuel consumption decreased by up to 10%.

Keywords: Biomass, Natural gas, Carbonless Heat, Polygeneration.

1. Introduction

When oil prices are high, there is significant incentive to use alternative methods of producing gasoline and diesel such as the gas-to-liquids process (GTL). Previous studies have shown that instead of using gas only, processes which integrate natural gas with other fuels can exploit certain synergies that yield both higher energy and carbon efficiencies (Khojasteh and Adams, 2013, Adams and Barton, 2011). In this process, natural gas and coal are used as the source of carbon, while heat and electricity are provided by an advanced type of nuclear energy source called a Modular Helium Reactor (MHR) (Adams and Barton, 2011). This forms the coal-gas-and-nuclear-to-liquids (CGNTL) process, which can be better both environmentally and economically than coal-to-liquids (CTL), coal-and-gas-to-liquids (CGTL), and other processes. However, even though the CO_2 can be eliminated during processing, one cannot prevent the CO_2 emissions from using the gasoline. Furthermore, coal is not of much interest to the Province of Ontario, Canada due to lack of local coal mines and the lack of political support. A recent study (Scott and Adams, 2016) presented a biomass-gas-and-nuclear-to-liquids (BGNTL) process to co-produce fuels and power which is meant to specifically take advantage of Ontario's interests and resources. In this process, nuclear

energy was used to power a copper-chloride cycle that produced hydrogen for syngas upgrading. However, it was found that it was not economical to use nuclear energy in this way (Scott and Adams, 2016). Instead, other approaches which take better advantage of the high-temperature (>800°C) heat produced by some nuclear reactors may be preferable. This study presents the BGNTL process which uses high temperature nuclear heat as the heat source of steam methane reforming process and compares the efficiency and environmental impacts of this process with the BGTL process.

2. Methodology

Figure 1 shows the schematic of the BGTL and BGNTL processes. The process starts with biomass gasification using the high purity oxygen from the air separation unit (ASU), steam, and CO_2. The produced hot syngas transfers its heat via a radiant syngas cooler (RSC) to either the integrated steam reforming process in the BGTL case or the steam generator in heat recovery steam generator (HRSG) section for BGNTL case. Then, the raw syngas is desulfurized in both cases and clean syngas is sent to the syngas mixing section. In the BGTL case, this CO-rich syngas is mixed with the hydrogen-rich syngas from the integrated RSC/SMR, syngas from the auto-thermal reforming (ATR) sections, and shifted syngas from the water gas shift (WGS) section to achieve a certain H_2/CO ratio for downstream processes. In the BGNTL case, CO-rich syngas is mixed with H_2 rich syngas from the integrated SMR/high temperature gas-cooled reactor (HTGR) to adjust the H_2/CO ratio. In this case, a WGS section is not necessary since nuclear-driven syngas has very high hydrogen content and all of the CO-rich syngas is required to obtain the desired H_2/CO ratio for Fischer-Tropsch (FT) synthesis and MeOH & DME processes.

The mixed syngas then is split into three streams and sent to either FT synthesis to produce gasoline and diesel, to the MeOH & DME section to produce DME and MeOH, or to the power generation section which includes gas turbine (GT) and solid oxide fuel cell (SOFC) sub-systems. The SOFC exhaust gas is mostly water and CO_2 which can be easily separated by CO_2 compression. The waste heat from the sections is recovered in the HRSG unit to produce steam for the plant needs and electricity via steam turbines if extra heat is available. Finally, 90% of the CO_2 in the FT feed syngas is removed using MDEA solvent, then this purified CO_2 and CO_2 from SOFC is compressed up to 150 bar for sequestration.

To simulate the BGTL and BGNTL processes, a combination of Aspen Plus V10, ProMax, gPROMS, and MATLAB software packages were used. Aspen Plus was used to model most of the process sections except CO_2 removal and integrated steam reforming sections. The PR-BM physical property package was used for most of the Aspen Plus simulations except the water-only streams in which NBS/NRC tables were applied, CO_2/water mixture at high pressures for which PSRK was used, and MeOH/DME separation for which NRTL-RK was used. ProMax software was employed to model the CO_2 removal section due to more accurate physical property models (TSWEET) for this system. This model was developed by Adams et al. (2014). A reduced order model (ROM) of this process was developed based on the ProMax results and implemented in Aspen Plus. Also, gPROMS was used to model the integrated RSC/SMR system and integrated HTGR/SMR processes. The RSC/SMR process used in the BGTL case was modeled and validated using experimental data by Ghouse et al. (2015). Scott et al. (2016) developed a ROM of this process based on the

results of this model and implemented that in Aspen Plus. In addition, the integrated HTGR/SMR section of BGNTL process was modeled in gPROMS by Hoseinzade et al. (2017) and validated using two pilot scale facility design data.

Both BGTL and BGNTL cases were sized to have 1270 MW_{HHV} thermal input including woody biomass, natural gas, and nuclear energy (in the BGNTL case only). The amount of biomass fed is 100 tonne/hr in both cases; however, the amount of natural gas and nuclear heat are varied accordingly, noting that the ratio between natural gas and nuclear heat in the integrated HTGR/SMR is fixed based on design limits. Table 1 shows the raw material and energy input to the base case BGTL and BGNTL plants. Note that the nuclear heat input is nearly identical to the thermal output (115 MW_{th}) of the Peach Bottom I helium-cooled reactor constructed in 1967 (LaBar et al., 2010). Utility requirements in the plant such as steam and electricity are generated in the plant. As a result of using nuclear energy in the BGNTL process, fossil fuels consumption approximately decreased by 10%.

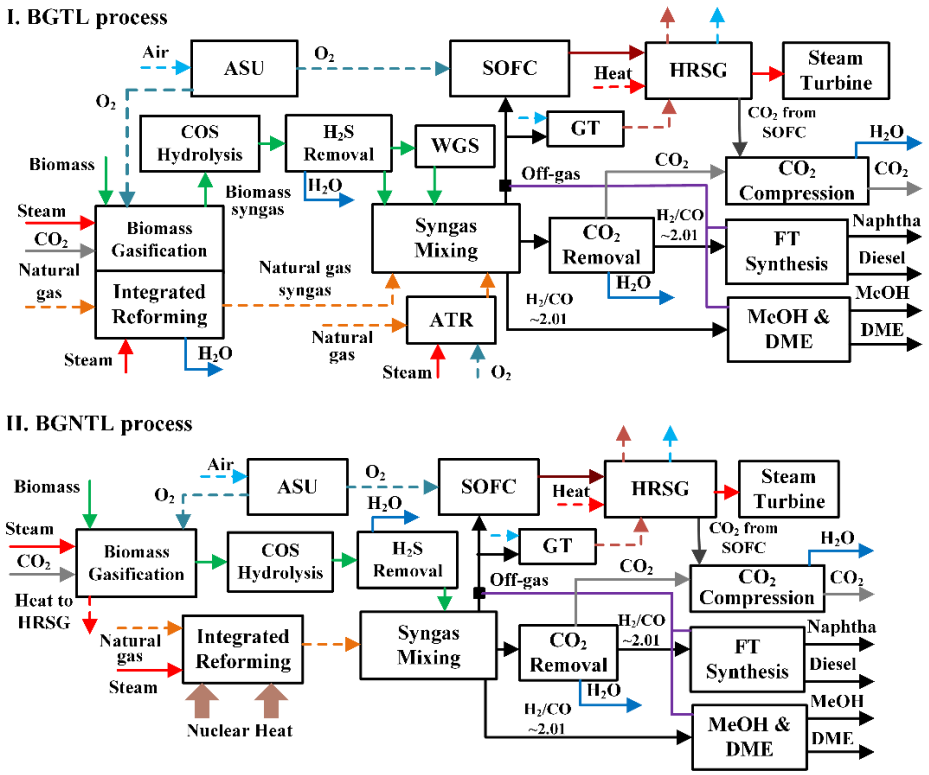

Figure 1. Schematic of BGTL and BGNTL processes.

Table 1. Thermal inputs to the plant (HHV basis where applicable).

Plant	Biomass (MWth)	NG feed to SMR (MWth)	NG feed to ATR (MWth)	Nuclear heat (MW)	Extra heat/ power (MW)
BGTL	550.0	169.3	550.7	-	-
BGNTL	550.0	600.5	-	119.5	-

3. Results and discussions

To evaluate the performance of the BGNTL process, its energy efficiency, carbon efficiency, and environmental impacts are compared to the BGTL process. To have a consistent basis for the comparison, the total thermal input, operating conditions, and CO_2 capture percentages are set to be the same. In addition, the syngas molar split fraction to each of the FT, MeOH & DME, SOFC, and GT routes, and the molar percentage of MeOH product used for DME production is fixed and the same for both cases.

To develop the reduced order model of the integrated HTGR/SMR system, the rigorous model developed in gPROMS by Hoseinzade et al. (2017) was applied. The studied HTGR/SMR plant is a shell and tube heat exchanger which high temperature helium gas is flowing in the shell side, and methane is reformed to syngas in the tube side. This system contains 199 SMR tubes placed in a shell with 14 (m) length and 2.7 (m) inner diameter. To collect the data from the model, the natural gas flow rate and steam to carbon ratio in the feed were selected as the independent variables. 55 data points were randomly generated using Latin Hypercube (LH) sampling, and the key output variables including the methane and steam conversions, heat duty, reformer exit temperature and pressure drop were recorded for each data point. 40 data points were used to train the model for each of the outputs, and 15 data points were applied to test the accuracy of the model. The MVR method was employed to develop the ROM for each of the outputs. For many of the variables, a second-order polynomial was the best fit. In addition, for all of the cases, R^2 of both training and testing was over 0.99.

In addition, the CO_2 removal process used a MDEA / piperazine blend as the solvent with a 90% CO_2 capture rate. This model then was used to build a ROM to implement in Aspen Plus. 100 data points were generated using LH sampling to train and test the developed ROM. 75% of the data were applied to the training, and the rest was used for the testing. Independent variables of this model include the CO_2 flow rate in the feed and solvent to feed molar ratio. Key output variables were the CO_2, H_2S, and water flow rate in the outlet streams, makeup solvent amount, reboiler and condenser duties in the stripper, different cooler duties, pump power, and outlet stream pressure. The ROM was developed based on the MVR as the previous case, and the model accuracy for the train and test were demonstrated by an R^2 over 0.98 for all the cases.

For the given feed conditions in Table 1, simulation results for the BGTL and BGNTL cases are shown in Table 2. The results show that electricity percentage of the BGNTL process is higher than the BGTL plant; however, liquid fuels and chemicals rate is slightly lower than the BGTL process due to lower natural gas feed rate.

Table 2. Simulation results.

Plant	Naphtha (tonne/hr)	Diesel (tonne/hr)	MeOH (tonne/hr)	DME (tonne/hr)	Electricity (MW)
BGTL	2.7	5.8	4.1	47.9	45.9
BGNTL	2.4	5.2	3.7	42.7	67.1

To evaluate the performance of the plants, energy efficiency is used as one of the indicators. Energy efficiency for a plant is defined as the ratio of the sum of produced power and HHV of produced fuels to the sum of total HHV of the feedstocks and

nuclear heat thermal input (Khojashteh and Adams, 2013). The energy efficiencies of plants with the given conditions in Table 1 and results in Table 2 are calculated as 47.27% for the BGTL case and 44.21% for the BGNTL process. The lower efficiency of the BGNTL plant is due to the lower fuel production rate comparing to the BGTL. The carbon efficiency is defined as the percentage of the carbon atoms in the feed converted into the liquid fuels (Khojasteh and Adams, 2013). The carbon efficiency is 40.06% for the BGNTL process and 41.57% for BGTL. The carbon efficiencies of the plants are close, however, the BGTL carbon efficiency is slightly higher.

To evaluate the environmental impacts of both processes, a cradle to grave GHG emission analysis was conducted. In both cases, all of the CO_2 produced in the SOFC section and 90% of the CO_2 in the FT feed syngas is captured. The only direct GHG emissions from the plant are the GT emissions. To estimate the cradle-to-plant-gate GHG emissions, woody biomass cradle-to-plant-gate emission was considered as 0.133 tonne CO_2e/tonne (Zhang et al., 2010) and natural gas well-to-plant-gate emission was counted as 7.2 g CO_2e/$MJth_{HHV}$ (Scott and Adams, 2016). Furthermore, a credit was considered for using biomass by estimating the equivalent CO_2 in biomass based on the carbon atom balance. The plant gate-exit-to-grave emissions include the GHG emissions from the produced fuels' dispensing, distribution and consumption stages. It is assumed that fuel dispensing and distribution GHG emissions are 138 g CO_2e/GJ and 575 g CO_2e/GJ, respectively; plant-to-grave emissions of gasoline and diesel are assumed to be 19.64 lbs CO_2e/gallon and 22.38 lbs CO_2e/gallon, respectively (Scott and Adams, 2016). The plant-to-grave emissions of methanol and DME were also estimated based on fully combusting those and calculated as 1.37 and 1.91 kg CO_2e/kg, respectively. Net sequestered CO_2 also represents the total CO_2 captured subtracted from any CO_2 input to the plant.

Table 3 shows the GHG emission results for the BGTL and BGNTL plants with and without CCS. The negative value for net CO_2e emissions represents the reduction in GHG emissions. Based on the results, both processes end up with a net reduction in GHG emissions, however, BGNTL process achieves 13.4% more life cycle GHG emission reduction and 5% less direct CO_2 emissions in the plant due to using nuclear energy. Based on the GREET (2017) model the cradle-to-plant gate-exit GHG emissions of coal-based DME is 92,700 gCO_2e/GJ_{DME} and its gate-exit-to-grave emissions are 60,280 gCO_2e/GJ_{DME} (Scott and Adams, 2016), so the cradle to grave GHG emissions of coal based DME is 152,990 gCO_2e/GJ_{DME}.

Table 3. Cradle to grave GHG emissions of the plants for 85% capacity.

GHG emission (tCO_2e/yr)	BGTL/CCS	BGNTL/CCS	BGTL/ woCCS	BGNTL/ woCCS
Direct GHG emissions	216,780	204,400	1,231,500	1,172,300
Cradle-to-plant-gate-entrance GHG emissions	-896,410	-916,940	-896,040	-916,940
Net sequestered	-941,210	-893,112	0	0
Plant-gate-exit-to-grave GHG emissions	914,990	814,310	911,450	813,390
Net Cradle-to-grave GHG emissions	-705,120	-791,340	1,327,700	1,149,500
Net Cradle-to-grave GHG emissions (gCO_2e/GJ_{HHV})	-48,372	-58,128	88,307	84,536

4. Conclusions

A base case design for the BGNTL process was presented and its performance was demonstrated by comparing the plant thermal and carbon efficiencies and life cycle GHG emissions to the base case BGTL process of the same size. It was found that both processes have significant negative net lifecycle GHG emissions owing to the sequestration of biogenic carbon. Even without sequestration, the lifecycle GHG emissions of the products are much lower than fossil fuels. However, BGNTL/CCS has 13% lower life cycle GHG emissions and 5% lower direct GHG emissions than BGTL/CCS owing to the use of nuclear energy. The BNGTL and BGTL have similar carbon efficiencies, but the BNGTL thermal efficiency is lower for this product mix.

In this work, the presented model used a mixture of products and technologies (such as both SOFCs and GT), but in practice, only a subset of these would be chosen. This was done because in future work, the model will be used in a superstructure optimization framework which will choose key process design parameters, outputs, and technologies based on a combination of economic and environmental objective functions. Based on the present results, the BGNTL process is expected to be more expensive but have less environmental impact than BGTL, and the optimization-based analysis will be used to better understand this trade-off. This will also determine if the integrated HTGR/SMR approach to integrating nuclear energy is preferable to the copper-chlorine cycle.

5. Acknowledgments

Financial support from the Ontario Ministry of Innovation via Early Researcher Award ER13-09-213 with matching support from the McMaster Advanced Control Consortium is gratefully acknowledged.

References

T. A. Adams II, P. I. Barton, 2011, Combining coal gasification, natural gas reforming, and solid oxide fuel cells for efficient polygeneration with CO_2 capture and sequestration, Fuel processing Technology, 92, 10, 2105-2115.

T. A. Adams II, Y. Khojestah Salkuyeh, J. Nease, 2014, Processes and Simulations for Solvent-based CO_2 Capture and Syngas Cleanup. In: Reactor and Process Design in Sustainable Energy Technology, ed: Fan Shi. Elsevier: Absterdam. ISBN 978-0-444-59566-9.

GREET 2017, U-Chicago Argonne LLC, Argonne, USA.

J. H. Ghouse, D. Seepersad, T. A. Adams II, 2015, Modelling, simulation and design of an integrated radiant syngas cooler and steam methane reformer for use with coal gasification, Fuel Processing Technology, 138, 378-389.

L. Hoseinzade, T. A. Adams II, 2017, Modeling and simulation of an integrated steam reforming and nuclear heat system, International Journal of Hydrogen Energy, 42, 39, 25048-25062.

Y. Khojasteh Salkuyeh, T.A. Adams II, 2013, Combining coal gasification, natural gas reforming, and external carbonless heat for efficient production of gasoline and diesel with CO_2 capture and sequestration, Energy Conversion and Management, 74, 492-504.M. P. LaBar, A. S. Shenoy, W. A. Simon, E. M. Campbell, Y. A. Hassan, 2010, The Gas-Turbine Modular Helium Reactor in: Nuclear Energy Materials and Reactors – Vol. II, Y.A. Hassan and R.A. Chaplin, eds., EOLSS Publications.

J. A. Scott, T. A. Adams II, 2016, Design, Simulation and Optimization of a Biomass-Natural-gas-and-Nuclear to Liquid Fuels and Power Process, Master's Thesis, McMaster University.

Y. Zhang, J. McKechnie, D. Cormier, R. Lyng, W. Mabee, A. Ogino and H. L. Maclean, 2010, Life Cycle Emissions and Cost of Producing Electricity from Coal, Natural Gas, and Wood Pellets in Ontario, Canada. Environmental Science & Technology, 44, 1, 538–544.

Chapter 5

Techno-economic and environmental analyses of a novel, sustainable process for production of liquid fuels using helium heat transfer

The contents of this chapter have been submitted for peer review in the following journal:

Hoseinzade L, Adams TA II. Techno-economic and environmental analyses of a novel, sustainable process for production of liquid fuels using helium heat transfer. Applied Energy 2018, Submitted.

Techno-economic and environmental analyses of a novel, sustainable process for production of liquid fuels using helium heat transfer

Leila Hoseinzade, Thomas A. Adams II*

Department of Chemical Engineering, McMaster University, 1280 Main St W,

Hamilton, Ontario, L8S 4L8, Canada

tadams@mcmaster.ca

Abstract

In this paper, several new processes are proposed which co-generate electricity and liquid fuels (such as diesel, gasoline, or dimethyl ether (DME)) from biomass, natural gas and heat from a high temperature gas-cooled reactor (HTGR). This carbonless heat provides the required energy to drive an endothermic steam methane reforming (SMR) process, which yields H_2-rich syngas (H_2/CO>6) with lower greenhouse gas (GHG) emissions than traditional SMR processes. Since downstream Fischer-Tropsch, methanol, or dimethyl ether synthesis is processes require an H_2/CO ratio of around 2, biomass gasification is integrated into the process. Biomass-derived syngas is sufficiently H_2-lean such that blending it with the SMR-derived syngas yields a syngas of the appropriate H_2/CO ratio of around 2. Chemical process simulations of several candidate processes were developed, which used a rigorous multi-scale, two-dimensional, heterogeneous model for the carbonless-heat-powered SMR reactor developed in a prior work in gPROMS. In addition, 1D

process models within Aspen Plus were also used (Aspen Plus simulation files are provided to the reader). The performance of the presented system was compared with a biomass-gas-to-liquids (BGTL) plant where heat from gasification drives the SMR instead of the HTGR. Techno-economic analyses and GHG life cycle analyses of each case were completed to investigate the economic and environmental impacts of the proposed processes. Optional carbon capture and sequestration (CCS) technology is also considered. The analysis demonstrates that carbonless heat integration leads to thermal efficiencies of up to 55 HHV% as well as suitable profits in the right market conditions. It is also found that net negative life cycle GHG emissions of the final products can be achieved owing to use of biomass, carbonless heat, and CCS. Even without CCS, the life cycle GHG emissions of the proposed process is 25-57% lower than traditional natural gas-to-DME and coal-to-DME processes.

Keywords: Biomass, Natural gas, Carbonless Heat, Dimethyl ether, Fischer-Tropsch Synthesis, Negative emissions.

1. Introduction

The gas-to-liquids (GTL) process can produce liquid fuels from natural gas by reforming natural gas into syngas (a mixture of H_2 and CO) and then converting syngas to synthetic diesel and gasoline using the Fischer-Tropsch (FT) synthesis route [1]. GTL processes can be more economical than traditional petroleum-based plants when natural gas prices are low [1]. The coal-to-liquid (CTL) process is another alternative which produces syngas from the gasification of before converting the syngas to liquid fuels via the FT process [2]. This process is also economic when the price of coal is low [2]. However, they both have significantly negative environmental impacts [3] that are even worse than traditional petroleum refining [4]. Carbon capture and

sequestration (CCS) technologies can be used to reduce the greenhouse gas (GHG) emissions of GTL and CTL plants, but unfortunately it causes the energy efficiency of the plants to drop remarkably [5]. However, GHG emissions can be reduced from GTL or CTL plants without the use of CCS by integrating them with other processes in a synergistic way that results in efficiency improvements [6, 7].

Polygeneration was introduced to efficiently utilize resources such as coal and gas [8]. Adams et al. defined polygeneration as a thermochemical process which simultaneously co-generates at least two products; one of the products is electricity and the other one is a fuel or a chemical [9]. Polygeneration systems are known by their improved efficiency and flexibility comparing to the standalone processes which produce only one product [9]. In most polygeneration systems, syngas is the main route to generate fuels, chemicals or electricity. To produce syngas in polygeneration processes, possible feedstocks and energy sources could include coal, natural gas, biomass, petroleum coke, nuclear energy, wind energy, steel refining off-gases, and so on, either alone or in combination. Based on Adams et al. [9], the products of the polygeneration plants include a wide range such as electricity, FT liquids (gasoline and diesel), alcohols, olefins, dimethyl ether (DME), H_2, syngas, heat, cooling and so on.

Adams et al. [10, 11] and Khojasteh et al. [12] have found that processes which combine natural gas (or coal) with other fuels can harness certain synergies that provide significant benefits. In the studies by Adams et al. [10, 11], natural gas reforming and coal gasification are integrated to poly-generate fuels, chemicals and electricity. It was demonstrated that by integrating the processes, the efficiency and profitability of the plant are significantly improved compared to the coal only and gas only processes.

In the study by Khojasteh et al. [12], an advanced type of nuclear reactor called a Modular Helium Reactor (MHR) is used as the source of heat and electricity, and coal and natural gas are employed as the carbon source. Heat from the high-temperature MHR is used to provide energy to the endothermic SMR reaction. This process is called coal-gas-and-nuclear-to-liquids (CGNTL), which is environmentally and economically superior to coal-to-liquids (CTL), coal-and-gas-to-liquids (CGTL), and other processes in most market conditions. However, even if all CO_2 emissions from the CGNTL plant can be captured, avoided, or eliminated, the CO_2 emissions from combusting the fuels downstream cannot be prevented. Furthermore, in some areas, the use of coal is either not permitted or not of interest due either to a lack of access, lack of political support, or other concerns. This is the case for the region considered in this study (the province of Ontario, Canada), which has eliminated coal from its power grid by public policy [13].

Scott et al. [14] recently presented an alternative to this process which used biomass instead of coal, called the biomass-gas-and-nuclear-to-liquids process (BGNTL). Unlike the process of Khojasteh et al. [12], the BGNTL process of Scott et al. used a Generation IV CanDu Supercritical Water Reactor which was not integrated with the SMR. Instead, heat from this reactor was used as the energy source of a copper-chloride (CuCl) cycle, which produces hydrogen that is blended into biomass-derived syngas for upgrading. This reduces the use of either biomass or gas combustion for heat production needs, thus lowering the amount of CO_2 that is generated during the process and increasing its carbon efficiency. However, it was found that comparing to a base case version that does not use nuclear energy (a biomass-gas-to-liquids process, or BGTL) at the same capacity, it was not economical to use nuclear energy in this way [14]. One of the key reasons for this is that the CuCl process is not particularly efficient at producing hydrogen, and the amount of fossil fuel consumption for hydrogen production that is avoided using this technique is limited.

Therefore, in this study, we propose a novel alternative to the BGNTL/CuCl process of Scott et al. [14] which avoids this limitation by using a high temperature gas-cooled reactor (HTGR) instead of a CanDU reactor. Our proposed process, which we call the BGTNL/HTGR process, uses heat at >800°C from the HTGR to provide energy for the endothermic SMR reaction. This allows a greater proportion of nuclear energy to be used in the process (thus displacing a greater amount of fossil fuel) and permits hydrogen production at greater efficiency. Our proposed process is similar in approach to the CGNTL process of Khojestah et al. [12], except for three important factors: (1) our process is designed for biomass instead of coal; (2) our process is designed to work with HGTRs with coolant temperatures in the 800-950°C range, while the process of Khojestah et al. is designed for very high temperature MHR reactors operating around 1200°C; and (3) our process uses a rigorous multi-scale model for the integrated HTGR/SMR system, with much more realistic properties. This is the primary novelty of the work. The use of biomass in our process is less efficient and less economical than coal, but can yield significant environmental benefits. The lower temperature HGTR used in our process has fewer practical limitations than the 1200°C MHR, but it also creates additional process challenges since it reduces the efficacy of the SMR reaction. For example, the SMR reactor designs are fundamentally different, since the helium-heated SMR in the present work is driven primarily by convection, while the helium-heated SMR in Khojestah et al. is driven primarily by radiative heat transfer.

In this paper the economic and environmental impacts of the proposed BGNTL/HGTR process is compared with a “best known” base case BGTL process with integrated biomass gasification and SMR. Other BGTL, GTL, or BTL processes were not considered for comparison since previous studies found that they were not as efficient or environmentally friendly than the base case used in our work [12].

The proposed BGNTL process is shown in Figure 1. In this process, biomass is gasified with steam and oxygen into syngas and wastes such as CO_2. The produced syngas contains a low amount of H_2 (molar H_2/CO ratio of about 0.75); However, a higher H_2 concentration ($H_2/CO \approx 2$) is required for the downstream use in either FT liquids synthesis or DME synthesis processes. To meet this need, natural gas and steam are converted into the hydrogen rich syngas through the steam reforming reaction ($CH_4 + H_2O \rightarrow CO + 3H_2$). This syngas has a high H_2 content ($H_2/CO > 6$), and it can be mixed with the biomass-derived syngas to produce syngas with a balanced H_2 content ($H_2/CO \approx 2$) required for the downstream processes. CO_2 produced in the process can be captured and sequestered, providing a process which produces near zero direct CO_2 emissions and uses enough biomass to offset the most of GHG emissions from the use of the fuels downstream (e.g. gasoline combustion).

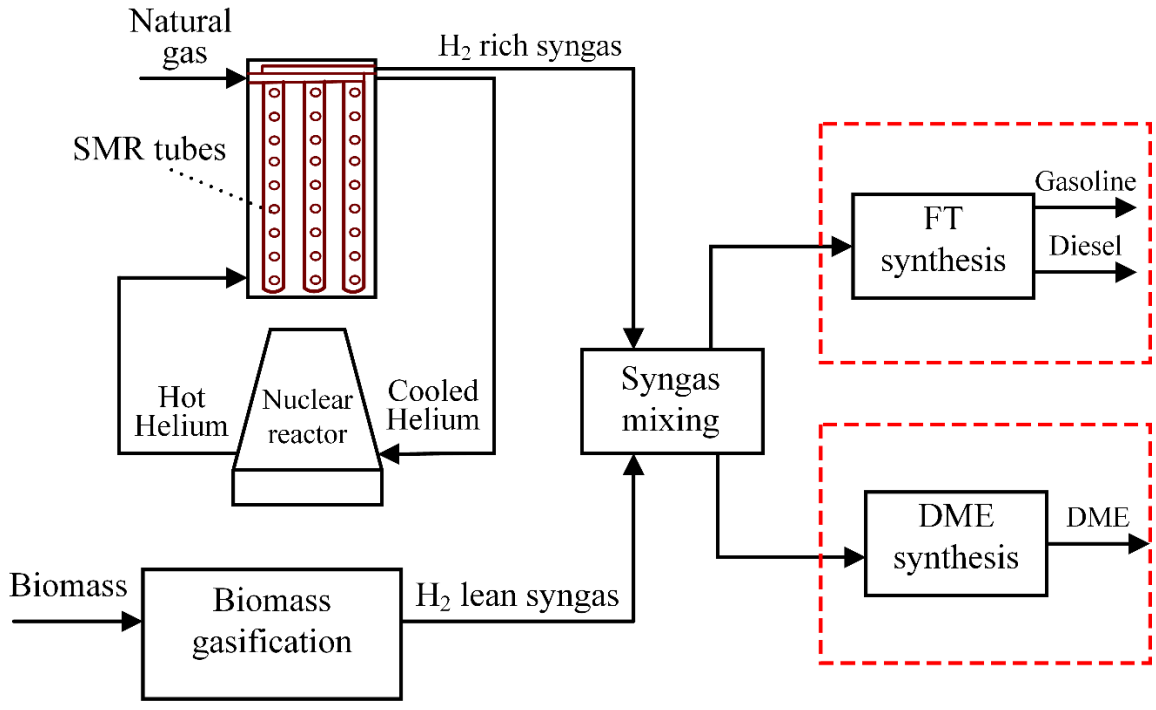

Figure 1. General overview of the BGNTL system superstructure.

The concept of using the heat from a HTGR to power SMR is not new. Several studies by the Research Center Julich and SIEMENS-INTERATOM research groups in Germany [15, 16, 17] and the Japan Atomic Energy Research Center [18] have examined the feasibility and safety of the concept when helium is used as a high-temperature transfer medium which carries heat from the HTGR to the SMR reactor. The studies included the demonstration of pilot scale versions of the helium-heated SMR unit. Hoseinzade et al. [19, 20] later developed a rigorous model for the helium-heated SMR reactor based on first principles and validated it against the design data of the prior work. We used this model in the present work in order to design a helium-heated SMR reactor suitable for use in a BGNTL system and predict the operating conditions pertinent to the system (such as temperature profiles, methane conversions and yields, steam and heat consumption, etc.). Then, we designed a BGNTL system which incorporates this reactor, and performed systems-level techno-economic and life cycle GHG emission analyses in order to evaluate the efficiency of the approach from a business, environmental, and technical perspective. Aspen Plus models were used to aid in these analysis, which have been made available to the public through LAPSE: the Living Archive for Process Systems Engineering at PSEcommunity.org.

2. Methodology

A recent literature review found that in the large majority of cases, creating multiple kinds of fuels in a polygeneration process is generally less economic than producing a single kind of fuel unless there are particular business reasons for needing to multiple kinds of fuels [9]. We found this to be true for the proposed BGNTL system as well [21]. Therefore, in this work, we considered BGNTL variants which produced either FT liquids or DME as products, but not both.

Eight different cases were studied in this work, each at steady state conditions. The cases are BGTL/FT to produce FT liquids (gasoline and diesel), BGTL/DME to produce DME with and without CCS, BGNTL/FT to produce FT liquids and BGTNTL/DME to produce DME with and without CCS. BGTL cases do not include a nuclear component but BGNTL cases contain a HTGR. Each case was sized to have 1070 MW_{HHV} thermal input including woody biomass, natural gas, and nuclear heat (in the BGNTL cases). It should be noted that nuclear heat amount does not represent the nuclear reactor size, it is the amount of heat delivered by the helium coolant to drive the SMR process. A combination of different software packages including Aspen Plus V10, ProMax, gPROMS, and MATLAB were used to simulate these processes. However, most of the process sections except CO_2 removal and integrated steam reforming systems were modeled using Aspen Plus. The Peng-Robinson equation of state with the Boston-Mathias modification (PR-BM) physical property package was used for most of the Aspen Plus simulations which is consistent with a prior work [10]. PSRK method was applied for the CO_2/water mixture at high pressures. In a prior study [22], the PSRK method was found to match experimental data for the property prediction of CO_2/water mixture at high pressures very well. For the MeOH/DME separation NRTL-RK was used [10] and NBS/NRC tables were used for the water-only streams. ProMax software was applied to model the CO_2 removal processes due to its superior physical property models (TSWEET) for this acid gas removal systems. The model of the CO_2 removal process was developed by Adams et al. [23]. The integrated RSC/SMR system and integrated HTGR/SMR processes were modeled in the gPROMS software package.

2.1 Steam Reforming Sections for BGTL Cases

Figure 2 shows the integrated RSC/SMR unit used in the BGTL cases. The model for this system, which was developed by Ghouse et al. [24], is based on first principles and validated in that work

using experimental data. The model is a rigorous, multi-scale, and two dimensional and accounts for both the bulk gas phase changes as well as spatial differences within the catalyst particles. The produced syngas in the gasifier is H_2-lean (H_2/CO ~1) and has the temperature as high as 1300°C. In order to cool down the gasifier derived syngas, it is integrated with a steam methane reforming process which is highly endothermic. Ghouse et al. [24] found that for safe operation of the integrated RSC/SMR process, the co-current configuration should be applied which assures the tube wall temperature remains below the structural integrity limit.

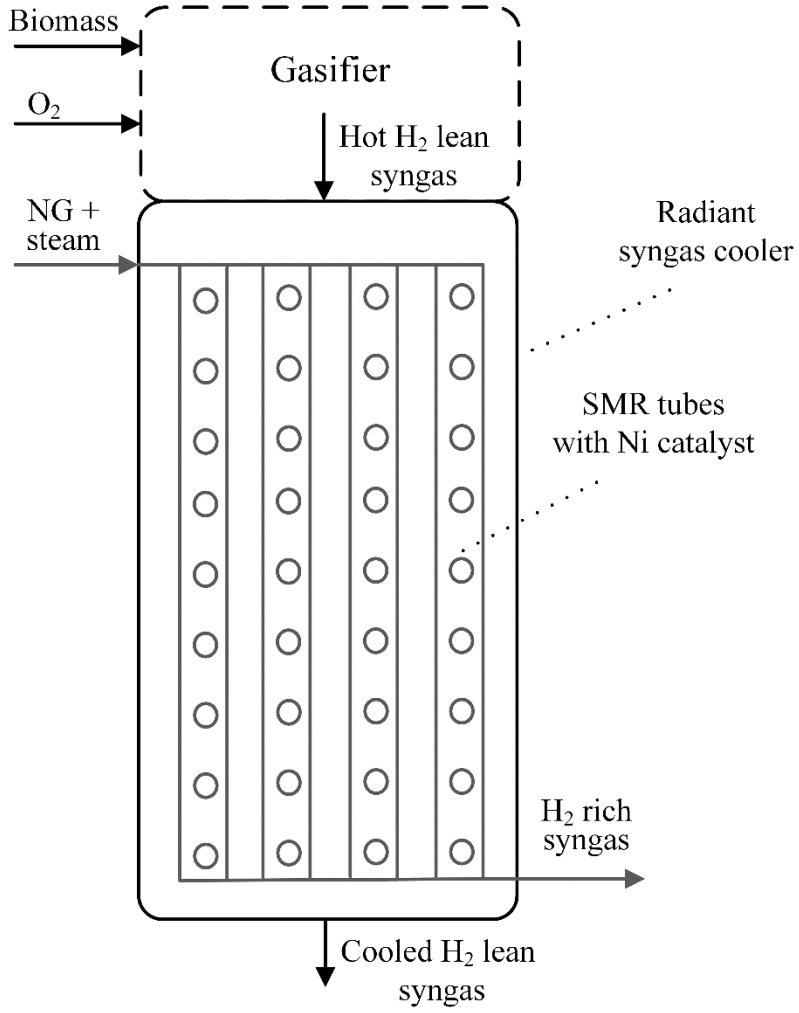

Figure 2. Integrated RSC/SMR system [24].

As Figure 2 shows, syngas from the gasifier flows through the radiant syngas cooler and transfers heat to the SMR tube walls mostly by the radiative heat transfer mechanism. In the tube side, methane and steam are mixed, receive heat from the tube walls, and then are converted to hydrogen rich syngas. The optimal design of the integrated system was presented in follow-up study by Ghouse et al. [25] and it was applied in the BGTL process design. The RSC/SMR system used in this study contains 200 SMR tubes with an outer tube diameter of 10 (cm), tube length of 20 (m), gasifier inner diameter of 4.572 (m) and catalyst particle diameter of 1.6 (cm). More details on the integrated RSC/SMR model can be find in the study by Ghouse et al. [24].

2.2 Steam Reforming Sections for BGTNL Cases

The BGNTL cases use an integrated HTGR/SMR approach shown in Figure 3. The model for this section was developed in gPROMS by Hoseinzade et al. [19] in a prior work, and is also rigorous and based on first principles. The model was validated in that work using design data from two pilot plants. As indicated in the figure, high temperature helium from an HTGR or an intermediate heat exchanger flows in the shell side of a shell and tube heat exchanger. The helium temperature at the shell entrance is 950°C, thus convection is the dominant heat transfer mechanism. Some disc type fins are installed in the outer surface of the SMR tubes to increase the flow turbulence and the heat transfer coefficient. Each SMR tube contains an inner tube (which is not packed with catalyst) to recover the heat of the produced high temperature syngas and increase the methane conversion. The designed system includes 199 SMR tubes with an outer diameter of 12 (cm), tube length of 14 (m), inner tube diameter of 6 (cm), refractory inner diameter of 2.7 (m), and a catalyst particle diameter of 1.2 (cm). Some of these design parameters where chosen to match the plant design by SIEMENS-INTERATOM, while others such as the catalyst particle size or inner tube

diameter were determined through a manual optimization procedure (a course-mesh sampling approach).

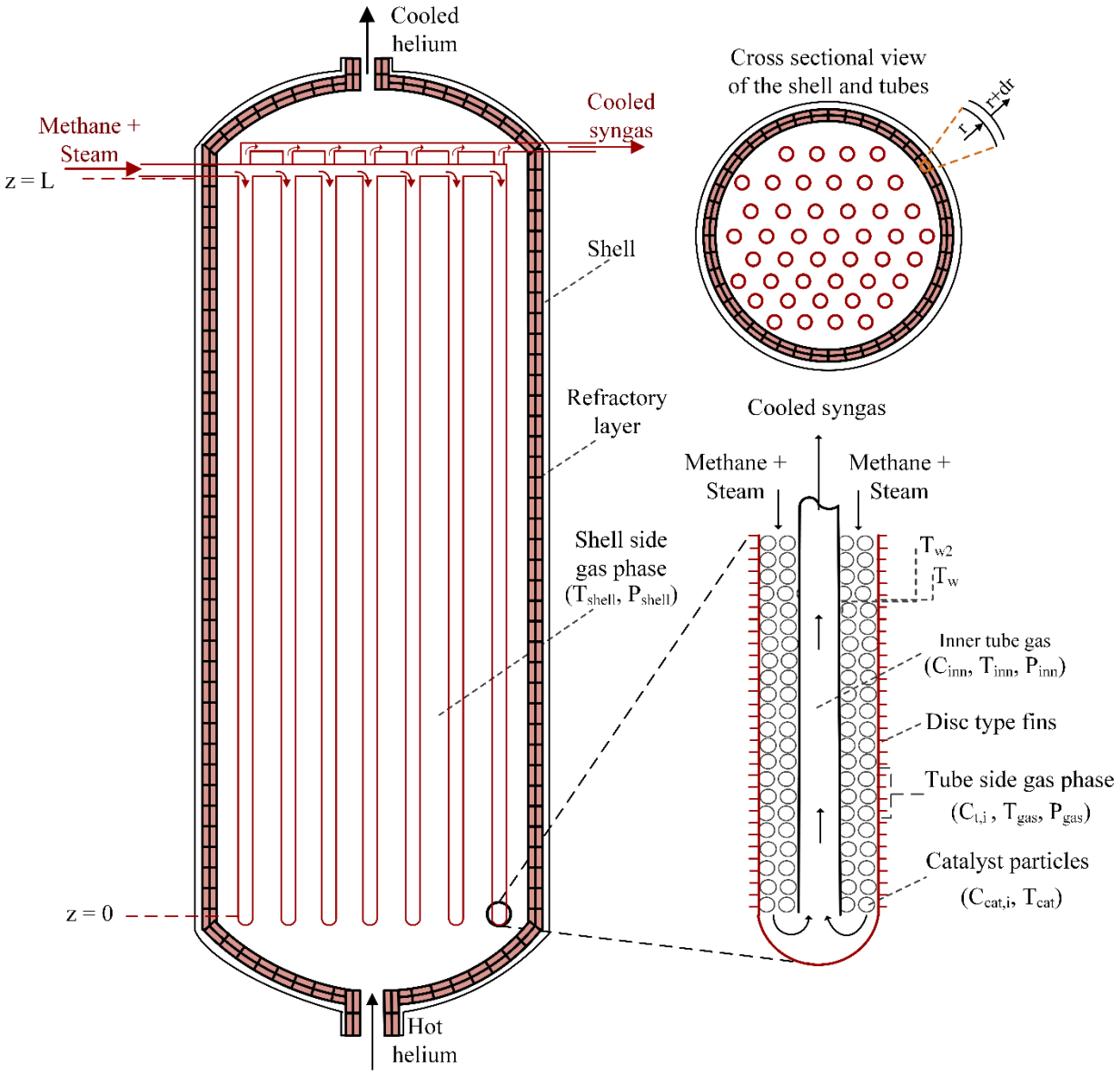

Figure 3. Integrated HTGR/SMR system super structure. This figure is reprinted from the study by Hoseinzade et al. [19].

2.3 Biomass Gasification and Biomass-Derived Syngas Upgrading

Much of the remaining portions of the Aspen Plus process models of the BGTL and BGNTL processes were based on individual model components which were each developed and optimized

in our prior works, including gasification [26], water gas shift [27], CO_2 removal [23], FT synthesis [10], and DME synthesis [28]. Therefore, most of the sections of the process are described briefly in this study and detailed descriptions of those sections can be found in the latter references. The biomass (Ontario cedar wood chips) and natural gas properties used in this study are given in Table 1. It is assumed that the average molecular weight of ash is 0.06515 (kg/mol), the mole fraction of Fe_2O_3 in ash is 2.613% [29], and natural gas is available at 30°C and 30 bar.

Table 1. Properties of wood and natural gas used in this study.

Wood: proximate analysis – as received (wt%) [30]					
Fixed carbon	Volatile matter	Ash	Moisture	HHV (kJ/kg)	LHV (kJ/kg)
58.16	39.94	1.90	8.00	19804.82	18790.00
Wood: ultimate analysis (dry wt%) [30]					
Carbon	Hydrogen	Nitrogen	Sulfur	Oxygen	Chlorine
48.620	5.991	0.478	0.005	43.006	0.209
Natural gas mole fraction (%) [12]					
Methane	Ethane	Propane	n-Butane	CO_2	N_2
93.9	3.2	0.7	0.4	1.0	0.8

Figure 4 and 5 show the schematic of the BGTL/FT, BGTL/DME, BGNTL/FT, and BGNTL/DME processes. The processes start with biomass crushing and feeding to an entrained-flow gasifier. It is assumed that 0.02 kWe is required to crush 1 kWth (HHV based) of wood [31]. Woody biomass, high purity oxygen from the air separation unit (ASU), steam, and CO_2 are fed into the gasifier to produce syngas. The biomass gasification model contains three stages: biomass decomposition, gasification, and cooling. The model was originally developed by Field et al. [32] for coal

gasification was adapted and modified for biomass gasification [14]. The produced high temperature syngas in the gasifier transfers its heat via a radiant syngas cooler to either the integrated steam reforming process in the BGTL cases or the steam generator in heat recovery steam generator (HRSG) section in BGNTL cases.

Then, the biomass-derived syngas is desulfurized before sending to the syngas mixing section. First, it is sent to a hydrolysis reactor where COS reacts with water, generating H_2S, which is easier to remove than COS from syngas, making downstream sulfur removal more cost efficient [10]. The H_2S amount in the raw syngas is low (in the range of 50 ppm) for wood gasification process, thus it is economic to remove it using the LO-CAT process [33]. The LO-CAT system uses a catalyst to oxidize the H_2S into solid sulfur [34]. This system is not modeled in Aspen Plus but it is accounted in the economic analysis. It should be noted that the ASU unit was not modeled in Aspen Plus either, however, it was considered in the economic and energy analysis. It is assumed that 1 MWe is required to produce 1 kg/s oxygen at 1 bar and 0°C [35].

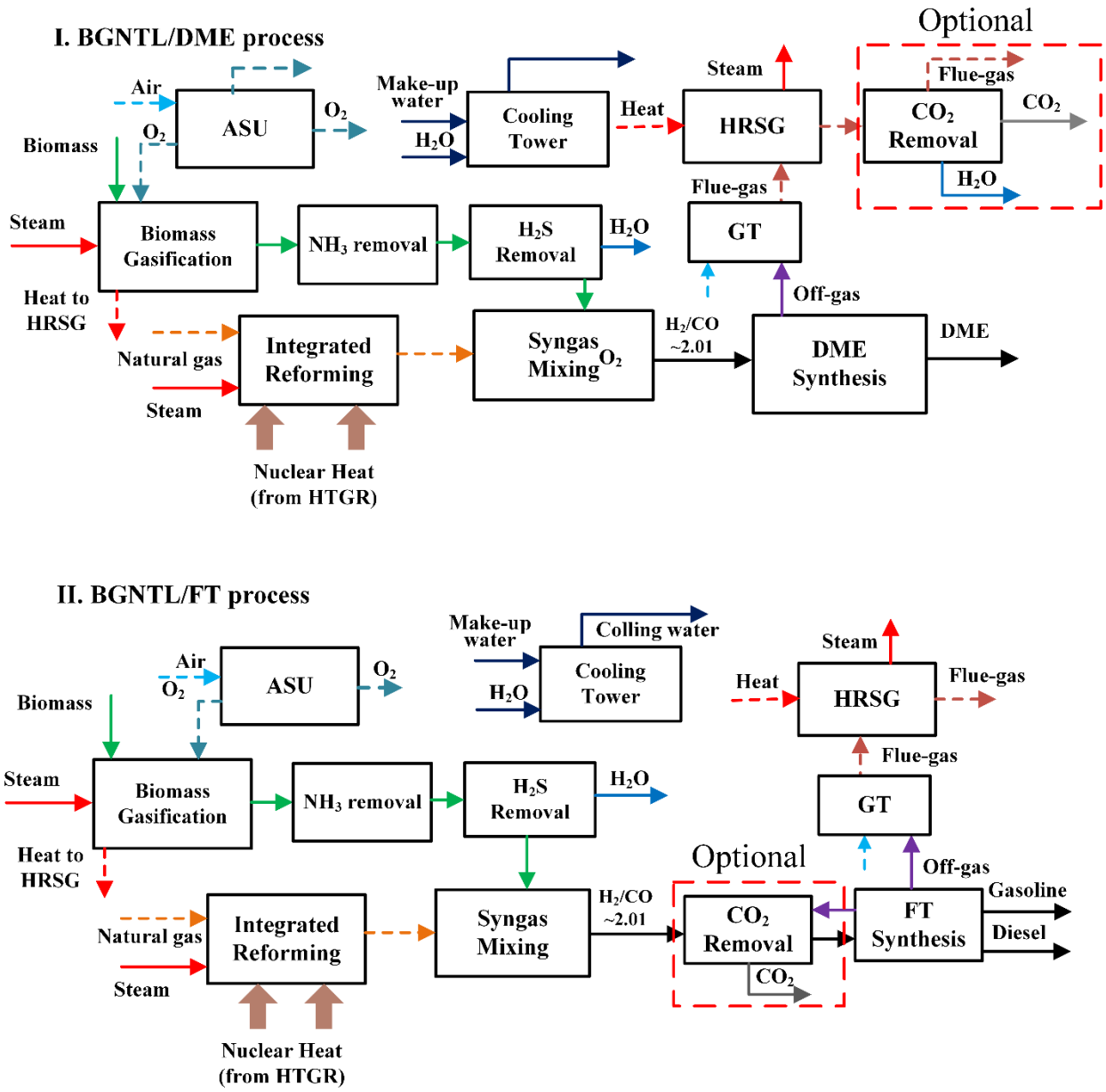

Figure 4. Schematic of BGNTL/DME and BGNTL/FT processes. (GT = Power generation using a gas combustion turbine)

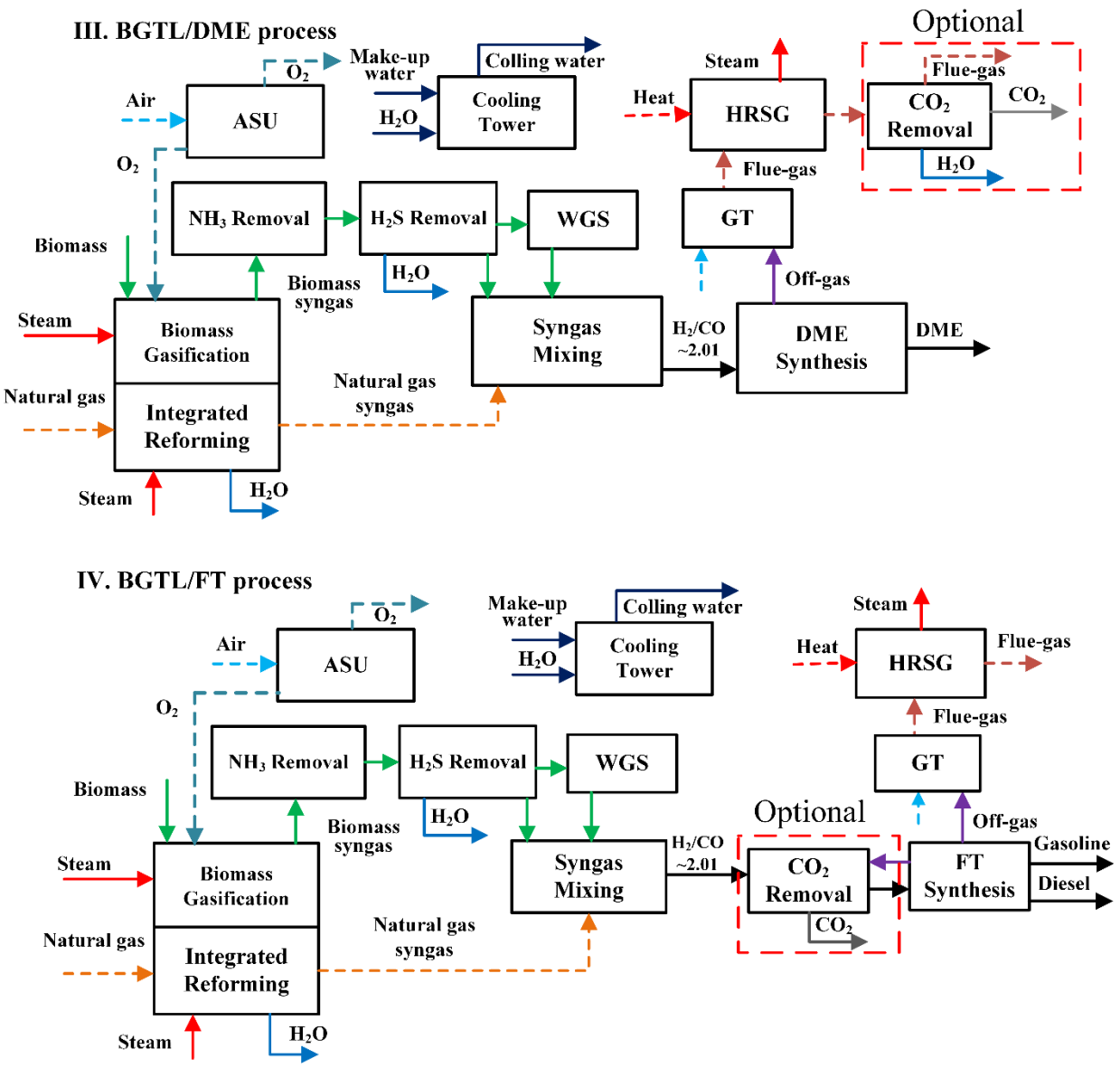

Figure 5. Schematic of the BGTL/DME and BGTL/FT processes.

In the BGTL processes, desulfurized syngas was upgraded to obtain the desired H_2/CO ratio for the Fischer-Tropsch (FT) and methanol/DME processes using the water-gas shift (WGS) reaction. The WGS section was modeled using series of three adiabatic-equilibrium reactors in Aspen Plus to benefit from the fast kinetics at higher temperature in the first two reactors and high conversion at low temperature in the last reactor [27].

2.4 Natural Gas Reforming

In the BGTL cases the integrated reforming section includes a pre-reformer and an integrated RSC/SMR system. The pre-reformer converts the C_2-C_4 hydrocarbons to syngas and is adiabatic. Methane is then reformed to H_2-rich syngas in the integrated RSC/SMR system. The latter design is similar to the integrated coal gasification and SMR system which was presented and modeled by Ghouse et al. [24]. The pre-reformer and reformer were modeled in Aspen Plus assuming chemical equilibrium.

Figure 6 shows a more detailed schematic for this system as modelled in Aspen Plus. As shown in the figure, a pre-reformer converts ethane, propane and butane to syngas first, then output gases are split into two streams of the equal molar flow rate and fed to two integrated HTGR/SMRs operating in parallel. The reason for using two HTGR/SMRs is to prevent high pressure drop in the SMR tubes. If only one reactor is used at this particular process capacity, the pressure drop exceeds 20 bar (as predicted by the rigorous model in gPROMS). The integrated HTGR/SMR system was modeled in Aspen Plus with a combination of a reactor model (specifically REQUIL with specified extents of conversions of the SMR and WGS reactions based on the gPROMS results) and a heater. The heater determines the outlet gas temperature. The results of the gPROMS model were directly entered into the Aspen Plus model of the integrated HTGR/SMR system.

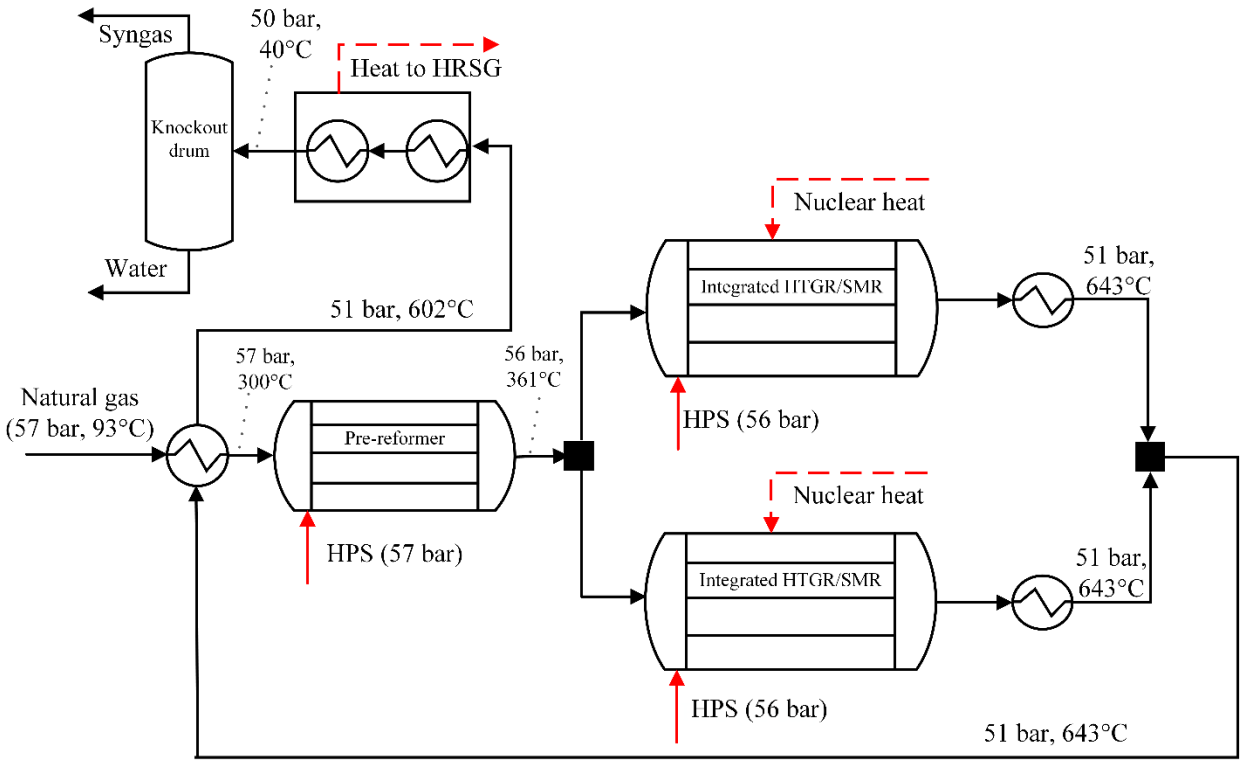

Figure 6. Flowsheet of the integrated HTGR/SMR system in Aspen Plus. HPS = High Pressure Steam.

In the BGTL cases, the CO-rich syngas is mixed with the hydrogen-rich syngas from the integrated RSC/SMR, and shifted syngas from the WGS section to achieve a certain H_2/CO ratio (=2.01) for downstream FT or DME processes. In the BGNTL cases, CO-rich syngas is mixed with H_2 rich syngas from the integrated HTGR/SMR to adjust the H_2/CO ratio. The WGS section is not required in the BGNTL cases since the ratio between biomass and natural gas used in the process can be freely chosen such that the correct H_2/CO ratio in the blended syngas can be obtained.

The mixed syngas then is sent to either FT synthesis to produce gasoline and diesel, DME synthesis. If there is any off-gas in the upstream processes, it is sent to the gas turbine (GT) section to generate electricity. The produced electricity is used for the process needs, and if there is extra electricity it is sold as a product. In the case that produced electricity cannot meet the process needs, it is purchased from the grid.

2.5 Carbon Dioxide Removal

In some of the cases, carbon capture and sequestration is enabled. Depending on the case, a pre-combustion or post-combustion capture process was applied. In the BGTL/FT and BGNTL/FT processes, CO_2 is captured from the syngas prior to entering the FT synthesis section using an MDEA/piperazine "pre-combustion" process. This is because the CO content in the FT process off-gases is small, CO_2 is more efficiently captured prior to combustion, and little additional CO_2 will be produced during combustion. CO_2/H_2 separation is normally less energy intensive than CO_2/N_2 separation, especially when a large amount of N_2 is present [5]. In addition, the portion of FT off-gases which are recycled are mixed with the fresh syngas feed before entering the CO_2 removal section.

In the BGTL/DME and BGNTL/DME processes, the off-gas of the DME synthesis process still contains a considerable amount of CO which ends as CO_2 in the gas turbine flue gas after combustion. Thus, pre-combustion capture is not a proper option for this case and a post-combustion capture process was applied. Based on the study by Adams et al. [5], an MEA based process is the most efficient and economic choice to capture CO_2 from the gas turbine flue gas.

Both CO_2 capture processes contain an absorption column to separate CO_2 from the syngas mixture, and a stripper column to recover the solvent and separate CO_2. The objective is to capture 90% of CO_2 in the either from syngas or flue gas. The captured CO_2 in this section is sent to the CO_2 compression section to remove water and compress up to 150 bar for sequestration. Both the CO_2 removal processes were based on the models of Adams et al. [23] and the reader is referred to that work for more details.

2.6 Fuel Production Sections

The FT process in the BGTL/FT and BGNTL/FT cases is based on converting syngas with a H_2/CO ratio of 2.01 to hydrocarbons with carbon atom counts from 1 to 60 over a Cobalt based catalyst. The FT reactor outlet is separated into light and heavy hydrocarbons in two flash drums in series. These light and heavy products are sent to a refinery column which was modeled using the PetroFrac block in Aspen Plus to upgrade the products to liquid hydrocarbons which forms diesel and gasoline. The vapor products from the column are sent to an autothermal reformer reactor in the FT unit to produce syngas in a H_2/CO ratio of 2. Depending on the case, this syngas is recycled to the FT reactor or sent back to the CO_2 removal section. The off-gases are sent to the power generation unit (GT). The heavy hydrocarbons from the refinery column are sent to a hydrocracker to break into smaller hydrocarbons using the hydrogen generated in the pressure-swing absorption column in the FT unit. For brevity we avoid providing detailed information on the FT model and instead refer the reader to Adams et al. [10].

The DME synthesis section was modeled based on the two-step (methanol intermediate) synthesis route model developed by Khojasteh Salkuyeh et al. [28]. In this section, methanol is synthesized using an adiabatic plug flow reactor over a Cu based catalyst. In addition to the methanol synthesis reaction, the water gas shift reaction, the ethanol synthesis reaction, and the methyl formate synthesis reaction are considered simultaneously in the Aspen Plus model of this reactor. The unreacted syngas is then recovered in a flash drum and sent back to the reactor except for a purge stream which is sent to the GT section for power generation. The liquid methanol product is recovered from the mixture in two distillation columns in series. Any off-gases from the distillation are sent to power generation. The distillation columns are modeled using RadFrac in Aspen Plus. The produced purified methanol is then sent to DME production. DME is synthesized in a plug

flow reactor over a γ-Alumina catalyst. The liquid product is then distilled (also modeled using a RadFrac block) to recover DME. The unreacted methanol is sent back to the methanol recovery unit and DME product is sent for sale.

2.7 Electricity Production Sections

The GT process, which combusts DME or FT synthesis off-gases, was modeled using an RGibbs block and compressor/ turbine models in Aspen Plus. Off-gases are fed with excess air to the combustion chamber. Some N_2 (from the ASU) is added to the fuel mixture to dilute the fuel and prevent very high temperatures in the combustion chamber [10]. It should be noted that some of the air is split and mixed with the combustion product to decrease the mixture temperature [10, 35].

The waste heat from various sections of the plant is recovered in the HRSG unit to produce steam for plant needs and electricity via steam turbines if extra heat is available. Steam is required in three levels in the plant: low pressure steam (LPS) at 5 bar and 180°C, medium pressure steam (MPS) at 20 bar and 300°C and high pressure steam (HPS) at 50 bar and 500°C. A minimum approach temperature of 10°C is assumed for the various heat exchangers in this unit [36]. This section was modeled in Aspen Plus using the heater, pump, and compressor blocks.

2.8. Cooling Tower

The cooling water required by the system is produced within the plant. The cooling tower was simulated in Aspen Plus using a two-stage equilibrium RadFrac column (with no condenser or reboiler). Air is blown using a fan to cool down the returning cooling water which is at 45°C. During this process some of the water is flees the tower, thus make-up water is added to the tower. This is based on the model of Scott et al. [14] and is described more fully in that work.

2. 9 Plant Sizing, Basis of Comparison, and Optimization

As mentioned previously, the basis of comparison used in this study was that the total thermal input of the feedstocks is 1070 $MW_{HHV.}$ In the BGTL processes, the mass ratio between biomass and natural gas is fixed based on the design requirements of the particular integrated RSC/SMR system which were developed in previous works (e.g. tube arrangements, lengths, wall thicknesses, and diameters; pressure drop; catalyst particle size and loading; material temperature structural limits; safety requirements, etc.), Similarly, in the BGNTL process, the mass ratio between the helium and the natural gas is fixed similarly based on the design requirements of the particular HTGR/SMR system used in this work. Also, in the BGNTL process, the mass ratio between biomass and natural gas is chosen to be the one that yields a syngas blend with the appropriate H_2/CO ratio in the feed to either the FT or DME synthesis process without requiring WGS (or reverse WGS). Thus, the ratios of all feedstocks are determined by process constraints and are not subject to optimization. The final feed rates are shown in Table 2. Note that the nuclear heat input to the BGNTL is nearly identical to the thermal output (103 MW_{th}) of the Peach Bottom I helium-cooled reactor constructed in 1967 [37].

Table 2. Thermal inputs to the plant (HHV basis where applicable).

Plant	Biomass (MWth)	NG feed to SMR (MWth)	Nuclear heat (MW)
BGTL	847.2	223.2	-
BGNTL	478.6	488.3	103.6

Electricity, steam, and cooling water, are produced within the plant boundaries using the waste off-gas and waste heat available (using a combination of the HRSG, GT, and Cooling Tower sections). In some cases, the available waste energy is not sufficient to meet all electricity and steam needs, and so our analysis assumes that the deficit is purchased from the market for cost purposes. In some cases, there is more waste energy available than can be used, and so this is converted to electricity for sale. All chilled water utility needs are similarly assumed to be purchased from the market.

Although, a formal optimization of the process as a whole was not carried out in this study, the individual sections within the BGNTL and BGTL processes were optimized individually. These section optimizations were either performed in the prior works or performed in the present work using industrial data and best practices. For example, the RSC/SMR design was optimized in a prior work [25] using mathematical programming based on factors such as maximizing methane conversion while meeting certain heat transfer and other constraints. The disadvantage of this approach is that the larger process as a whole was not optimized with an economic objective, but given the very large size of some of the models used for the process, this is not tractable with current computing power. The advantage of this approach is that the resulting processes are likely still sufficiently close to optimality that it is quite suitable for drawing conclusions about the technical and economic feasibility and making value judgements.

3. Results and discussion

3.1 Thermal and Carbon Efficiency

A summary of the simulation results for the BGTL and BGNTL cases are shown in Table 3. In the BGTL case, more biomass feed is introduced to the plant comparing to the BGNTL cases. This is

due to the low heating value of biomass which demands more biomass to reform a certain amount of natural gas. In the BGNTL process, a smaller amount of biomass is required to meet the desired H_2/CO ratio due the contribution from nuclear heat.

Table 3. Simulation results.

Case	BGTL/ FT	BGTL/ FT	BGTL/ DME	BGTL/ DME	BGNTL/ FT	BGNTL/ FT	BGNTL /DME	BGNTL /DME
CCS used?	Yes	No	Yes	No	Yes	No	Yes	No
Nuclear heat used?	No	No	No	No	Yes	Yes	Yes	Yes
Energy input (MWe or MW_{HHV})								
Biomass	847.2	847.2	847.2	847.2	478.6	478.6	478.6	478.6
NG	223.2	223.2	223.2	223.2	488.3	488.3	488.3	488.3
Nuclear heat	-	-	-	-	103.6	103.6	103.6	103.6
Extra steam	179.9	89.8	77.6	42.5	132.5	103.2	75.8	63.7
Electricity	133.5	41.8	1.5	-	66.6	2.7	-	-
Energy output (MWe or MW_{HHV})								
Naphtha	172.8	172.9	-	-	167.9	168.1	-	-
Diesel	369.4	369.8	-	-	359.1	359.7	-	-
DME	-	-	489.8	489.8	-	-	546.6	553.9
Electricity	-	-	-	27.0	-	-	38.4	59.2
Thermal efficiency (%)	39.2	45.2	42.6	46.4	41.5	44.9	51.0	54.1
Carbon efficiency (%)	45.1	45.2	36.3	36.3	55.3	55.4	51.1	51.8

The required extra steam and electricity purchases were determined by the simulations and are given in the table. The results show that in three of the four DME production cases (except

BGTL/DME with CCS), the plant itself generates more electricity than process needs; however, in the FT cases, some extra electricity must to be purchased from the grid. The reason is that in the FT cases, the available off-gas contains large quantities of CO_2 rather than CO and H_2 and cannot generate the required power. In contrast, in the DME production cases off-gases contain less CO_2 and more CO which can be combusted in the GT and produce more electricity. In the cases with CCS, more electricity is required due to adding CO_2 capture and compression systems. For cost and environmental analysis purposes, it is assumed that the required extra electricity is purchased from the grid in Ontario, Canada. We do not assume that extra electricity is provided by traditional nuclear power (for the BGNTL cases) because the motivating factor for the research is to explore how nuclear energy can be used for non-electricity purposes.

Thermal and carbon efficiencies are employed as indicators to assess the performance of the different plans. The thermal efficiency of a process is defined as the ratio of the sum of all energy outputs divided by all energy inputs on a thermal higher heating value (HHV) basis [12] as given as follows:

$$Thermal\ Efficiency\ (HHV\ based) = \frac{HHV_{Gasoline}+HHV_{Diesel}+HHV_{MeOH}+HHV_{DME}+Power}{HHV_{biomass}+HHV_{NG}+Q_{HTGR}+Q_{Extra}} \quad , \qquad (2)$$

where $Power$ is the electricity output of the system (or 0 if electricity is instead purchased from the grid), Q_{HTGR} is the thermal energy delivered from the nuclear source, and Q_{Extra} is the extra steam or power purchased from the market. For cost and environmental impact purposes, it is assumed that steam is produced from natural gas combustion on an equivalent energy basis.

The carbon efficiency metric uses the definition of [12], which is the carbon atoms in the DME or FT products divided by the carbon atoms in the biomass and natural gas feedstocks. This metric does not consider carbon atoms in any fuels used in the production of steam or electricity purchased

from the market, but rather is an indication of the percentage of the feedstock carbon is converted into useful products within the plant boundaries.

The thermal and carbon efficiencies of the different cases are given in Table 3. Comparing the thermal efficiencies indicates that DME production is more efficient than FT liquids production, due to co-producing electricity as another product in the DME cases. Furthermore, the BGNTL/ DME plant is the most efficient since integrated HTGR/SMR process is efficient. However, comparing the carbon efficiencies depicts that FT liquid production better uses primary feedstock carbon, thus resulting in lower direct CO_2 emissions. Of course, since the FT cases require a greater amount of steam and electricity purchases, this may be offset by higher indirect CO_2 emissions depending on the way in which those utilities were made. The carbon efficiency is higher in the nuclear integrated cases, since carbonless nuclear heat displaces biomass or natural gas combustion for the thermal needs of the endothermic SMR reaction.

In our prior study, the efficiency of the BGNTL process in polygenerating FT liquids, MeOH, DME and electricity was studied [21]. Comparing the results of that study with Table 3 indicates that producing one product at a time and using waste off-gases for power production is remarkably more efficient than polygenerating several products.

3.2 Cost Estimation

Raw material, product and utility prices are given in Table S1 in the supplementary material section. All the prices are in Canadian dollars and given in the original year. If the April 2018 price was available for the raw material, product or utility, we used that in the cost analysis. If not, it was updated to 2018 prices using the inflation rate given in Table S3 in the supplementary material section. As shown in the table, high temperature helium is assumed to be a utility which is available

in 0.0293 $/kWh (in 2011 dollars). Therefore, the capital cost of purchasing an HTGR will not be considered in the analysis but is instead incorporated indirectly via treating it as a utility.

To estimate the plant capital cost, equipment cost estimates from the literature were used as given in Table S2 in the supplementary materials. The costs in Table S2 are given for the base size, in the base year, and in US dollars. Thus, they were updated to the considered plant size using the power law rule and updated to 2018 Canadian dollar using the latest Chemical Engineering Plant Cost Index (CEPCI) [38]. The installation cost is assumed to be proportional to the equipment cost. These factors as shown in Table S2 were derived from the literature for different equipment types and taken into account in the cost estimation. The direct cost was approximated as the sum of the equipment and installation costs. Based on Peters et al. [39], the indirect costs were assumed to be 20% of the direct costs and working capital investment was assumed to be 15% of the fixed capital investment. Furthermore, to estimate plant depreciation, the MACRS depreciation tax table was used. The profitability of the studied cases were evaluated by net present value (NPV). The cost data and parameters used to estimate NPV are given in Table S3 in the supplementary material section.

To approximate the capital and operating costs, all the process units shown in Figure 4 and 5 were considered in the cost analysis. The high temperature helium from the HTGR, steam, water, the LO-CAT process and purchased electricity were considered as utility.

The operating cost of the plant was estimated based on the procedure presented by Peters et al. [39] which assumed different components of the operating cost is a function of fixed capital cost, raw material cost or operating labour cost. A summary of these assumptions is given in Table S4 in the supplementary material section.

With these assumptions, the NPV was calculated for each of the studied cases. It should be noted that all the plants were assumed to operate at 85% designed capacity and carbon tax is not considered in the NPV analysis. Instead carbon tax impact on the profitability of the processes is investigated in the sensitivity analysis section. The summary of the cost analysis including the direct costs of each section, fixed capital, revenue from product sales, total production cost and NPV is given in Table 4.

Table 4. Techno-economic analysis results (in 2018 CAD). TPC = Total Product Cost; FCI = Fixed Capital Investment

Case	BGTL/ FT	BGTL/ FT	BGTL/ DME	BGTL/ DME	BGNTL/ FT	BGNTL/ FT	BGNT L/DME	BGNT L/DME
CCS used?	Yes	No	Yes	No	Yes	No	Yes	No
Nuclear heat used?	No	No	No	No	Yes	Yes	Yes	Yes
Direct capital cost of process sections (million $)								
ASU	141	141	120	120	122	122	90	90
Gasifier	182	182	182	182	122	122	122	122
Integrated RSC/SMR	18	18	18	18	-	-	-	-
WGS	21	21	21	21	-	-	-	-
Integrated HTGR/SMR	-	-	-	-	16	16	16	16
CO_2 removal and compression	71	-	74	-	48	-	53	-
FT	217	215	-	-	237	239	-	-
DME	-	-	368	368	-	-	319	333
Compressors	20	18	18	18	21	20	14	14
GT	14	-	55	54	18	19	54	53
HRSG	80	89	76	68	98	114	87	95
Cooling towers	15	1	3	2	4	1	2	2.0
FCI ($M)=1.2×Direct costs	**935**	**822**	**1,121**	**1,021**	**824**	**783**	**909**	**871**

Gasoline sales ($M/yr)	128	128	-	-	124	125	-	-
Diesel sales ($M/yr)	322	322	-	-	313	313	-	-
DME sales ($M/yr)	-	-	487	487	-	-	543	551
Electricity sales ($M/yr)	-	-	-	16	-	-	23	35
Electricity purchase ($M/yr)	79	25	1	-	39	16	-	-
Helium purchase ($M/yr)	-	-	-	-	26	26	26	26
TPC ($M/yr)	**409**	**304**	**425**	**324**	**307**	**272**	**357**	**280**
NPV ($M)	**-1,129**	**-56**	**-686**	**65**	**-228**	**173**	**281**	**697**

In the gasoline & diesel production cases, the FT section is the most expensive section which accounts for 23-30% of the fixed capital investment (FCI) depending on the case. In the DME cases, the DME synthesis section contributes to 32-38% of the fixed capital investment. In all cases, the ASU and gasifier are the two other primary contributors to the capital cost. The fixed capital cost varies from $783 million for BGNTL/FT/woCCS to $1121 million for the BGTL/DME/CCS. The DME cases require 10-24% more capital investment, since the DME synthesis section is more expensive and they require a larger GT unit. The nuclear integrated cases (BGNTL) needs 5-19% less FCI than the non-nuclear once, since they have a smaller gasifier, ASU, and carbon capture sections. However, this is somewhat misleading since the capital cost of the nuclear reactor is not included in the FCI and instead accounted in the form of an annual utility expense.

Comparing the sales of the different cases indicates sales of diesel and gasoline are almost the same regardless of the process; however, in the DME cases, DME sales are larger in the BGNTL process. This represents higher production rate of DME in the BGNTL cases. The reason is that in the BGNTL process, even though total syngas rate is smaller than the syngas rate in the BGTL, it contains more $CO+H_2$ and less CO_2 than the BGTL process. In the DME cases some electricity is

sold as a side product. In contrast, in the FT cases electricity is purchased from the grid. All of these lead a higher profit for the BGNTL/DME process (with and without CCS). The BGNTL/FT process is only profitable without CCS (note that no carbon taxes are considered in Table 4). Based on the economic analysis results, with the current prices of biomass and natural gas BGTL process is not economic and for an investment of $800-900 million, and building BGNTL/DME process is the most profitable option and results in an NPV in the range of $281-697 million.

3.3 Environmental impacts

The environmental impacts of the different cases were assessed by computing the life cycle GHG emissions. In the FT cases with carbon capture and storage, 90% of the CO_2 in the syngas is captured and the CO_2 from the gas turbine is emitted. In the analysis, emissions from the GT is considered as the direct emissions for the FT cases. In the DME cases with carbon capture, 90% of the CO_2 from the flue gas is captured in the MEA process and the rest is emitted to the atmosphere as vent. The vent gas in this case considered as the direct emissions. In the non-CCS cases flue gases of the gas turbine are the direct emissions. If extra steam is required in a process, it is assumed that it is produced using the heat from natural gas combustion on site. The CO_2 emissions from this natural gas combustion is also considered as direct emissions.

Table 5 gives the cradle-to-plant entrance gate emissions in carbon dioxide equivalents (CO_2e) for the natural gas and woody biomass, as well as the plant gate-exit-to-grave CO_2e emissions. The gate-exit-to-grave emissions include the GHG emissions associated with fuel dispensing, distribution, storage, and combustion of the fuels by the end-user. The DME combustion emissions were approximated assuming the fuel is fully combusted. In addition, we assume that all of the carbon contained in the biomass originated from atmospheric CO_2 and so a credit for CO_2 removal

from the atmosphere is assumed based on the carbon content. Net sequestered CO_2 is determined by subtracting the CO_2 feedstock to the biomass gasification process from the total captured CO_2.

Table 5. CO_2e GHG emissions assumptions of the upstream and downstream processes.

Emission source	Value	Reference
Cradle-to-plant entrance gate CO_2e emissions		
Natural gas cradle-to-plant entrance gate CO_2e emissions	7.2 g CO_2e/MJ_{HHV}	[40]
Woody biomass cradle-to-plant-gate emission (including the harvesting and transportation)	0.133 tonne CO_2e / tonne of biomass	[41]
Plant gate-exit-to-grave CO_2e emissions		
Fuel dispensing	138 g CO_2e/GJ	[42]
Fuel distribution and storage	575 g CO_2e/GJ	[42]
Combustion emissions of gasoline	2.35 kg CO_2e/L	[43]
Combustion emissions of diesel	2.68 kg CO_2e/L	[43]
Combustion emissions of DME	1.91 kg CO_2e/kg	Calculated

The detailed GHG emissions accounting of each process are given in Table 6. In the cases that CCS is enabled, net negative GHG emissions are achieved, meaning that even including the combustion of the fuel, there is a net migration from CO_2 in the atmosphere into underground sequestration. Figure 7 compares the cradle-to-grave CO_2e emissions of the different cases with and without CCS. The results show that the DME route has 30-40% less life cycle GHG emissions

than FT liquids production when there is no-CCS and significantly lower emissions when CCS is enabled, even when accounting for the lower energy density of DME. Also, BGTL cases have 11-37% larger direct emissions than BGNTL cases and 38-48% larger (negative) cradle-to-gate entrance emissions due to using more biomass as the feedstock, although the amount of CO_2 that needs to be sequestered is nearly double.

Table 6. Cradle to grave GHG emissions of the plants for 85% capacity.

GHG emission (tCO_2e/yr)	BGTL/ FT	BGTL/ FT	BGTL/ DME	BGTL/ DME	BGNTL/ FT	BGNTL/ FT	BGNTL/ DME	BGNTL/DME
CCS used?	Yes	No	Yes	No	Yes	No	Yes	No
Nuclear heat used?	No	No	No	No	Yes	Yes	Yes	Yes
Direct GHG emissions	287,400	1,234,500	230,340	1,411,900	254,670	892,890	173,790	882,780
Cradle-to-plant-gate-entrance GHG emissions	-1,503,100	-1,518,800	-1,521,000	-1,527,100	-923,300	-785,690	-790,480	-792,580
Net sequestered	-985,740	0	-1,123,060	0	-596,890	0	-664,430	0
Plant-gate-exit-to-grave GHG emissions	1,273,700	1,275,100	724,160	724,160	1,238,000	1,239,300	808,040	818,970
Net Cradle-to-grave GHG emissions	-927,850	1,115,200	-1,689,500	733,300	-27,517	1,416,800	-473,080	979,450
Net Cradle-to-grave GHG emissions (gCO_2e/GJ_{HHV})	-70,610	84,780	-142,319	58,548	-2,155	110,753	-33,368	65,908

Since each DME production process both is more profitable than and has lower GHG emissions than its FT equivalent under the base case market conditions, we compared the life cycle GHG emissions of different cases with standalone NG-to-DME and coal-to-DME processes. The cradle-to-plant gate-exit GHG emissions of a coal-based and natural gas-based DME plants based on the GREET model [44] are 92,700 gCO_2e/GJ_{DME} and 27,310 gCO_2e/GJ_{DME}, respectively. The gate-

exit-to-grave emissions of DME are 60,288 gCO_2e/GJ_{DME} from Table 5 results. Thus, the life cycle GHG emissions of coal based and natural gas based DME are 152,988 gCO_2e/GJ_{DME} and 87,598 gCO_2e/GJ_{DME}. These are compared in Figure 8. Based on the results, the BGNTL/DME process without CCS, which is the most efficient and most profitable process among the other studied cases, has GHG emissions that are 57% lower than the traditional coal-to-DME process and 25% lower than the traditional NG-to-DME process.

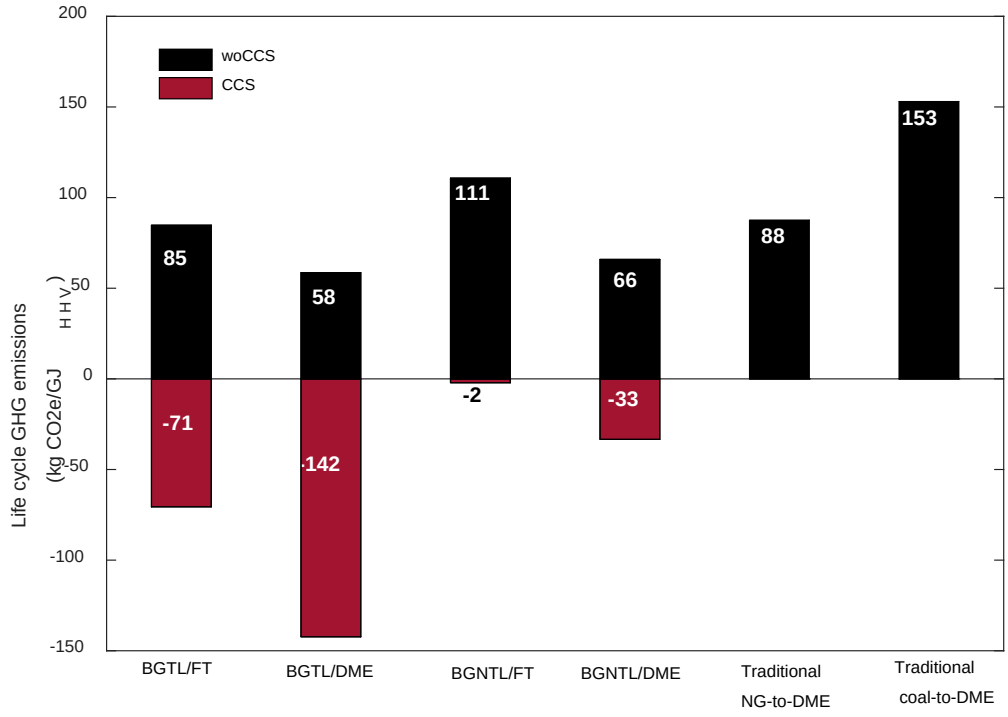

Figure 7. Life cycle GHG emissions of the different cases.

3.4 Sensitivity Analysis

In this section the impact of the uncertain and key parameters on the profitability of the studied systems is considered. The sensitivity analyses were conducted only for the BGNTL/FT/woCCS and BGNTL/DME with or without CCS cases, since the others are not economically promising. The selling price of the fuels (gasoline, diesel and DME), the capital cost of the integrated

HTGR/SMR process, the carbon tax, and the wood price are considered as the most uncertain and key parameters in determining the profitability of the systems. Although, the fuel and raw material prices were taken from the most updated sources, they are always subject to change and it is important to analyze the system performance for the possible changes. Furthermore, the capital cost of the integrated reforming systems (HTGR/SMR) is unknown and we assumed that to be the same as a conventional reformer in the HTGR/SMR case, which causes a large uncertainty in the analysis. The carbon tax is also an important factor which strongly influences the inclusion of the CCS system on the studied processes. It should be noted that in the economic analysis in section 3.2, carbon taxes were not included.

The key parameters were perturbed from their base case values as follows: carbon tax was varied between 0 to 100 $/tonne; the integrated HTGR/SMR capital cost was changed from 1 to 7 times its base case value; and the FT liquids, DME ,and wood prices were changed from -20% to +20% of their base case values. The performance of the system under these uncertainties is best demonstrated by the NPV of the different cases. Figure 8 shows the NPV for the different scenarios for each of the studied changes in the parameters. Based on the Figure 8.a., for the considered carbon taxes, non-CCS cases are more profitable than the CCS cases. The BGNTL/DME design without CCS is profitable for carbon taxes smaller than $100 /tonne. Furthermore, it should be noted that with a carbon tax of $50 /tonne all the cases are still profitable. Figure 8.b. shows that even if the integrated reformer price increases by 7 times from its base case value, still all the plants will remain profitable. This implies that NPV of the plants is less sensitive to the integrated reformer capital cost because it is a small portion of the overall process.

Figure 8.c. shows that the NPV of the plants is very sensitive to fuel selling price. Based on this graph, for more than a 10% decrease in the base case diesel and gasoline or DME selling price,

both BGNTL/FT and BGNTL/DME designs with CCS become non-economic, however, the BGNTL/DME non-CCS case is still profitable.

Figure 8.d. shows NPV change for a 20% change in the wood purchase price. The results indicate that NPV is less sensitive to this change compared to fuel selling price changes. In this case for a 20% increase in the wood price, all of the plants remain suitable business investments (has a positive NPV).

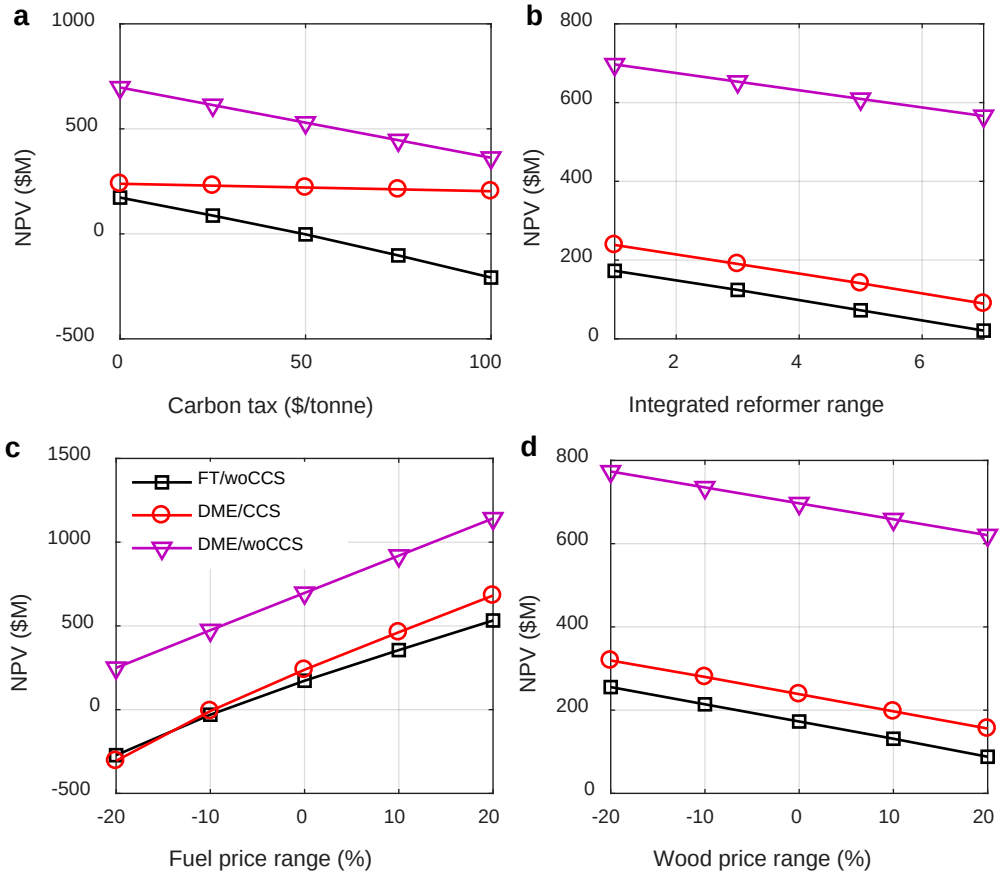

Figure 8. Sensitivity analysis results.

4. Conclusions

A novel combined biomass, gas, and nuclear heat to liquid fuels process was presented for gasoline and diesel or DME production. The BGNTL process was compared against a non-nuclear process of biomass and gas to liquids of the same size to examine nuclear heat integration impact. The key conclusions of the study are listed below:

- The BGNTL process yields high thermal and carbon efficiency. The thermal efficiency can go up to 54 HHV% in the DME production case and carbon efficiency as high as 55% for the FT production case.
- Systems which produce DME result in surplus electricity generation from the off-gases in the plant, thus resulting in a higher thermal efficiency and avoiding the need for importing grid electricity
- With the current prices, the FT liquid production is only profitable if it is produced from the BGNTL process, CCS is not enabled, and there is no carbon tax.
- The most profitable and efficient design, which is the BGNTL/DME, has 57% lower cradle-to-grave GHG emissions than a traditional coal-to-DME plant and 25% lower than a traditional gas-to-DME plant.
- The BGNTL/DME process has 37% lower direct GHG emissions than BGTL/DME when there is no CCS and 25% lower direct emissions when CCS option is enabled.
- All the cases with CCS lead to a negative cradle-to-grave GHG emissions due to using biomass, carbonless heat (in some cases) and a carbon capture system.
- The sensitivity analysis shows that the profitability of the different cases is subject to the current prices and will be affected if market conditions change. Due to the large uncertainty in the fuel and feedstock prices, in the future work it is necessary to conduct an optimization under uncertainty to study the flexibility of the different designs when fluctuation in the market conditions happens.

Acknowledgments

Financial support from the Ontario Ministry of Innovation via Early Researcher Award ER13-09-213 with matching support from the McMaster Advanced Control Consortium is gratefully acknowledged.

Appendix A. Simulation file of the studied designs

The Aspen Plus simulation file of the studied designs can be found in LAPSE (the Living Archive for Process Systems Engineering) with tag LAPSE:2018.0126v1 at the following link:

http://psecommunity.org/LAPSE:2018.0126

Nomenclature

Acronyms

BGNTL	Biomass-gas-nuclear heat-to-liquid
SMR	Steam methane reforming
FT	Fischer-Tropsch
DME	Dimethyl ether
GHG	Greenhouse gas
BGTL	Biomass-gas-to-liquid
CCS	carbon capture and storage
GTL	Gas-to-liquids process
MHR	Modular helium reactor

CGNTL	Coal-gas-and-nuclear-to-liquids
CTL	Coal-to-liquids
CGTL	Coal-and-gas-to-liquids
MeOH	Methanol
HTGR	High temperature gas-cooled reactor
RSC	Radiant syngas cooler
HHV	High heating value
LHV	Low heating value
WGS	Water gas shift
LHS	Latin hypercube sampling
GT	Gas turbine
ASU	Air separation unit
LPS	Low pressure steam
MPS	Medium pressure steam
HPS	High pressure steam
NG	Natural gas
MDEA	Methyl di-ethanolamine
CEPCI	Chemical Engineering Plant Cost Index
NPV	Net present value
FIC	Fixed capital investment
TPC	Total product cost

References

[1] Baliban RC, Elia JA, Floudas CA. Novel natural gas to liquids processes: Process synthesis and global optimization strategies. AIChE J 2013; 59:505-31.

[2] Liu G, Yan B, Chen G. Technical review on jet fuel production. Renew Sustain Energy Rev 2013;25:59–70.

[3] Mantripragada HC, Rubin ES. CO_2 reduction potential of coal-to-liquids (CTL) process: effect of gasification technology. Enrgy Proced 2011;4:2700–7.

[4] Jaramillo P, Griffin WM, Matthews HC. Comparative analysis of the production costs and life-cycle GHG emissions of FT liquid fuels from coal and natural gas. Environ Sci Tech 2008;42:7559-65.

[5] Adams TA II, Hoseinzade L, Madabhushi, PB and Okeke IJ. Comparison of CO_2 capture approaches for fossil-Based power generation: review and meta-study. Processes 2017; 5(3): 44.

[6] Zhang X, Li S, Jin H. A polygeneration system based on multiinput chemical looping combustion. Energies 2014; 7:7166-77.

[7] Khojasteh Salkuyeh Y, Adams TA II. Co-production of olefins, fuels, and electricity from conventional pipeline gas and shale gas with near-zero CO_2 emissions. Part I: Process development and technical performance. Energies 2015; 8:3739-61.

[8] Serra LM, Lozano MA, Ramos J, Ensinas AV, and Nebra SA. Polygeneration and efficient use of natural resources. Energy 2009; 34(5):575-86.

[9]Adams TA II, Ghouse JH. Polygeneration of fuels and chemicals. Curr Opin Chem Eng 2015;10:87-93.

[10] Adams TA II, Barton PI. Combining coal gasification and natural gas reforming for efficient polygeneration. Fuel Process Technol 2011;92:639-55.

[11] Adams TA II, Barton PI. Combining coal gasification, natural gas reforming, and solid oxide fuel cells for efficient polygeneration with CO_2 capture and sequestration. Fuel Process Technol 2011;92:2105-15.

[12] Khojasteh Salkuyeh Y, Adams TA II. Combining coal gasification, natural gas reforming, and external carbonless heat for efficient production of gasoline and diesel with CO_2 capture and sequestration. Energ Convers Manage 2013;74:492-504.

[13] Government of Ontario. Ontario's Five Year Climate Change Action Plan 2016-2020 (p86). http://www.applications.ene.gov.on.ca/ccap/products/CCAP_ENGLISH.pdf

[Accessed Aug 2017].

[14] Scott JA, Adams TA II. Biomass-gas-and-nuclear-to-liquids (BGNTL) processes Part I: model development and simulation. Canadian J Chem Eng 2018; in press, CJCE-18-0053.R2.

[15] Yan XL, Hino R. Nuclear hydrogen production handbook. CRC Press; 2011.

[16] Fedders H, Harth R, Höhlein B. Experiments for combining nuclear heat with the methane steam-reforming process. Nucl Eng Des 1975;34(1):119-27.

[17] Höhlein B, Niessen H, Range J, Schiebahn HJ, Vorwerk M. Methane from synthesis gas and operation of high-temperature methanation. Nucl Eng Des 1984;78(2):241-50.

[18] Inagaki Y, Nishihara T, Takeda T, Hada K, Ogawa M, Shiozawa S, Miyamoto Y. Development programme on hydrogen production in HTTR. No. IAEA-TECDOC--1210 2001.

[19] Hoseinzade L, Adams TA II. Modeling and simulation of an integrated steam reforming and nuclear heat system. Int J Hydrogen Energy 2017;42(39): 25048-62.

[20] Hoseinzade L, Adams TA II. Dynamic modeling of integrated mixed reforming and carbonless heat systems. Ind Eng Chem Res 2018;57:6013-23.

[21] Hoseinzade L, Adams TA II. Combining biomass, natural gas, and carbonless heat to produce liquid fuels and electricity. Comput Aided Chem Eng 2018;43:1401-06.

[22] Adams TA II, Barton PI. High-efficiency power production from coal with carbon capture. AIChE J 2010;56:3120-36.

[23] Adams TA II, Khojasteh Salkuyeh Y, Nease J. Processes and simulations for solvent-based CO_2 capture and syngas cleanup. In: reactor and process design in sustainable energy technology, ed: Fan Shi. Elsevier: Amsterdam. ISBN 978-0-444-59566-9, 2014.

[24] Ghouse JH, Seepersad D, Adams TA II. Modelling, simulation and design of an integrated radiant syngas cooler and steam methane reformer for use with coal gasification, Fuel Process Technol 2015;138:378-89.

[25] Ghouse JH, Adams TA II. Optimal design of an integrated radiant syngas cooler and steam methane reformer using NLP and meta-heuristic algorithms. Comput Aided Chem Eng 2016;38:1431-36.

[26] Adams TA II, Barton PI. High-efficiency power production from coal with carbon capture. AIChE J 2010;56:3120-36.

[27] Adams TA II, Barton PI. A dynamic two-dimensional heterogeneous model for water gas shift reactors. Int J Hydrogen Energy 2009;34:8877-91.

[28] Khojasteh Salkuyeh Y, Adams TA II. A new power, methanol, and DME polygeneration process using integrated chemical looping systems. Energ Convers Manage 2014;88:411-25.

[29] Zhang L, Ninomiya Y, Wang Q, Yamashita T. Influence of woody biomass (cedar chip) addition on the emissions of PM10 from pulversied coal combustion. Fuel 2011;90:77-86.

[30] Hewson D, Oo A, Albion KJ, Keir A. Biomass residuals study for OPG repowering program. Report of the University of Western Ontario Research & Development Park, Sarnia-Lambton Campus; 2011,

http://www.canadiancleanpowercoalition.com/pdf/BM22%20-%20Biomass%20Residuals%20Study%20for%20OPG%20Repowering%20Program.pdf

[31] Van der Drift A, Boerrigter A, Coda H, Cieplik B, Hemmes MK, Van Ree K, Veringa HJ. Entrained flow gasification of biomass. Report ECN-C--04-0.39 of Energieonderzoek Centrum Nederland, Revision A; April 2004. Accessible at

https://www.ecn.nl/docs/library/report/2004/c04039.pdf

[32] Field RP, Brasington R. Baseline flowsheet model for IGCC with carbon capture. Ind Eng Chem Res 2011;50:11306-12.

[33] Feedstock EW. Equipment design and cost estimation for small modular biomass systems, synthesis gas cleanup, and oxygen separation equipment. Nat Renew Energy Lab 2006.

[34] Okoli C, Adams TA II. Design and economic analysis of a thermochemical lignocellulosic biomass-to-butanol process. Ind Eng Chem Res 2014;53:11427-41.

[35] Clausen LR, Elmegaard B, Houbak N. Technoeconomic analysis of a low CO_2 emission dimethyl ether (DME) plant based on gasification of torrefied biomass. Energy 2010;35:4831-42.

[36] Seider WD, Seader JD, Lewin DR, Widago S. Product and process design principles: synthesis, analysis and design.3rd ed. Hoboken, NJ: Wiley; 2008.

[37] LaBar MP, Shenoy AS, Simon WA, Campbell EM, Hassan YA. The gas-turbine modular helium reactor in: nuclear energy materials and reactors – Vol. II, Hassan YA and Chaplin RA, eds. EOLSS Publications; 2010.

[38] Chemical engineering cost index, 2017.

[39] Peters M S, Timmerhaus K D. Plant design and economics for chemical engineers. 4th ed. New York: McGraw-Hill; 1991.

[40] ICF Consulting Canada. Life Cycle Greenhouse Gas Emissions of Natural Gas, A LITERATURE REVIEW OF KEY STUDIES COMPARING EMISSIONS FROM NATURAL GAS AND COAL. The Canadian Natural Gas Initiative (CNGI); 2012,

http://www.capp.ca/~/media/capp/customer-portal/documents/215278.pdf

[41] Zhang Y, McKechnie J, Cormier D, Lyng R, Mabee W, Ogino A, Maclean HL. Life cycle emissions and cost of producing electricity from coal, natural gas, and wood pellets in Ontario, Canada. Environ Sci Technol 2010; 44:538–44.

[42] S&T Consultants Inc. The addition of Bio-Butanol to GHGenius and a review of the GHG Emissions from Diesel Engines With Urea SCR; 2007,

http://www.ghgenius.ca/reports/ButanolGHGenius.pdf

[43] How much carbon dioxide is produced by burning gasoline and diesel fuel? - FAQ - U.S. Energy Information Administration (EIA),

http://www.eia.gov/tools/faqs/faq.cfm?id=307&t=11

[Accessed 6 May 2016].

[44] GREET. U-Chicago Argonne LLC, Argonne, USA 2017.

[45] Natural Gas Rate Updates. (n.d.),

http://www.ontarioenergyboard.ca/OEB/Consumers/Natural+Gas/Natural+Gas+Rates /

[Accessed 30 Jan 2018].

[46] Government of Canada, N. R. C. (n.d.-a). Average Gasoline Retail Prices in Canada,

http://www2.nrcan.gc.ca/eneene/sources/pripri/prices_bycity_e.cfm

[Accessed 30 Jan, 2018].

[47] Dimethyl Ether Prices - Alibaba.com. (n.d.),

https://www.alibaba.com/showroom/dimethyl-ether-prices.html

[Accessed 30 Jan, 2018].

[48] Ontario electricity pricing,

http://www.ieso.ca/en/learn/electricity-pricing/for-residents-and-small-businesses

[Accessed 30 Jan, 2018].

[49] Perales AV, Valle CR, Ollero P, Gómez-Barea A. Technoeconomic assessment of ethanol production via thermochemical conversion of biomass by entrained flow gasification. Energy 2011;36(7):4097-4108.

[50] Hamelinck CN, Faaij AP, den Uil H, Boerrigter H. Production of FT transportation fuels from biomass; technical options, process analysis and optimisation, and development potential. Energy 2004;29(11):1743-71.

[51] Larson ED, Tingjin R. Synthetic fuel production by indirect coal liquefaction. Energy Sustain Dev 2003;7(4):79-102.

[52] Larson ED, Jin H, Celik FE. Gasification-based fuels and electricity production from biomass, without and with carbon capture and storage. Princeton Environmental Institute, Princeton University; 2005.

[53] Kreutz TG, Larson ED, Liu G, Williams RH. Fischer-Tropsch fuels from coal and biomass. In 25th annual international Pittsburgh coal conference. Princeton University Pittsburg; 2008.

[54] Hoseinzade L, Adams TA II. Supply chain optimization of flare-gas-to-butanol processes in Alberta. Canadian J Chem Eng 2016;94:2336-54.

[55] Historic inflation Canada – historic CPI inflation Canada. (n.d.).,

http://www.inflation.eu/inflation-rates/canada/historic-inflation/cpi-inflation-canada.aspx

[Accessed 30 Jan, 2018].

[56] Government of Canada, C. R. A. Corporation tax rates,

http://www.cra-arc.gc.ca/tx/bsnss/tpcs/crprtns/rts-eng.html

[Accessed 30 Jan, 2018].

Supplementary materials

Table S1. Raw material, utility and product prices in CAD.

Raw material, product or utility	Price	Year	2018 Price	Unit
Wood	100	2011	110.6	$/tonne [30]
Natural gas	0.106499	2018	0.106499	$/m^3(std) [45]
Gasoline	0.898	2018	0.898	$/L [46]
Diesel	0.93	2018	0.93	$/L [46]
DME	1.300	2018	1.300	$/kg [47]
Electricity	0.0878	2018	0.0878	$/kWh [48]
High temperature helium	0.0293	2011	0.0313	$/kWh [12]
Process steam	0.246	2006	0.291	$/m^3 [36]
Boiler feed water	0.615	2006	0.728	$/m^3 [36]
Cooling water	0.0246	2006	0.0291	$/m^3 [36]
Chilled water	4.92	2006	5.82	$/GJ [36]
Waste water treatment	1.193	2012	1.298	$/tonne [34]
LO-CAT process	717.240	2012	780.3	$/tonne-sulfur [34]
CO_2 transport and sequestration cost	12.3	2010	13.4	$/tonne [10]

Table S2. Capital cost data of different equipment in US$.

Equipment	Base cost ($M)	Base size	Scale factor	Installation factor	Base year	Reference
ASU	141	52 kg O_2/s	0.5	1	2007	[35]

Gasifier island	120.05	730 MW_{th} LHV of biomass	0.7	1	2006	[49]
COS removal	2.949	1 Kmol/hr COS fed	0.65	1	2012	[7]
Integrated RSC/SMR	10% of gasifier capital cost					
Integrated HTGR/SMR	11.817	56862 kg/hr of NG	0.7	1.32	2011	[12]
Water gas shift reactor	9.02	8819 Kmol/hr of CO + H_2	0.65	1.81	2002	[50]
CO_2 removal section	43.38	327 CO_2 removed in tons / hour	0.67	1	2002	[51]
CO_2 compression	9.52	13 MWe of power	0.62	1.32	2007	[35]
FT reactor	10.5	2.52 Million scf/hr of feed	0.72	1.52	2003	[52]
Pressures swing absorption column	5.46	0.294 Purge gas flow kmol/s	0.74	1.52	2003	[52]
Pressure swing absorption purge compressor	4.83	10 MWe of power	0.67	1.52	2003	[52]
Pressure swing absorption CO_2 rich compressor	4.83	10 MWe of power	0.67	1.52	2003	[52]
FT hydrocarbon recovery unit	0.56	14.44 Thousands lbs/hr feed	0.7	1.52	2003	[52]

FT Hydro treater	7.21	8.984 Thousands lbs/hr feed	0.7	1.52	2003	[52]
FT Autothermal reformer	29.9	365 Million scf/day of feed gas	0.67	1.32	2007	[53]
Methanol reactor	81.77	10.81 Syngas fed in kmol/s	0.65	1	2002	[51]
Methanol separation	1.72	4.66 Methanol production in kg/s	0.291	1	2002	[51]
DME reactor	15.8	2.91 Feed rate of MeOH to DME reactor	0.65	1.52	2003	[52]
DME separation	21.3	6.75 DME produced in kg/s	0.65	1.52	2003	[52]
Plant Compressors	6.3	10 MWe of power	0.67	1.32	2007	[35]
HRSG – Steam turbines and condenser	66.7	275 MWe of power generated	0.67	1.16	2007	[35]
HRSG – Heat exchangers	41.2	355 MW_{th} of heat exchanger duty	0.67	1.16	2003	[52]
Cooling plant	1.7	3.3 MWe of cooling fan	0.7	1.32	2007	[35]
Gas turbine	73.2	266 MWe of power generated	0.75	1.27	2007	[35]

Table S3. General economic data used in this work.

Parameter	Value	Reference

Working days in a year	330 day/yr	[54]
Plant life time	30 years	[54]
Interest rate on loan	10%	[54]
Inflation	1.7%	[55]
Debt percentage	50%	[54]
Tax rate (in Ontario)	38%	[56]
Equity return rate	20%	[54]
Loan life time	30 yr	[54]
Plant life time	30 yr	[54]
Plant production capacity	85%	[22]
Carbon tax	0	[12]

Table S4. Operating cost estimation [39].

	Plant Costs/income component	Estimated cost/income
1	Total capital investment ($)	fixed capital investment/0.85
2	Working capital investment ($)	Total capital investment – fixed capital investment
3	Operating labour cost ($/year)	10/50 of raw materials cost
4	Operating supervision($/year)	0.10×operating labour
5	Utilities($/year)	Estimated based on simulation results
6	Maintenance and repairs($/year)	0.05× fixed capital investment
7	Operating supplies ($/year)	0.10×maintenance and repairs
8	Laboratory Charges ($/year)	0.10×operating labour
9	Patents and Royalties($/year)	0.01×fixed capital investment
10	Catalysts and Solvents($/year)	Calculated based on the simulation results
11	Direct Production Costs($/year)	Sum of 3 to 10+ raw materials
12	Insurance($/year)	0.01×fixed capital investment
13	Local taxes($/year)	0.02×fixed capital investment

14	Rent($/year)	0
15	Fixed Charges($/year)	sum of lines 12 to 14
16	Plant Overhead Costs($/year)	0.5×(operating labour + operating supervision + maintenance &repairs)
17	Manufacturing Costs($/year)	Direct Production Costs+ Fixed Charges+ Plant Overhead Costs
18	Administrative Costs($/year)	0.15×(operating labour + operating supervision + maintenance and repairs)
19	Distribution and Selling Costs($/year)	2/50 raw materials cost
20	Research and Development($/year)	2/50 raw materials cost
21	General Expenses ($/year)	Administrative Costs+ Distribution and Selling Costs+ Research and Development
22	Total Production cost ($/year)	Manufacturing Costs + General Expenses

Chapter 6

Conclusions and Recommendations

6.1. Conclusions

In this thesis, the economic feasibility of several novel alternatives to generate liquid fuels in Ontario province of Canada, with negative GHG emissions is investigated. The general findings of this project are: 1) it is beneficial from both economic and environmental perspectives to displace fossil fuels with nuclear energy to provide heat for the SMR process; 2) an efficient process is presented to combine biomass, natural gas and nuclear heat to produce liquid fuels; and 3) an alternative sustainable feedstock and process is offered to produce liquid fuels without using biomass.

The primary conclusions of this study are as follows:

- A dynamic, multi-scale and mechanistic model was presented for the integrated HTGR/SMR system for the first time and its validity was proven using existing design data in the literature (chapter 2). This model is applicable for controllability, safety, start-up, optimality studies and techno-economic and environmental impact analysis of the integrated system.
- In the HTGR/SMR system, using high steam to carbon ratio in the feed is necessary for sufficient conversions of methane. This leads to a very hydrogen rich syngas with an H_2/CO ratio of up to 6.3. To apply this syngas for the downstream FT and MeOH/DME conversions, it needs to be blended with a low hydrogen content syngas.
- The concept of using nuclear heat for the mixed steam and dry reforming process was presented and investigated for the first time. The rigorous and dynamic model of the HTGR/SMR system was extended to the HTGR/MRM process and a large scale design was developed for this system (chapter 3).

- It was found that flexible H_2/CO ratios can be obtained from HTGR and MRM integration. This process can be directly applied for the downstream FT or MeOH/DME conversions. This system is a potential alternative for the BGNTL process, however, its efficiency and profitability to produce liquid fuels is subject to future research.
- The HTGR/SMR process was combined with biomass gasification to balance the hydrogen amount in the syngas and produce liquid fuels and power. First, BGNTL process superstructure was investigated for polygenerating fuels, chemicals and power (chapter 4). Then, an optimal and efficient design of BGNTL process was presented which targets producing one fuel at a time (chapter 5).
- Comparing the efficiency results of the BGNTL process in chapter 4 and 5 indicates that producing one fuel in the process and using wastes of the plant to co-generate power is remarkably more efficient than polygenerating several products in the plant. It is also found that producing only DME in the plant with electricity from the waste off-gases is significantly more efficient than simultaneously producing FT liquids, DME and power in the plant.
- Producing the same product (or products) from the BGNTL route is remarkably more efficient than the BGTL route. This states that using nuclear heat for the SMR process is more efficient than using biomass gasification heat.
- With current market conditions, producing DME and power from the waste off-gas is the most efficient, most profitable and environmentally friendly option than producing gasoline and diesel. This suggests that replacing diesel with DME is a sustainable option.
- Net negative life cycle greenhouse gas emissions can be achieved in all the proposed designs, owing to converting biomass to fuels and using carbon capture technology.

- It was determined that producing DME from the BGNTL process has 25-57% lower cradle-to-grave GHG emissions when there is no carbon capture and sequestration.
- All of the results on the BGNTL and BGTL processes are subject to the current market prices. The sensitivity analysis shows that the profitability of the different cases will be affected if market conditions change.

6.2. Recommended Future Work

The following section describes the research areas that require further analysis and investigation. Some of these important projects are listed below:

- The optimal design of the HTGR/SMR system: The integrated HTGR/SMR system has been designed mostly based on an industrial case and its unknown parameters were fit to minimize the model predictions from the reported data. This assures that in the analysis of this thesis an efficient and practical design has been applied. However, it is shown in chapter 2 that there is a trade-off to choose the catalyst particle size, inner tube diameter and the pitch ratio of the SMR tubes in the shell side. These parameters affect the heat transfer, pressure drop, methane conversion and capital cost of building the equipment. In the analysis, those parameters were determined based on trial and error while considering design limits and conversion of reactants. However, an optimization to determine the key parameters of the system with an objective function to minimize the overall cost of the system can improve the design. This optimization can be conducted in gPROMS using the developed model for the HTGR/SMR system. Similar analyses are recommended to be carried out to the HTGR/MRM system.

- The start-up and controllability studies of the integrated HTGR/SMR process: Before large scale implementation of the system, its start-up studies are necessary. Any possible failure situation, possibility of forming hot and cold spots in the catalyst, and any unexpected behaviour and unsafe situation during the transients needed to be identified. Then controllability of the system is required to be studied to avoid all of the possible failure and unsafe situations. Based on studies by Japan Atomic Energy [1], the pressure different between the shell and tube in the HTGR/SMR system is one of the key variables determining the safety of the system and needed to be controlled. Furthermore, exit temperature of the helium from the shell is required to be stayed within the bounds. High exit temperature of helium causes inefficient cooling of the nuclear reactor and low exit temperature leads to overcooling of reactor.
- Performance analysis of the HTGR/MRM process to produce liquid fuels: Chapter 3 shows that HTGR/MRM system is capable of producing a syngas with proper H_2/CO ratios for the FT and MeOH/DME synthesis. This process is a potential alternative to the BGNTL process when biomass is not available. However, applying this option to generate liquid fuels was not studied in this thesis. It is recommended that the gas, nuclear, to liquids process is investigated via a large scale simulation in Aspen Plus to determine its carbon and thermal efficiency in producing fuels and power. Furthermore, its economic and environmental performance needed be evaluated and compared with the BGNTL process to decide on the best route of converting feedstocks. The developed model in gPROMS can be applied to simulate this process in Aspen Plus; however, before using HTGR/MRM system for other applications, more analysis and probably optimization needed to improve the conversion of CO_2 in the HTGR/MRM system.

- Optimization under uncertainty for the BGNTL process: As discussed in chapter 5, the profitability of the proposed designs are subject to the current raw materials and product prices. Hence, uncertainties in the market conditions and environmental regulations are inevitable. Other studies showed that flexible design considering the uncertainties in the design can significantly improve the profitability [2] and robustness [3] of the polygeneration process. Therefore, an optimal design under uncertainty is recommended to be carried out to probe possibility to improve the performance of the presented systems.

References

[1] Inagaki Y, Nishihara T, Takeda T, Hada K, Ogawa M, Shiozawa S, Miyamoto Y. Development programme on hydrogen production in HTTR. No. IAEA-TECDOC--1210 2001.

[2] Chen Y, Adams TA II, Barton PI. Optimal design and operation of flexible energy polygeneration systems. Ind Eng Chem Res 2011;50:4553-66.

[3] Liu P, Pistikopoulos EN, Li Z. Decomposition based stochastic programming approach for polygeneration energy systems design under uncertainty. Ind Eng Chem Res 2010;49: 3295-3305.

Appendix

A.1. Clarification on the model validation and fitting in chapter 2:

In chapter 2, the developed model is fitted and validated based on the design data from two pilot scale plants. It is clarified that the data used for model fitting are not experimental data since the experimental data were not reported; however, based on reference [29] of chapter 2, the design data are close to the experimental data from testing the pilot-scale facilities.

A.2. The transient behavior of integrated HTGR/SMR without SMR reactions

Figure A.1 shows the impact of SMR reaction on the transition time of the HTGR/SMR system. The red curve represents the exit temperature dynamics when SMR reaction in the tube is happening and the blue curve shows the transition of exit temperature when the SMR reaction is switched off. In both cases simulation was started from the same steady state condition. In the non-reacting system, it is assumed that in the tube side methane and steam are mixed and receive heat from the shell and leave the tube with converting into syngas. As the graph indicates, when SMR reaction is turned off in tube side, it almost takes twice time for the system to reach its steady state condition comparing to the case with reaction. This is due to high heat rate required for the reforming reaction which derives the system to reach the steady state faster than non-reacting system.

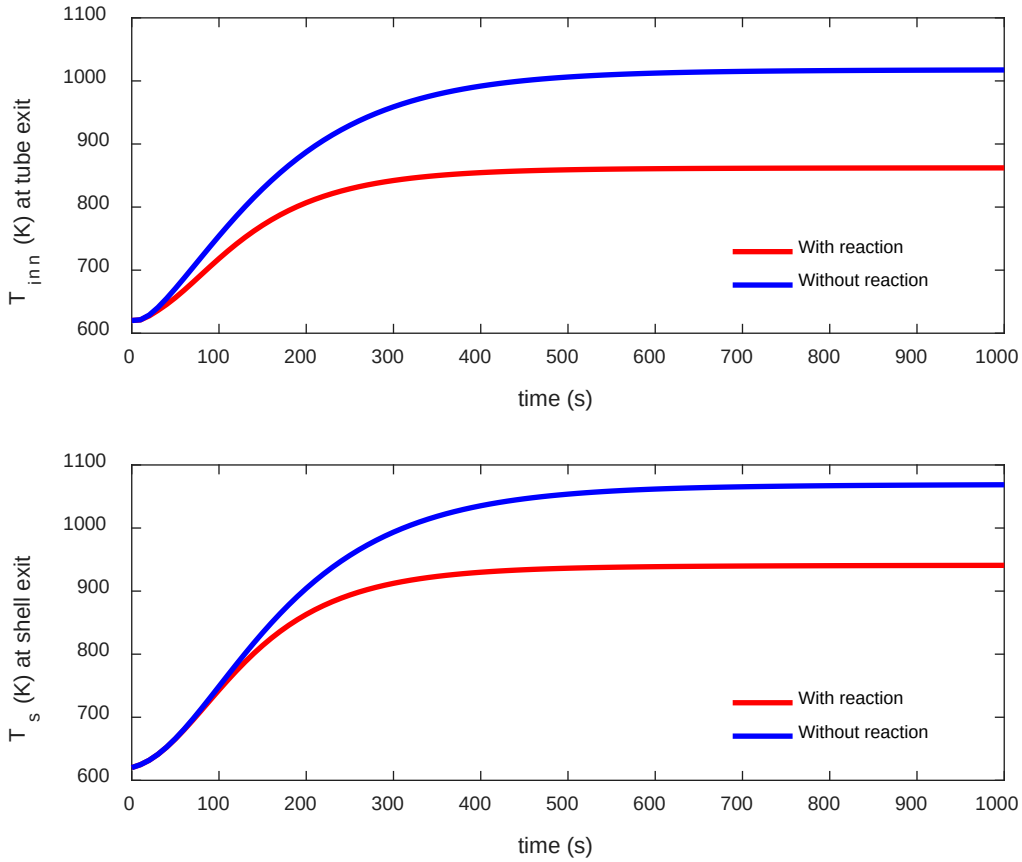

Figure A. 1. Reaction impact on transition behaviors of HTGR/SMR system from a steady state to a new steady state.

A.3. Transient behaviors of the HTGR/SMR system for the changes in the tube feed composition

Another disturbance investigated in the HTGR/SMR system is the impact of the change in the steam to carbon ratio (with constant total molar flow rate) on the system behavior from the base case steady-state conditions. Several step changes in the steam to carbon (S/C) ratio are introduced to the system at different times in sequence. The disturbances are steam to carbon ratio changes from 4 to 3.5 at 0 (s), from 3.5 to 3 at 2000 (s), and from 3 to 2.5 at 4000 (s). Figure A2 shows the dynamic responses of the outlet temperatures and methane conversion to these disturbances. As a result of these disturbances, the shell and inner tube outlet temperatures are change slightly from their previous steady states, with a worst-case change of only an 8 K reduction in the outlet

temperatures. The cooling duty also changes only slightly as a result of the S/C disturbances. However, methane conversion shows a significant change; it changes from 0.73 to 0.67, 0.67 to 0.61 and 0.61 to 0.54, respectively, when the S/C changes from 4 to 3.5, 3.5 to 3 and 3 to 2.5. Also, methane conversion (in Figure A2) overshoots whenever a step disturbance introduced to the system. Analyzing the results indicates that diffusion and mass transfer coefficient of the methane suddenly increases due to a step decrease in the S/C ratio. This sudden increase causes more methane consumption and, thus the overshoot in the methane conversion at that moment. Then both the diffusion and mass transfer coefficients of methane begin to decrease and result in lower methane conversion, as shown in Figure A3.

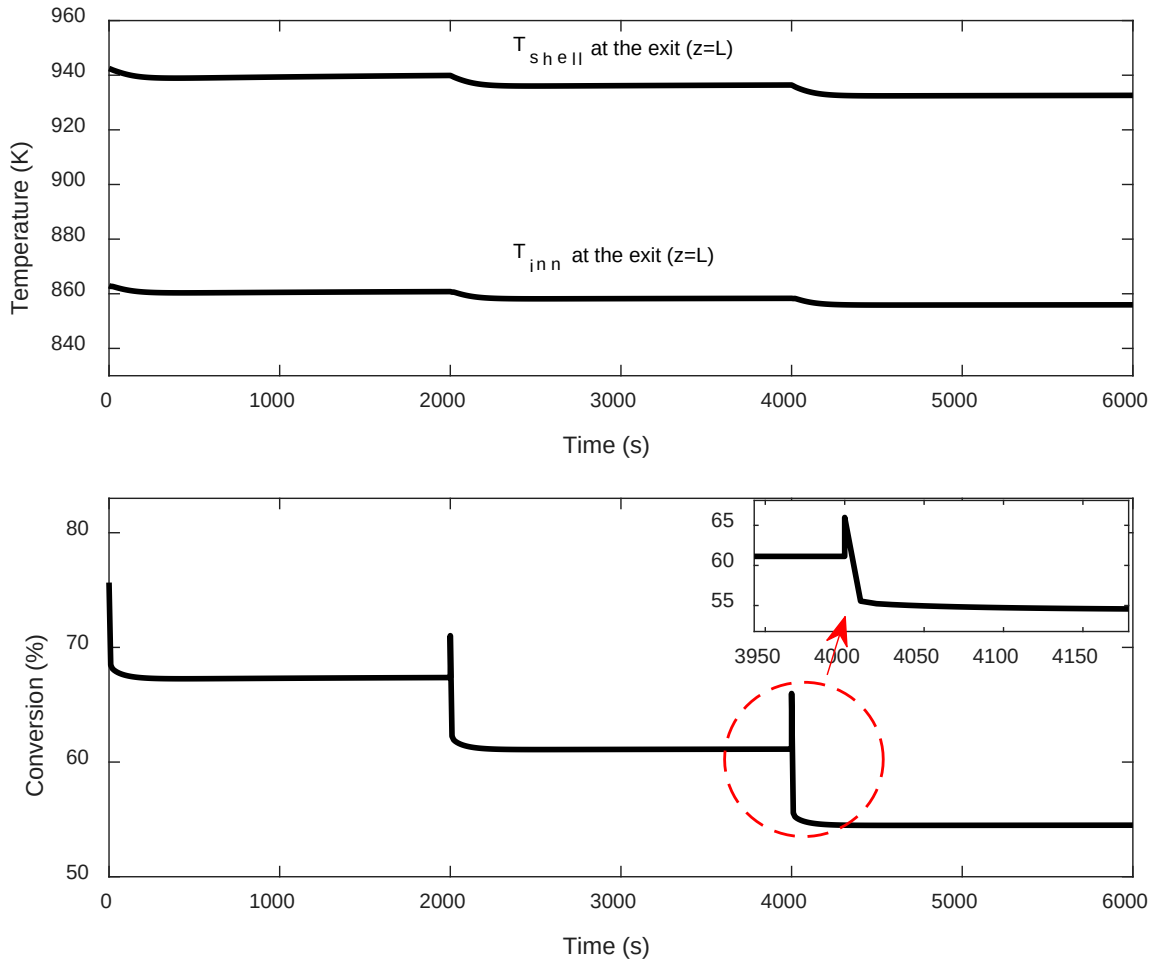

Figure A. 2. Dynamic response of the shell and inner tube outlet temperatures and methane conversion to the steam to carbon ratio changes from 4 to 3.5 at 0 (s), from 3.5 to 3 at 2000 (s), and from 3 to 2.5 at 4000 (s).

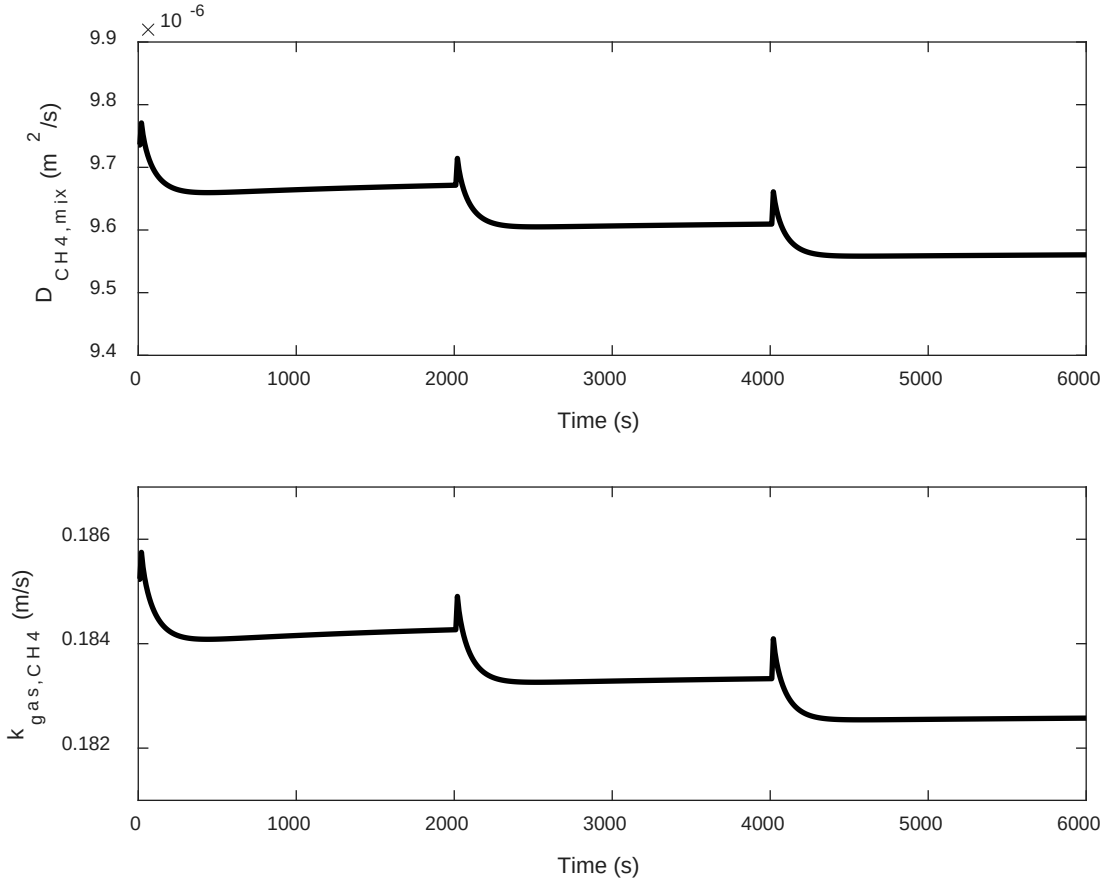

Figure A. 3. Methane diffusivity and mass transfer coefficients dynamic trajectories in the mixture in response to the steam to carbon ratio changes from 4 to 3.5 at 0 (s), from 3.5 to 3 at 2000 (s), and from 3 to 2.5 at 4000 (s).

A.4. Heat recovery steam generator (HRSG) unit simulation

Figure A.4 shows the schematic of the HRSG unit simulated in Aspen Plus. This system is simulated using the heater, pump and compressor blocks in Aspen Plus. Some of the HPS and LPS is used in the plant as process steam, thus some make-up boiler feed water is required to be continuously fed to the HRSG unit.

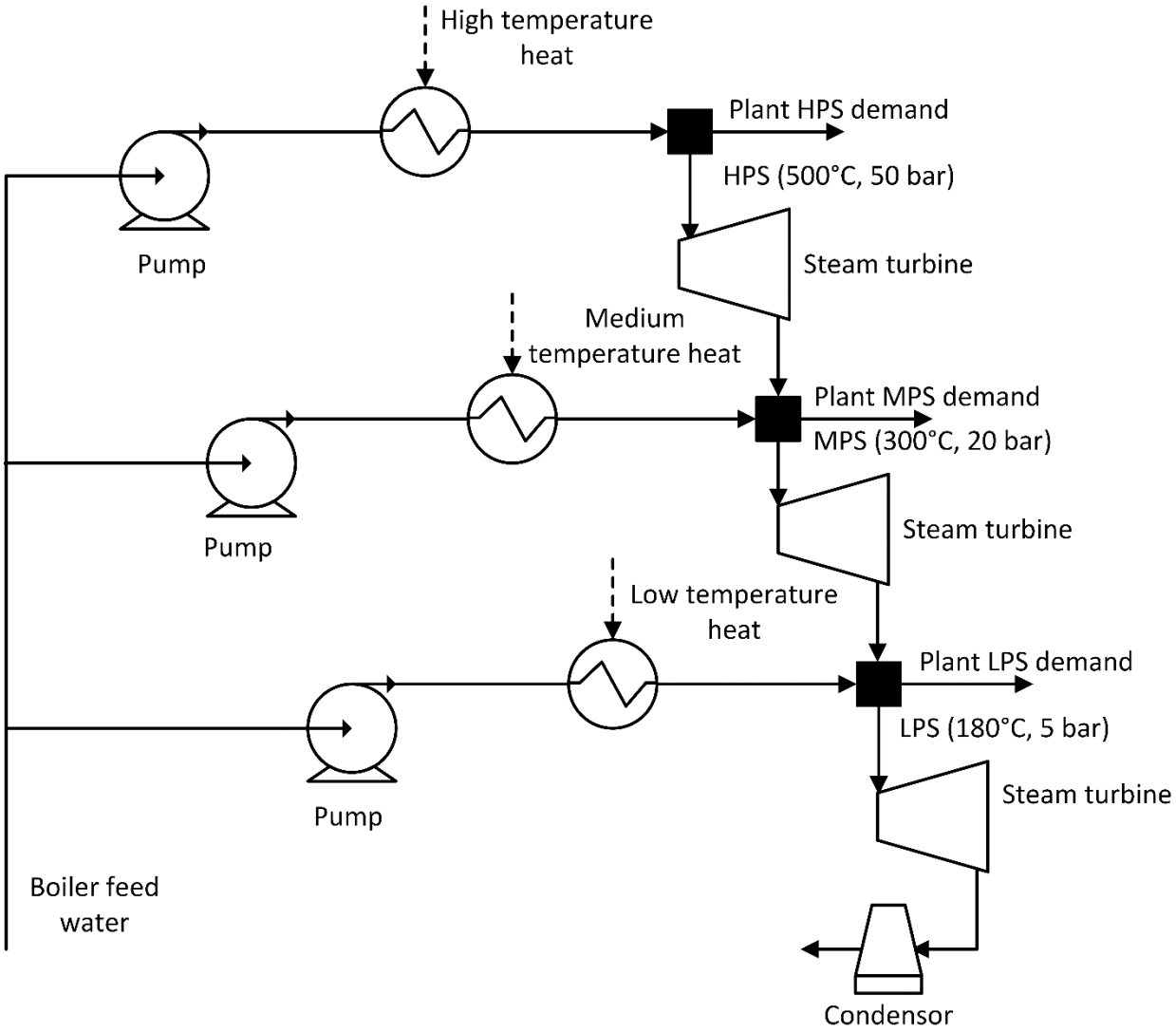

Figure A. 4. HRSG unit flowsheet.